Functional Characterization of a Homozygous *TRAF6* Mutation Causing NF-κB Signaling Defects and Human Immunodeficiency Disease

by
Allison Christina Lewis

A thesis submitted in partial fulfillment for the degree of

Master of Science

Medical Sciences-Medical Genetics
University of Alberta

Abstract

As many as 80,000 Albertans are affected by rare diseases; with the greatest prevalence in children such diseases dramatically impact the lives of both those suffering and the families caring for them. Severe combined immunodeficiency (SCID) represents a group of inherited disorders characterized by immune system impairment due to dysfunctional lymphocytes. Ectodermal dysplasia with immunodeficiency (EDA-ID) is a rare disorder where patients experience abnormalities of the ectodermal structures in addition to immunodeficiency. EDA-ID is most often caused by mutations in the gene encoding NEMO, a critical regulator of the NF-κB pathway. This study focused on finding the cause of a life-threatening immunodeficiency with ectodermal dysplasia features affecting a child of Cree descent born to consanguineous parents from Alberta. Conventional genetic testing for SCID was unable to provide a diagnosis prompting an in-depth investigation for possibly novel genetic causes. A combined bioinformatics method of homozygosity mapping, whole-exome sequencing, and *in silico* modelling was used to identify candidate genes according to an autosomal recessive mode of inheritance. Sanger sequencing was used to determine which candidates segregated with the phenotype in the family. A single candidate gene, *TRAF6* (NM_145803 c.G269T; [p.C90F]), was identified according to these criteria.

This gene is a component of the NF-κB pathway and required for NEMO activation, and the mutation is harbored in a domain that is critical for protein structure and function. The functional consequences of the TRAF6 C90F variant at the protein level, and on the NF-κB pathway were determined using patient derived cell lines. Western blotting shows that the mutant protein is present at much lower levels in patient cells than WT protein in control cells, and translational repression of patient cells using cycloheximide suggests that the mutation impacts protein stability. Molecular analysis of NF-κB signaling in patient cells by western blotting, a high-content assay

for nuclear translocation, and RT-qPCR showed that NF-κB signaling is impaired or abolished in patient cells. Significantly, introduction of WT *TRAF6* gene expression in patient cells rescues signaling defects, confirming that the C90F mutation, and not another unidentified signaling component, is underlying the impairment in pathway activation. Elucidating the causative gene of the disorder in this family has had direct implications for the therapeutic choice to treat the deficiency in this child: a bone marrow transplant, as well as on the family through personalized genetic counselling. This work describes a novel phenotype in a family of Cree descent and proposes a molecular basis for the disease in a gene not definitively known to cause human disease. This research provides an example of a translational study using deep sequencing to identify the cause of a genetic disorder with direct implications for the practice of precision genetics.

Preface

This thesis contains an original work completed by Allison Lewis in partial fulfillment towards a Master of Science degree. The research project, of which this thesis is a part, received research ethics approval from the University of Alberta Research Ethics Board, *Investigating the Cause of Rare Disorders in Children*, Project ID: RES0018693; July 3, 2014.

Some of the research for this thesis is a part of a research collaboration at the University of Alberta, led by Dr. Oana Caluseriu in the Department of Medical Genetics, and with Dr. David Eisenstat from the Department of Medical Genetics, Dr. Edan Foley from the Department of Medical Microbiology and Immunology, and Dr. Leo Spyracopoulos from the Department of Biochemistry. RNA extraction and RT-qPCR experiments for Figures 12 & 22 were performed by Min Ku Kang from the Caluseriu Lab; I performed data analysis and prepared figures. I assisted with transfections for Figure 23 and Min Ku Kang performed RNA extraction and RT-qPCR; I performed data analysis and prepared figures. I performed FPLC experiments for Figures 14, 15 & 16 with the assistance of Brian Le from the Spyracopoulos Lab; Brian Le took the NMR spectrum for Figure 15. Brittany Fraser from the Foley Lab contributed the algorithm for high content analysis for Figure 19 and assisted with imaging and contributed the algorithm for high content analysis for Figure 20.

Dedication

To my Mom, Dad, Terri-Ann, and Kailey for getting me here.
To Minou, Oswald, and Tully for keeping me here.

To Adrian, for getting me here, keeping me here, and everywhere we will go together.
I love you.

Tomorrow can be a wonderful age.

-*Walt Disney*

Acknowledgments

When I was in the 4th grade I was asked what I wanted to be when I grew up, I said an archeologist because the bones look cool. In the 5th grade I thought I might own my own business, and by the 8th grade I wanted to be an engineer for NASA; in the 10th grade I took physics and changed my mind. When I graduated high school I thought: Doctor? Grad school never made the list. Growing up we would travel to Vancouver Island and visit my Dad's Ph.D. supervisor, Fred. My Dad would take me and my sisters out into the forest and show us where he would pitch his tent in the summer in search of Blue Grouse with his dog Puddles. Camping with your dog in B.C. made research seem pretty awesome. I've been lucky to have teachers who have ensured that science has lived up to the "awesomeness" I had in my head. I had a great Biology teacher in high school, Mr. Case, who made me realize how much I love genetics. George Owttrim took me on as a 499 student even though I nearly failed his class. I look back on the work we accomplished together and see the kind of scientist I hope to become. When I finally finished my bachelor's degree I had no clue what to do with it other than keep going to school. I remember telling my Dad that I thought I'd go to grad school, and he asked me why. I honestly hadn't thought very hard about it. I figured I like science, and maybe I'd get a better job. My Dad told me something that has stuck with me all through grad school, and I come back to it when things seem particularly grim. He said more school won't necessarily mean a better job, and I should only do it if I love it. Research can be demanding, you need to love it. Everyone one tells you grad school is hard, but you assume they're exaggerating, you assume the tetchy grad students are just jaded, that it will be different for you. Grad school is hard; I can see now why you have to love it.

I am incredibly proud of the work and relationships I have built the past three years. None of it would have been possible without the support of my committee members, and everyone in the Department of Medical Genetics. Thank you, David, and the Eisenstat Lab, for being an unwavering champion of this project and supporter of all my endeavors both experimental and professional. Edan, I can't express my gratitude for all the encouragement and help you have provided throughout this project. Thank you for your guidance for my Ph.D. applications, and for being an amazing mentor to me. You are a role model as a scientist and a supervisor. Thank you to the entire Foley Lab for making me so welcome and providing an inspiring intellectual environment to grow in. You have all made me a better scientist. Oana, thank you so much for taking me on as a graduate student and giving me the independence to be a driving force in this project. I'm so grateful for the trust you have put in me. Thank you for your unconditional support of all my goals and for always being there to remind me I can do anything I set my mind to. You have always made me feel my opportunities were boundless. Thank you to Min for all the amazing work you have contributed to this project, it's been so nice to have another person in our TRAF6 world to share ideas with and keep moving forward. I'm so proud of what we have all accomplished together. Finally, thank you Mike and Sarah for making sure this wasn't the hill I died on.

Three years later I still love science. It was made easier to love by the friends I made along the way. Kim, Nicole, Tim, Lance, Vanessa, and Jamie. Kim, thank you for always having a fun plan to get me out of the lab; an escape room or board game café, but usually something to do with food. For being an expert in all things food, new places to eat and exotic fruit, and how to get it all without leaving the house. Nicole, I'm glad I've found someone who shares my unsettling obsession with cats and being able to unapologetically gush over how adorable they are. Thank

you for always making sure I take care of myself, mostly going to the gym and eating enough fatty potatoes, but so much more. Tim, thank you for being the ultimate lab Dad, for advice on controls and your perfectly organized spreadsheets. Thank you for helping me realize how much I love board games and what a total nerd I really am. I'm lucky to have you and Stacey making sure I eat more than McDonalds and chips when Adrian is away. Adrian is grateful too. I can't imagine my degree or my life without Lance. You're always there for me for anything at a moment's notice. Thank you for taking a whole morning to help me analyze qPCR data before I was supposed to be on a flight to Germany and reassuring me that I was (am) not actually a total dummy. Thank you for being such a true and dependable friend to me and Adrian; I can't think of anyone more suited to be Best Man, finally. You know I could go on, but let's keep this thesis respectable. BASALSTATE! Vanessa, you are the sweetest soul I know. I remember when I realized we were going to be friends: Chez Pierre and dancing till our legs hurt. Now it's red wine and a movie at home, picking dresses, flower arrangements and carpets for the wedding. I don't know what I'd do without you. Early in my degree, but not soon enough I found a best friend in Jamie. Thank you for taking me under your wing in the lab, at the gym, and in life. You are the true embodiment of charisma, uniqueness, nerve, and talent. I never thought I'd enjoy being stuck at the lab late but hanging around with you, listening to Disney sing-a-longs and waiting for the exodus of bros from the gym was worth it. You are an incredible scientist and from your help I hope one day some grad student might say the same about me. Seeing you graduate was inspiring and saddening; I've always been terrible at staying in touch, but I'm glad we've made it work. Thank you for the time we spent together in Winnipeg; I'm looking forward to going back. I hope you and Marino have already booked your trip to Dresden. The couch is always yours.

Thank you to my family for always being supportive of my goals, no matter how unlikely they seem. I would not be where I am today or had the courage to apply for a Ph.D. at MPI without you. Thank you, Dad, for sharing your experience as a grad student with me and helping me approach school with the right mindset of curiosity and discovery. This perspective helped get me through when things seemed most challenging. Mom, thank you for always believing in me, even when I was failing a class back in third year; I'm glad you talked me out of dropping it or things would be very different now. Terri-Ann and Kailey, you have always been my best friends, and I'm glad I have someone reminding me not to take myself too seriously; you guys keep me humble. I'm grateful for how close we have all always been and the memories we share together: trips to Disneyland and the East Coast, movie nights, and just spending time in the yard as a family. It is reassuring to know that no matter where my life takes me I will always have your love and support, and we will remain close as ever. I love you all.

Adrian, there isn't enough time or words in the world to thank you for everything you do for me, but I'll try my best. Thank you for going on this journey with me and being endlessly supportive of all my unlikely dreams and sharing that crazed ambition with me. Thank you for seeing strength in me even when I am to grouchy and gloomy to see it myself. You make me a better scientist and I know I wouldn't have been able to accomplish any of this without you by my side. You inspire me to achieve all my goals and with you I feel like everything is possible, no matter how farfetched it seems. Thank you for loving me. I can't wait to marry you in September. I love you deeply.

I'm still not sure what I want to be when I grow up, but I suppose I'm on track to become a doctor of sorts. I'm excited to see what the future holds.

Table of Contents

List of Tables

List of Figures

List of Abbreviations

ADA	Adenosine Deaminase Deficiency
ANOVA	Analysis Of Variance
ATP	Adenosine Triphosphate
BCL10	B-Cell Lymphoma/leukemia 10
BCR	B Cell Receptor
BMT	Bone Marrow Transplant
BSA	Bovine Serum Albumin
C90F	Cysteine 90 Phenylalanine
CC	Coiled-Coil
CD40	Cluster of Differentiation 40
CD40L	Cluster of Differentiation 40 Ligand
CHUK	Conserved Helix-loop-helix Ubiquitous kinase K
CHX	Cycloheximide
CLDN16	Claudin 16
COQ2	Coenzyme Q10
CRISPR	Clustered Regularly Interspersed Short Palindromic Repeats
D_2O	Deuterium Oxide
dk	Donkey
DMEM	Dulbecco's Modified Eagle Medium
DPBS	Dulbecco's Phosphate Buffered Saline
dsRNA	Double Stranded RNA
EBV	Epstein Barr Virus
ED	Ectodermal Dysplasia
EDA	Ectodysplasin
EDAR	Ectodysplasin Receptor
EDARADD	Ectodysplasin Receptor Associated Death Domain
ELISA	Enzyme Linked Immunosorbent Assay
F360fs	Phenylalanine 360 Frame Shift
FBS	Fetal Bovine Serum
FPLC	Fast Protein Liquid Chromatography
GARD	Genetic And Rare Diseases
GBS	Group B Streptococcus
GMNC	Geminin Coiled-coil domain containing
GST	Glutathione-S-Transferase
GUSB	Glucaronidase beta
GVGD	Grantham Variation Grantham Deviation
HDR	Homology Directed Repair
hg19	Human Genome build 19
HSQC	Heteronuclear Single Quantum Correlation

HZM	Homozygosity Mapping
IκB	Inhibitor of Kappa B
IKBKB	Inhibitor of Kappa B Kinase Beta
IKBKG	Inhibitor of Kappa B Kinase Gamma
IKK	Inhibitor of Kappa B Kinase
IL-1	Interleukin-1
IL-1β	Interleukin-1 Beta
IL-1R	Interleukin-1 Receptor
IL-8	Interleukin-8
indel	Insertion/Deletion
INF-γ	Interferon-gamma
IP	Incontentia Pigmenti
IRAK	Interleukin-1 Receptor Associated Kinase
K48	Lysine 48
K63	Lysine 63
LCL	Lymphoblastoid Cell Line
LMP-1	Latent Membrane Protein 1
LOH	Loss Of Heterozygosity
LPS	Lipopolysaccharide
LZ	Leucine Zipper
MAMP	Microbe Associated Molecular Pattern
MHC	Major Histocompatibility Complex
ms	Mouse
MWCO	Molecular Weight Cut Off
MYD88	Myeloid Differentiation Primary Response 88
NAD+	Nicotinamide Adenine Dinucleotide +
NADH	Nicotinamide Adenine Dinucleotide + Hydrogen
ncRNA	Non-Coding RNA
NEMO	Nuclear factor kappa B Essential Modulator
NF-κB	Nuclear Factor Kappa B
NFKBIA	Nuclear Factor Kappa B Inhibitor Alpha
NGS	Next Generation Sequencing
NHDF	Normal Human Dermal Fibroblasts
NHEJ	Non-Homologous End-Joining
NK	Natural Killer
NMD	Nonsense Mediated Decay
NMR	Nuclear Magnetic Resonance
OLEDAID	Osteopetrosis and/or Lymphedema with Ectodermal Dysplasia and Immunodeficiency
OPG	Osteoprotegrin
PBS	Phosphate Buffered Saline

PBS-T	Phosphate Buffered Saline-Tween
PFA	Paraformaldehyde
PNP	Purine Nucleoside Phosphorylase
PRR	Pathogen Recognition Receptor
PTC	Premature Termination Codon\
RAG1	Recombination Activating Gene 1
RAG2	Recombination Activating Gene 2
RANK	Receptor Activator of Nuclear Factor Kappa B
RANKL	Receptor Activator of Nuclear Factor Kappa B Ligand
rb	Rabbit
RING	Really Interesting New Gene
RPM	Rotations Per Minute
RPMI	Roswell Park Memorial Institute
RT-qPCR	Reverse Transcriptase Quantitative Polymerase Chain Reaction
SCID	Severe Combined Immunodeficiency
SDS-PAGE	Sodium Dodecyl Sulfate Polyacrylamide Gel Electrophoresis
SIFT	Sorting Intolerant From Tolerant
SNP	Single Nucleotide Polymorphism
SNV	Single Nucleotide Variant
TAB2	TGF-beta Activated Kinase 1/MAP3K7 Binding protein 2
TAGC	The Applied Genomics Core
TAK1	TGF-beta Activated Kinase 1
TBS	Tris Buffered Saline
TCAG	The Centre for Applied Genomics
TCR	T Cell Receptor
TLR	Toll-Like Receptor
TLR4	Toll-Like Receptor 4
TNF	Tumor Necrosis Factor
TNF-α	Tumor Necrosis Factor Alpha
TNFAIP3	Tumor Necrosis Factor Alpha Induced Protein 3
TNFR	Tumor Necrosis Factor Receptor
TNFRSF11A	Tumor Necrosis Factor Receptor Superfamily member 11a
TNFRSF11B	Tumor Necrosis Factor Receptor Superfamily member 11b
TRADD	Tumor Necrosis Factor Receptor Associated Death Domain
TRAF	Tumor Necrosis Factor Receptor Associated Factor
UBC13	Ubiquitin-conjugating enzyme E2 N
UCLA	University of California Los Angeles
UCSC	University of California Santa Cruz
UEV1A	Ubiquitin-conjugating enzyme E2 variant 1
UMKC	University of Missouri Kansas City
UPS	Ubiquitin Proteasome System

VUS..... Variant of Unknown Significance
WES ..... Whole Exome Sequencing
WGS..... Whole Genome Sequencing
WT..... Wild-Type
ZF ..... Zinc Finger

Chapter One:

Diseases and Molecular Biology of the Human Immune System

1.1 The Human Immune System

Human immune defenses consist of physical barriers to prevent infection, and the innate immune and adaptive immune systems to respond to infection (Figure 1a). Barrier tissues, such as skin, epithelial linings, and mucous secretions, exist as a physical structure to protect organisms from environmental threats. Sweat and sebaceous secretions from the skin create an inhospitable environment for many pathogens, and mucous membranes help to remove invading materials.[1] In the interest of maintaining organismal homeostasis it is preferable to prevent, rather than respond to an infection. However, the human body is constantly faced with external threats, and infection cannot always be avoided. The innate and adaptive immune responses are responsible for recognizing and eliminating infectious microbes that have invaded barrier tissues.[2] It is important that immune responses occur efficiently and proportionally to the threat, such that there is a balance of eliminating pathogens while avoiding self-damage that can lead to conditions such as infections, allergy, and autoimmunity.[3] These risks associated with a protracted immune response highlight the importance of barrier tissues, and tight regulation of the immune system is essential to maintain organismal homeostasis.

The *innate immune system* provides the next line of defense should physical barriers be breached. Recognition of microbe associated molecular patterns (MAMPs), conserved characteristics of infectious agents, by host pathogen recognition receptors (PRRs) triggers a swift and broad range of cell-mediated immune responses.[4] Toll-like Receptors (TLRs) are a family of PRRs expressed on macrophages. For example, TLR-4 binds to lipopolysaccharide (LPS), which is a major component of the cell wall in gram-negative bacteria (Figure 1b).[5] The innate immune system may respond to invading microbes by the secretion of bactericidal proteins such as lysozyme which breaks up bacterial cell walls,[6] and complement proteins which are involved in

inflammation, cell lysis, and phagocytosis.[1] Lysozyme is expressed by both macrophages and neutrophils; the two major cells of the innate immune system.[7] All cells of the immune system (leukocytes or white blood cells) are produced in the bone marrow as pluripotent hematopoietic stem cells, which then divide into a common myeloid or lymphoid progenitor. The common myeloid progenitors produce the cells of the innate immune system including: mast cells, eosinophils, neutrophils and monocytes.[8] Neutrophils circulate in the blood and represent the first line of defense of the innate immune system;[9] under non-infectious conditions they are unable to permeate tissues due to the number of destructive enzymes contained within their cytoplasm.[1] Macrophages are produced from monocyte precursors which circulate in the blood before arriving at their destination tissue and differentiating into a resident macrophage, such as microglial cells in the brain, alveolar cells in the lungs, or osteoclasts in the bone.[8,10] Macrophages can detect invading pathogens and become activated when the PRR on its surface encounters a pathogen; the cell is now able to engulf invading microbes more effectively and begins secreting cytokines and chemokines to amplify the immune response. Secretions from macrophages initiate the inflammatory response to a breach of barrier tissues, which includes swelling, capillary dilation (redness), pain, and heat. These secretions also recruit other cells of the immune system, and the dilation and increased permeability of endothelial tissues allows cells to infiltrate the site of infection. Activated macrophages secrete chemokines such as interleukin-8 (IL-8) which attract additional neutrophils to the site of infection. The cytokines Tumor Necrosis Factor-alpha (TNF-α) and Interleukin 1-beta (IL-1β) are also secreted by macrophages and allow neutrophils to adhere to tissue at the site of infection where they can release their destructive enzymes or engulf the assaulting pathogen (Figure 1b).[1]

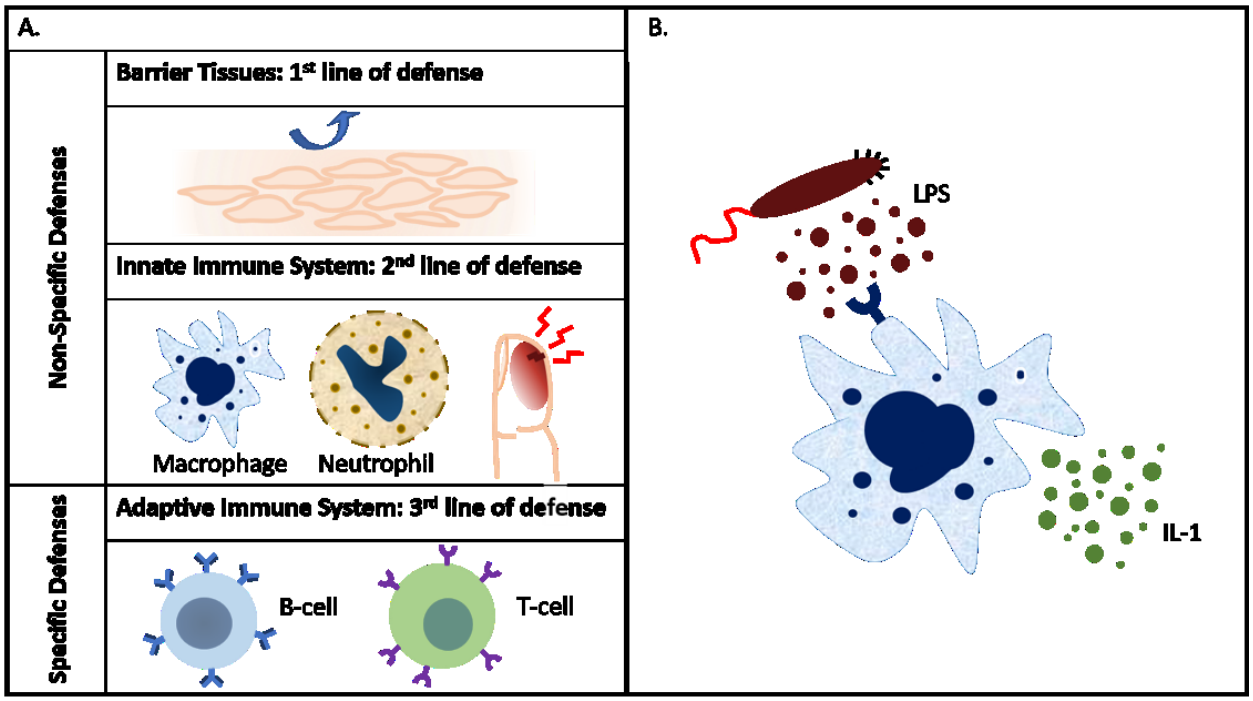

Figure 1. The Human Immune System. A. The human immune system consists of barrier tissues to prevent infection, the innate immune response which rapidly detects and responds to many types of pathogens, and the adaptive immune response which provides a response to the specific invading pathogen but takes time to activate. B. Macrophages are an important cell of the innate immune system for detecting pathogens and initiating an immune response. Toll-like Receptors (TLRs) on the macrophage surface detect lipopolysaccharide (LPS) in the bacterial cell wall which prompts the secretion of cytokines (such as IL-1) to amplify the immune response and activate the adaptive immune system.

Common lymphoid progenitors give rise to the cells of the *adaptive immune system*: T- and B-lymphocytes, and Natural Killer (NK) cells.[11] NK cells are derived from the lymphoid cell lineage but play a significant role in the innate immune response.[1] Macrophages and neutrophils are excellent at responding to infectious threats in the extracellular space but are ill-equipped to sense and react to pathogens such as viruses that have managed to infiltrate intracellular regions.[1] Infecting viruses will often attempt to evade the immune system by interfering with the major histocompatibility complex (MHC), which is present on all cells of the human body and help the immune system recognize self from non-self.[12] NK cells protect the host by recognizing cells that are expressing abnormal MHC proteins.[13] The human body is able to mount a quick response to numerous pathogens through the constant presence of neutrophils in the blood, and the rapid recruitment of additional immune cells by macrophages to the site of infection. However, microbes evolve rapidly, which presents a challenge for the invariant innate immune system. The adaptive immune system provides the perfect complement: a delayed but specifically tailored response to the pathogen in question. Cells of the adaptive immune system can rearrange their cell surface receptors such that they can target the infecting agent with a much more specific response than the innate immune system.[2] However, this plasticity can make cells of the adaptive immune system less adept at recognizing self from non-self; these rearrangements can produce receptors that recognize host characteristics, which can manifest as allergies or autoimmune disease.[1] However, these reactions are rare as self-recognizing immune cells are generally identified and eliminated by negative selection during development.[14] A critical aspect of the adaptive immune system is immunological memory, which allows for an immune response that is both rapid and specific to a pathogen that has been encountered before.

1.2 Diseases of the Immune System: Severe Combined Immunodeficiency

Severe combined immunodeficiencies (SCID) represent a heterogenous group of inherited disorders that cause impairment of the immune system resulting in the absence or dysfunction of T and B cells that are important for maintaining both innate and adaptive immunity.[15] SCID is a rare disorder with an incidence of 1 in 100,000, although a more recent epidemiological study detected a much higher incidence of 1 in 58,000 live-births, and in over 15% of cases the genetic cause was unknown.[15,16] Prompt diagnosis is critical for this condition as it is generally fatal in the first two years of life if the appropriate treatment to restore the immune system is not administered. Some patients can be cured by hematopoietic stem cell transplantation.[15] A number of patients receive a clinical diagnosis of SCID but the underlying molecular defect remains elusive. Therefore, the genetic study of these individuals is essential if we are to advance our understanding of this condition and provide the best care to these patients and their families.

SCID has considerable variability in immunological phenotype, and can be classified according to the major pathway(s) that the molecular defect is disrupting (when known), or the specific leukocyte abnormalities related to a given mutation.[17] The latter method was generally considered sufficient to describe the various presentations of SCID; however, as molecular knowledge of the condition has increased, and specific genetic defects are being associated with atypical symptoms, this classification system is losing its utility.[15] SCID can be divided into different syndromes; this classification includes a unique collection of symptoms associated with a given syndrome along with a causative genetic mutation if identified. For example, Omenn Syndrome (MIM 603554) is a form of SCID that can be identified by a characteristic skin rash that can lead to loss of the hair and eyebrows, in addition to opportunistic infections.[18] Atypical SCID represents another variation that is characterized by recurrent infections; although this form

generally presents after the first year of life.[17] This heterogeneity is a significant feature of SCID as it can often impede a timely diagnosis with life-threatening consequences. In addition to a diversity of symptoms SCID is also not characterized by a single mode of inheritance, with both X-linked and autosomal inheritance patterns observed. Additionally, SCID is no longer considered to be restricted to recessive inheritance, as dominant gain-of-function mutations have been identified.[19] Patients with SCID are generally normal at birth and present in the first few months of life with persistent respiratory and gastrointestinal infections that fail to clear; and general failure to thrive throughout the first year of life.[17] The initial transfer of maternal antibodies at birth allows infants with SCID to fight early infections; however, as these antibodies decline they become predisposed to severe bacterial, viral and fungal infections. Indeed, oral candidiasis is a common finding among SCID infants.[15] When examining an infant presenting with symptoms of SCID it is important to consider a family of complicated infections or unexplained infant deaths, and parental consanguinity as these provide additional clues to diagnose this heritable condition.[17]

SCID can be limited to the immune system or can include symptoms involving other tissues such as ectodermal structures: hair, teeth, nails, and sweat glands, and this association is delineated as ectodermal dysplasia with immunodeficiency (MIM 300291).[20] In the vast majority of cases this is an X-linked recessive condition due to hypomorphic mutations to the coding region of the Inhibitor of nuclear factor Kappa B Kinase subunit Gamma (*IKBKG*) gene; whereas, complete amorphic mutations to *IKBKG* result in a condition called Incontinentia Pigmenti (IP MIM 308300).[21] Loss-of-function mutations result in embryonic lethality in males and the phenotype experienced by females generally does not include immunodeficiency.[22] Hypomorphic mutations to *IKBKG* can also cause a more severe allelic disorder: osteopetrosis and/or lymphoedema with ectodermal dysplasia and immunodeficiency (OLEDAID Syndrome MIM 300301), which is

caused by mutations that induce premature stop codons.[22] *IKBKG* encodes the Nuclear Factor kappa B (NF-κB) essential modulator (NEMO) protein, which is required for activation of the NF-κB pathway. Mutations in *IKBKG* result in a wide variety of phenotypes; some without immune deficiency, and complex disorders such as OLEDAID. Many different mutations to *IKBKG* have been documented, and it is this mutational diversity that results in the clinical heterogeneity observed in this condition (Table 1). In a few reported cases an autosomal dominant form of ectodermal dysplasia with immunodeficiency has been caused by hypermorphic mutations to the NF-κB Inhibitor Alpha (*NFKBIA*) gene, which encodes another protein critical for NF-κB signalling.[23]

1.3 NF-κB Signaling

NF-κB signaling is an important mechanism controlling gene expression required for regulating immunity, stress responses, apoptosis and differentiation.[24] NF-κB represents a family of transcription factors that is composed of two subfamilies: the NF-κB proteins, which is composed of the proteins p105/p50, p100/p52; and the Rel proteins, which consist of RelA (aka p65), RelB, C-Rel.[25] These two subfamilies come together to form protein dimers that activate gene expression in response to a multitude of stimuli.[24,25] NF-κB signaling can be divided into the canonical and non-canonical pathways. The canonical pathway is comprised of p105/p50 and RelA, RelB, and C-Rel and is induced by many physiological stimuli; whereas, the non-canonical pathway is composed of p100/p52 and RelB and is activated by select members of the TNF superfamily of cytokines.[24] Prior to nuclear translocation of NF-κB these pathways share a common upstream mechanism: activation of the inhibitory of κB (IκB) kinase (IKK) complex.[25] The IKK complex is composed of NEMO along with two additional proteins IKKα and IKKβ, and

is activated through the post-translational modification of these proteins. The non-canonical pathway relies primarily on the IKKα induced phosphorylation of p100 and RelB heterodimers; after phosphorylation p100 is processed to the shorter p52 subunit and the heterodimer can enter the nucleus and activate gene transcription.[25] The analysis presented in this work focuses exclusively on the canonical NF-κB pathway. NEMO and IKKβ are the main signaling molecules of the canonical pathway and result primarily in phosphorylation of IκB-α and the subsequent nuclear translocation of RelA containing NF-κB dimers.[24] In canonical signaling activation of the IKK complex requires the K63-linked polyubiquitination of NEMO and the phosphorylation of IKKα and IKKβ, this activated complex is now capable of phosphorylating IκB and targeting it for degradation by the ubiquitin proteasome system (UPS).[26] Both ubiquitination of NEMO and phosphorylation of IKKα and IKKβ is required for activity of the IKK complex, yet neither modification alone is sufficient. Negative regulation of canonical NF-κB signaling is accomplished by IκB proteins, which sequester the NF-κB dimer in the cytoplasm to repress transcription of target genes (Figure 1). As there are multiple NF-κB proteins there are also multiple IκB proteins, which have differing affinities for the various NF-κB dimers. NF-κB signaling is activated by a complex cascade of events that ultimately results in the degradation of IκB allowing for nuclear translocation of the NF-κB transcription factor.[25] Classic inducers of the canonical NF-κB pathway include: TNF-α, interleukin-1, lipopolysaccharide, and double stranded RNA (dsRNA). Given the essential role of NEMO in IKK complex activation it has been suggested that anything that impairs its function will also impair the function of the entire complex.[26] NEMO is predicted to be comprised primarily of extended α-helices and three coiled-coil domains: CC1-3, a leucine-zipper (LZ) motif, and a c-terminal zinc finger (ZF). The ZF seems to be required for the binding of K63-linked polyubiquitin, and mutation of this domain has been shown to cause ectodermal dysplasia

with immunodeficiency.[26] The binding of Lysine 63 (K63) linked polyubiquitin to NEMO is the first step in IKK complex activation and this post-translational modification is believed to serve as a binding site for additional signaling molecules that are required for the activation of IKKβ. E3 ubiquitin ligases are required for protein tagging with ubiquitin, and NEMO has multiple E3 ligases for the numerous pathways that function through NEMO.[27]

Our understanding of NF-κB signaling comes primarily from immunology studies, since in many instances the transcription factor mediating both innate and adaptive immune responses is NF-κB. This function of NF-κB as an immune regulatory is highly conserved from mammals to *Drosophila melanogaster*. NF-κB plays critical roles in numerous immunological processes such as hematopoiesis, which produces B cells, T cells, NK cells, dendritic cells, monocytes, macrophages, basophils, eosinophils, neutrophils and mast cells. These cells represent the major players of both the innate and adaptive immune response.[28] The NF-κB pathway can be activated by multiple immune receptors, including the cytokine receptors IL-1 and tumor necrosis factor (TNF) receptor (TNFR) superfamily, and the TLR4 PRR.[24] NF-κB signaling through these different receptors converges on activation of the IKK complex, upstream of the IKK complex signaling through individual receptors is mediated through specific cytoplasmic proteins.[24,25] Canonical NF-κB signaling can be activated by the binding of LPS to TLR4 on the surface of macrophages, and results in recruitment of the myeloid differentiation primary response 88 (MYD88) protein which contains an N-terminal death domain for interacting with the interleukin-1 receptor associated kinase (IRAK) family of proteins. IRAK also binds tumor necrosis factor receptor associated factor (TRAF) 6 to activate the IKK complex.[29–31] IL-1 and TNF-α are secreted by macrophages after engagement of PRRs, and can activate NF-κB signaling in innate immune cells and fibroblasts to amplify the immune response through the induction of additional cytokines

which recruit and activate other cells of the immune system.[29] IL-1 secreted by macrophages can also activate the NF-κB pathway by binding to the IL-1 receptor (IL-1R); similar to TLR4 signaling this process also requires MYD88 and IRAK proteins together with TRAF6.[30,31] The TNFR superfamily of proteins can induce both canonical and non-canonical NF-κB activation; for example, activation of canonical signaling through TNFR1, and non-canonical signaling through the cluster of differentiation 40 (CD40) receptor have been extensively studied.[29,32] Canonical NF-κB signaling is activated through the TNFR1 receptor by the cytokine TNF-α, and requires the additional proteins TNFR1 associated death domain (TRADD) and tumor necrosis factor receptor associated factor (TRAF) 2 and TRAF5 resulting in IKK complex activation.[24,32] Mutations in different members of the NF-κB pathway cause its impairment and lead to a group of rare congenital disorders of significant morbidity, including SCID (Table 1).[20,22,41–46,33–40] This heterogenous group of inherited disorders causes impairment of the immune system resulting in the absence or dysfunction of T and B cells that are important for maintaining both innate and adaptive immunity.[15] Patients with mutations in the *IKBKG* gene, which encodes the NEMO protein, have a complex phenotype characterized by immune, ectodermal, and osseous abnormalities.[20] Mutations in the interacting gene *IKBKB* have been documented as a cause of SCID in the Cree population;[36] this gene encodes the IKK-β protein which interacts with NEMO and IKK-α to form the IKK complex.[25]

The NF-κB pathway does not just regulate the immune system; it also regulates other developmental processes such as bone growth and remodeling, and the development of the structures arising from the ectoderm. Ectodysplasin (EDA) signaling regulates ectodermal development through the binding of EDA to the ectodysplasin receptor (EDAR) to activate the transcription of NF-κB target genes. This process requires the receptor adapter EDAR Associated

Death Domain (EDARADD), which binds to the cytoplasmic component of EDAR. The EDARADD death domain is homologous to that of MYD88, the protein which mediates NF-κB signaling through the Toll/IL-1 receptors, and also interacts with TRAF6 and the TGF-Beta Activated Kinase 1 (TAK1)/TGF-Beta Activated Kinase 1/MAP3K7 Binding Protein 2 (TAB2) complex similar to Toll/IL-1 signaling.[47] Mutations in EDA, EDAR, and the receptor adapter EDAR Associated Death Domain (EDARADD) are known causes of human ectodermal dysplasia (Table 1).[22,48–50] Bone development and homeostasis process involves the breakdown and rebuilding of bone tissue by osteoclasts and osteoblasts respectively.[51,52] The receptor activator of nuclear factor kappa-B ligand (RANKL)-receptor activator of nuclear factor kappa-B (RANK)-osteoprotegrin (OPG) system regulates the development and function of osteoclasts to mediate bone development.[53,54] RANK is a member of the TNFR superfamily, and stimulation by RANKL activates NF-κB signaling to drive differentiation of monocytes into osteoclasts.[55,56] This process is also mediated by TRAF6, TAK1, and TAB1/TAB2, which form a complex with the RANK receptor.[57] Mutations in RANK, RANKL, and OPG have been documented as causes of human bone disease (Table 1).[58–62]

This thesis presents the work to characterize the molecular basis of a new SCID in a family of Cree descent for which we propose the pathogenic cause is a recessive mutation in a gene that belongs to the NF-κB pathway.

Gene	Protein	Disease	MIM (Phenotype)	Inheritance	Location	Reference
IKBKG	NEMO	Incontentia Pigmenti	300308	X-linked		Smahi et al., 2002
IKBKG	NEMO	OLEDAID Syndrome	300301	X-linked		Doffinger et al., 2001
IKBKG	NEMO	Isolated Immunodeficiency	300584	X-linked	Xq28	Orange et al. 2004
IKBKG	NEMO	Immunodeficiency + ED	300291	X-linked		Zonana et al., 2000
IKBKG	NEMO	Immunodeficiency 33	300636	X-linked		Filipe-Santos et al., 2006
IKBKB	IKK-β	Immunodeficiency	615592	Autosomal Recessive	8p11.2	Pannicke et al., 2013
CHUK	IKK-α	Cocoon Syndrome	613630	Autosomal Recessive	10q4.3	Lahtela et al., 2010
NFKBIA	IκB-α	Immunodeficiency + ED	612132	Autosomal Dominant	14q13.2	Courtois et al., 2003
TAK1	TAK1	Frontometaphyseal Dysplasia 2	617137	Autosomal Dominant	6q15	Wade et al., 2016
TAK1	TAK1	Cardiospondylocarpofacial Syndrome	157800	Autosomal Dominant		Le Goff et al., 2016
TAB2	TAB2	Cardiac Defects	614980	Autosomal Dominant	6q25.1	Thienpont et al., 2010
IRAK4	IRAK4	IRAK-4 Deficiency	607676	Autosomal Recessive	12q12	Picard et al., 2003; Medvedev et al., 2003
IRAK4	IRAK4	Invasive Pneumococcal Disease	610799	Autosomal Recessive		Ku et al., 2007
MyD88	MYD88	Recurrent pyogenic bacterial infections	612260	Autosomal Recessive	3p2.2	Von Bernuth et al., 2008
MyD88	MYD88	Waldenstrom Macroglobulinemia	153600	Autosomal Dominant		Treon et al., 2012
EDA	EDA	Hypohidrotic Ectodermal Dysplasia	305100	X-linked	Xq13.1	Smahi et al., 2002
EDA	EDA	Selective tooth agenesis	313500	X-linked		Tao et al., 2006
EDAR	EDAR	Hypohidrotic Ectodermal Dysplasia	224900	Autosomal Recessive	2q13	Smahi et al., 2002
EDAR	EDAR	Hypohidrotic Ectodermal Dysplasia	129490	Autosomal Dominant		Monreal et al., 1999
EDARADD	EDARADD	Hypohidrotic Ectodermal Dysplasia	614941	Autosomal Recessive	1q42-q43	Smahi et al., 2002
	EDARADD	Hypohidrotic Ectodermal Dysplasia	614940	Autosomal Dominant		Bal et al., 2007
TNFRSF11A	RANK	Familial Expansile Osteolysis	174810	Autosomal Dominant		Hughes et al., 2000; Johnson-Pais et al., 2003
TNFRSF11A	RANK	Osteopetrosis	612301	Autosomal Recessive	18q21.3	Guerrini et al., 2008
TNFRSF11A	RANK	Paget Disease of Bone	602080	Autosomal Dominant		Hughes et al., 2000
TNFSF11	RANKL	Osteopetrosis	259710	Autosomal Recessive	13q14.1	Sobacchi et al., 2007
TNFRSF11B	OPG	Paget Disease of Bone	239000	Autosomal Recessive	8q24.1	Whyte et al., 2002
TNFAIP3	A20	Familial Behcet-like Autoinflammatory Syndrome	616744	Autosomal Dominant	6q23.3	Zhou et al., 2016

Table 1. Genes in the NF-κB pathway that cause associated with human phenotypes.

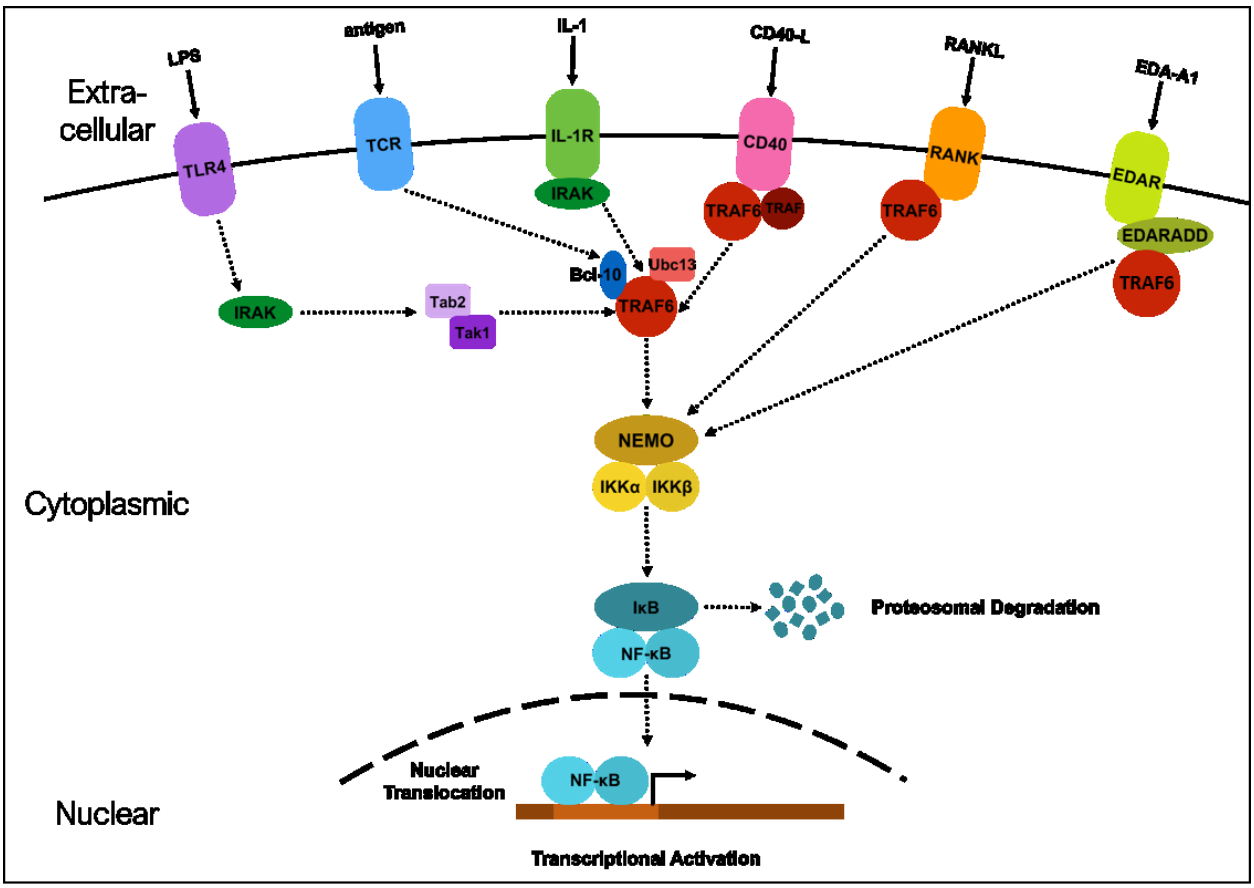

Figure 2. The NF-κB Signalling Pathway. Many receptors exert their function through the NF-κB pathway, including the Toll-like Receptor (TLR), T-cell Receptor (TCR), Interleukin-1 Receptor (IL-R1), Cluster of Differentiation-40 Receptor (CD40), Receptor Activator of Nuclear Factor kappa B receptor (RANK), and Ectodysplasian A receptor (EDAR). Signals from these receptors are mediated by different cytoplasmic protein complexes but ultimately all signals converge at the IκB kinase (IKK) complex, which includes NEMO, IKK-α, and IKK-β. The activated IKK complex is competent to phosphorylate the Inhibitory kappa B (IκB) complex for proteasomal degradation, which reveals the nuclear localization signal of the NF-κB dimer allowing for nuclear translocation and target gene transcription.

Chapter Two:

Identification of a candidate gene for an undiagnosed immunodeficiency in a family of Cree descent

2.1 **Rare disorders and their impact in medicine**

Rare diseases, while individually uncommon, jointly represent a considerable health challenge. Over 7000 rare diseases are documented by the Genetic and Rare Disease (GARD) Information Centre and coming to a correct diagnosis can become a serious barrier to patient care.[63] As many as 80,000 Albertans are affected by rare diseases and with the greatest prevalence in children such diseases dramatically impact the lives of both those suffering and the families caring for them. Next-generation sequencing (NGS) approaches have provided a powerful tool to practitioners faced with a difficult to diagnose disorder.[64] Whole-genome sequencing (WGS) allows for the analysis of the entire human genome within a single experiment, but still represents a tremendous challenge in analysis and interpretation. Whole-exome sequencing (WES) restricts the sequencing analysis to only the coding exons of the genome and makes evaluation much less difficult. Coding regions only make up 1-2% of the genome but harbor as much as 85% of pathogenic mutations; making WES a much more economical option.[65,66] Clinical WES has differing levels of success but generally provides a diagnostic rate of 25-30%, with different phenotypes having varying success rates.[67] WES is useful for detecting single-nucleotide variants (SNVs) and small insertions or deletions (indels) but is limited in its ability to ascertain larger indels and incapable of detecting trinucleotide repeats. WES also has uneven coverage of the exome, with only 90-95% of genes having a depth of coverage sufficient to make an accurate variant call.[63] Additionally, WES data interpretation is based on a statistical analysis for mapping reads, and large gene families or the presence of pseudo genes can affect the accuracy of the interpretation. A concern regarding the use of NGS for patient care is the frequency with which variants of uncertain significance (VUS) are found. VUS present challenges for clinicians, as they are generally not helpful in modulating patient care.[68] However, as this technology grows the

significance of these variants may become clearer; from an analysis perspective it is as helpful to know which variants are polymorphisms as it is to know which are pathogenic. Awareness of these advantages and limitations of WES are critical for its appropriate use in patient care. Since Ng *et al*. in 2010 demonstrated the use of WES to identify the cause of a Mendelian disorder, hundreds of human phenotypes have been characterized each year.[64,69] Single families with unique phenotypes present a challenge in identifying a definitive molecular cause of their disorder, as multiple families are generally required to provide strong evidence of genetic causation. In the cases of individual families, functional studies are necessary to understand the underlying mechanism and significance of the variant in terms of pathogenicity. This study is a translational research project that identifies a novel genetic cause for a new human disorder. It begins with defining the clinical phenotype and uses a multi-level approach to identify a candidate gene. The functional consequences of the identified genetic variant on a signaling pathway are determined using a patient derived cell lines.

2.2 Materials & Methods

Study Family

This project examines a consanguineous family of Cree descent who has had 2 children affected with a severe, congenital immunodeficiency.

Homozygosity Mapping

HZM was derived from raw data obtained following a clinical single nucleotide polymorphism (SNP) array. HZM analysis was performed by Dr. Paulo Nuin, bioinformatician in the Department of Medical Genetics to identify the regions of homozygosity. Homozygous regions were applied to the patient's whole exome sequencing data set to restrict filtering to regions

inherited from a common ancestor.

Whole-Exome Sequencing

WES was performed by Macrogen using the *SureSelect Target Enrichment System Capture Process*.[70] Reads were mapped against University of California at Santa Cruz (UCSC) genome browser human genome build 19 (hg19) (http://genome.ucsc.edu/) by Burrows-Wheeler Aligner (http://bio-bwa.sourceforge.net/); SNVs and Indels were detected by SAMTOOLS (http://samtools.sourceforge.net/) and called against the variant databases dbSNP (https://www.ncbi.nlm.nih.gov/projects/SNP/) and 1000 Genomes (http://www.internationalgenome.org/). HMZ data was applied to patient exome data to isolate regions of interest according a recessive mode of inheritance. Variants within the loss of heterozygosity (LOH) regions obtained by HZM were then filtered to remove SNVs that were documented as common in the dbSNP database, and intergenic/intronic/3'UTR/5'UTR regions. Common SNPs were removed since we hypothesized that the patient had a rare disorder, and non-exonic regions were removed since these variants tend to be less deleterious.[66] Remaining SNVs were then examined by quality score, and low quality SNVs (quality score <150) were retained before applying additional filtering. SNVs were grouped into: synonymous SNVs, non-coding RNA (ncRNA), downstream regions, upstream regions, and exonic regions. Exonic SNVs were sub-grouped into: frameshifts, non-frameshift indels, and non-synonymous SNVs. SNPs were subsequently filtered assuming an autosomal recessive inheritance pattern to remove SNPs that were heterozygous in the affected patient and homozygous in the unaffected parents. Variants in the three individuals were then cross-referenced to identify common variants that were homozygous in the patient and heterozygous in the parents.

In silico Analysis for Predicted Pathogenicity

The software Alamut was used to assess the predicted *in silico* pathogenicity of the candidate genes identified by the whole-exome sequencing trio. Alamut integrates the prediction algorithms of Align GVGD (Grantham Variation Grantham Deviation), SIFT (Sorting Intolerant From Tolerant), MutationTaster, and PolyPhen-2 to give an integrated pathogenicity score particularly applied for missense variants according to 5 classes: 1-certainly not pathogenic, 2-unlikely pathogenic, 3-unknown pathogenicity, 4-likely pathogenic, and 5-definitely pathogenic (Alamut Focus version 1.0 (Interactive Biosoftware, Rouen, France, www.interactive-biosoftware.com).

Align GVGD scores missense mutations by evaluating species sequence conservation and properties of the amino acids when making predictions.[71] Mutations are given a GD score and a GV score; in general if the score is between 5-60 the change is considered conservative, 60-100 is non-conservative, and greater than 100 is a radical change. Based on GD and GV scores mutations are classed on a spectrum from C0, C15, C25, C35, C45, C55, and C65; where C0 changes are the least likely to affect protein function, and C65 are the most likely.[72]

SIFT is a sequence homology-based tool that **s**orts **i**ntolerant **f**rom **t**olerant amino acid substitutions and predicts whether a given substitution in a protein will have a phenotypic effect. SIFT is based on the premise that protein evolution is correlated with protein function. Positions important for function should be conserved, whereas unimportant positions should be diverse (sift.jcvi.org). SIFT gives three kinds of outputs: a SIFT score, a median sequence conservation score, and the number of sequences represented at the position of interest. The SIFT score will range from 0-1, with anything less than 0.05 predicted to be damaging and scores above 0.05 are predicted to be tolerated. Scores approaching 0 or 1 are predicted with greater confidence. Median sequence conservation scores measure the diversity of the sequences used for prediction and range

from 0 to 4.32; scores should fall between 2.75 and 3.5 and a warning will occur if it is greater than 3.25 which indicates the prediction was based on closely related sequences.[73]

Mutation Taster analyzes evolutionary conservation, splice-site changes, loss of protein features, and changes that may affect the amount of RNA produced by integrating information from various databases for analysis. The output will indicate if the change is a polymorphism or predicted to cause disease.[74]

PolyPhen-2 examines numerous sequence and structure-based features of the missense mutation and classifies them qualitatively as benign, possibly damaging, or probably damaging based on pairs of false positive rate thresholds and gives a score of 0-1 where scores closer to 1 are predicted to be more damaging.[75,76]

PCR and Sanger Sequencing

The third exon of *TRAF6* (NM_145803) was amplified by PCR using the forward primer 5'-TGAACTTCTGAAGGGACCCAG-3'and the reverse primer 5'-GAGAGGAGGAGATTCAAGTCAC-3' to yield a 793 base pair product. Econotaq 2x PLUSGreen (Lucigen Cat. No. 30033-1) was used according to manufacturer's instructions with 0.2 μM each primer and 50 ng genomic DNA. DNA was initially denatured at 95°C for 3 minutes, followed by cycling 34x through denaturation at 95°C for 30 seconds, primer annealing at 56°C for 45 seconds, and extensions proceeded at 72°C for 1.5 minutes. After cycling a final extension for 10 mins at 72°C was performed. The PCR product was purified by ExoSAP (ThermoFisher Cat. No. 78201.1.ML) according to the manufacturer's instructions, and the concentration was determined using band intensity quantified against the GeneRuler 100 bp PLUS DNA ladder (ThermoFisher Cat. No. SM0321)) by running samples in a 0.8% agarose gel. 0.5 ng/μL of PCR

amplified DNA was sequenced in both directions by Sanger sequencing at The Applied Genomics Core (TAGC) at the University of Alberta using the above primers at a concentration of 0.3 μM.

2.3 Results

The family under examination is of Cree origin from a consanguineous Northern Alberta community; the parents are second cousins who have had two children with an extremely severe congenital immunodeficiency (Figure 3). The first child (II-2) died at 40 days of life from fulminant pertussis infections, and the second (II-3) has been permanently hospitalized with life-threatening recurrent infections, osteoporosis, and ectodermal dysplasia. Patient II-3 (Figure 4) presented with seizures and difficulty breathing at 2 weeks of age and was admitted to the hospital. Blood work revealed group-B streptococcus (GBS) in blood and cerebrospinal fluid, and the patient was diagnosed with meningitis. GBS is a gram-positive microbe normally found in the human intestinal and genital tracts; it exists as a commensal bacterium of the microbiome and is generally not a cause of invasive infections.[77] While in hospital a skeletal survey showed pathological fractures and abnormal wide metaphysis of the long bones. The patient was treated and released from hospital but continued to experience recurrent infections resulting in her permanent admission to the hospital due to concerns of an underlying immunodeficiency disorder. The patient's severe, life-threatening infections to generally non-pathogenic and pathogenic microbes suggested that the underlying defect was related to the innate immune system and cytokine signaling. As development progressed the patient was found to have a more complex phenotype with features of ectodermal dysplasia (Figure 3b) including a skin rash, alopecia, abnormal nails, an absence/defect of sweat glands, and absent or malformed teeth, in addition to metaphyseal splaying of the long bones and osteoporosis (Figure 3c). The patient underwent

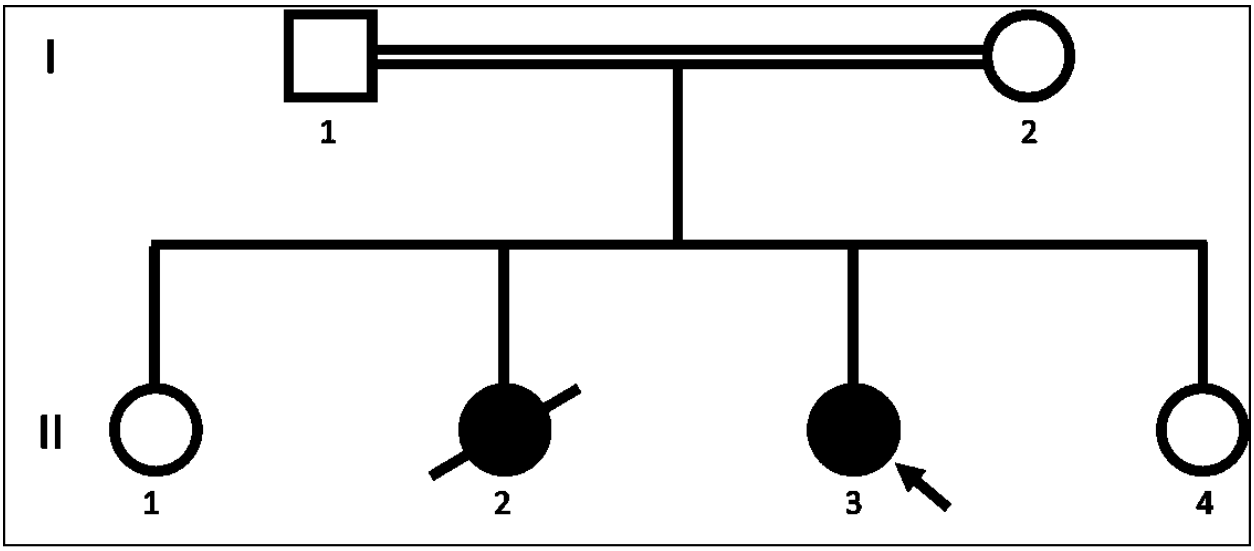

Figure 3. Family pedigree with two affected individuals. Pedigree of the family under investigation. Family is from a consanguineous Cree community and individuals I-1 and I-2 are 2nd cousins. Individual II-2 died at 40 days of life due to an infection, and II-3 (index case) began experiencing life-threatening infections at 2 weeks of age. II-1 and II-4 are unaffected.

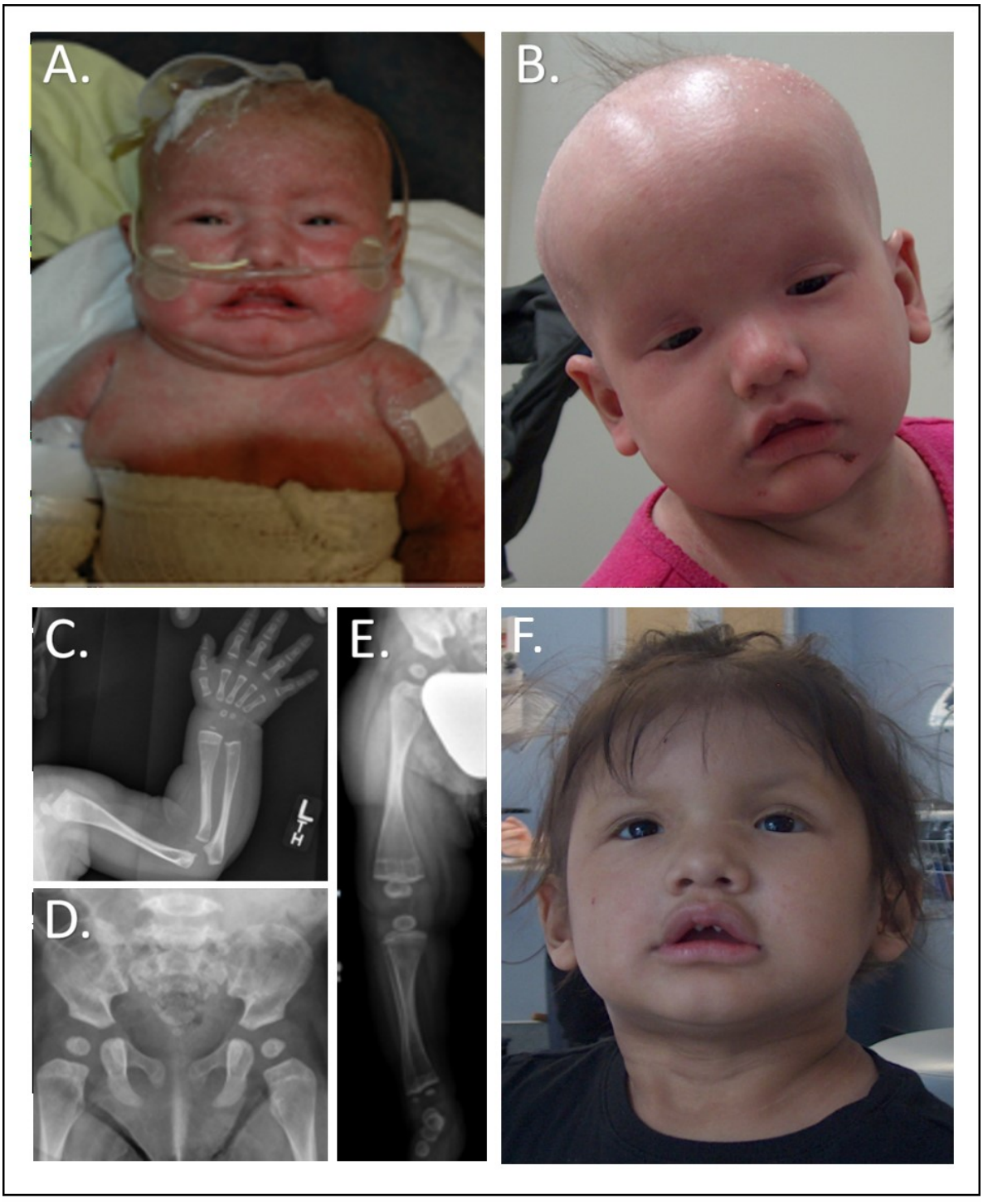

Figure 4. Index case congenital phenotype. A. The patient presented at 2 weeks with meningitis and was permanently hospitalized at 2 months of age due to recurrent life-threatening infections, dysmorphic features and skin rash present. B. Features of Ectodermal Dysplasia (ED), including alopecia and a skin rash, and at 2 years of age she only had 2 malformed teeth. C-E. Skeletal scans revealed osteoporosis and metaphyseal splaying of the long bones. F. Patient 2 years 11 months old and post-transplant, showing improvement of some ectodermal features; note peg-shaped teeth characteristic of ED.

clinical genetic testing for known causes of SCID through a commercially available gene panel including: Adenosine Deaminase (*ADA*) and Purine Nucleoside Phosphorylase (*PNP*) deficiency, and Inhibitor of nuclear factor Kappa B Kinase Beta (*IKBKB*) which is known to cause SCID in the Cree community.[36] Differential diagnoses included Omenn Syndrome, Cartilage Hair Hypoplasia, Stuve-Wiedmann Syndrome, and Cranioectodermal Dysplasia. Furthermore, clinical Enzyme Linked Immunosorbent Assay (ELISA) showed that the patient had a distinct inflammatory response that was not associated with a particular type of immunodeficiency. Extensive medical and genetic testing failed to identify the cause of the child's ailment, which initiated the search for novel causes of immunodeficiency using WES.

The severe and complex congenital phenotype and the early death of a sibling to infection suggested the condition in this family was genetic, and consanguinity between the parents supported an autosomal recessive mode of inheritance; X-linked inheritance was unexpected as both patients were female and an X-inactivation skew occurring in 2 individuals is statistically unlikely. It was hypothesized that the candidate gene might be in the NF-κB pathway due to similarities between our patient and males who have hypomorphic mutations in *IKBKG*.[20] These individuals have a clinical phenotype characterized by immunodeficiency, bone and skin disorder in keeping with ED summarized under the abbreviation OLEDAID (MIM300301, Table 1). The methodology to look for candidate genes combined homozygosity mapping (HZM) and trio exome sequencing, and a filtering approach assuming an autosomal recessive mode of inheritance. Variants or interest were assessed by *in silico* modelling for predicted pathogenicity and family segregation studies to confirm the variant(s) segregated with the phenotype (Figure 3).

Consanguinity in the patient's family suggested autosomal recessive inheritance and prompted the use of homozygosity mapping (HZM) to isolate regions of the genome that were

inherited from a common ancestor. Regions of homozygosity (loss of heterozygosity) were found on chromosomes 1, 2, 3, 4, 5, 6, 7, 8, 11, 12, 13, 14, 18, and 20 in the patient; allowing subsequent analysis to be restricted to 14 chromosomes (Table 2). Whole-exome sequencing was performed as a trio for the patient at an average depth of 209.9 and the mother and father at average depths of 213.6 and 207.9, respectively. Approximately 75,000 variants were called in each individual. Applying the HZM mapping results to the patient's exome data yielded 1,369 variants and initial filtering steps reduced the number of variants to 41 homozygous mutations in the patient. Subsequent comparison of these 41 variants with variants in the parents further reduced the analysis to 3 candidate genes (Table 3): *CLDN16* (NM_006580 c.166delG; [p.A56fs]) *GMNC* (NM_001146686 c.G142A; [p.D48N]), and *COQ2* (NM_015697 c.T1178C; [p.V393A]). *TRAF6* (NM_145803 c.G269T; [p.C90F]) was an additional variant among the 41 candidate genes identified in the patient by HZM and exome filtering, but had poor depth of coverage and failed to amplify in either parent and was therefore eliminated by the filtering strategy. Due to phenotypic similarities with boys who have mutations in *IKBKG* we hypothesized that the causative gene might be in the NF-κB pathway. TRAF6 is a central mediator for many of the receptors which activate this pathway and was added to the 3 candidate genes for further analysis (Table 3).

Alamut software predicted that only the variants in *GMNC* and *TRAF6* were pathogenic (Table 4), and these candidates were prioritized for segregation analysis in additional family members. The mutant variants in *GMNC* and *TRAF6* were analyzed by Sanger Sequencing in the patient's family; *GMNC* did not segregate with the phenotype as the other affected child was heterozygous for the variant allowing it to be eliminated as a candidate gene. The *TRAF6* homozygous variant was consistent with the presence of the phenotype in the family. Both affected siblings were homozygous for the missense variant, both parents and one sibling are carriers for

CHROMOSOME	LOCATION	SIZE (Mb)
1 (3 regions)	77,992,150-197,870,521	4.4
2 (2 regions)	81,340,758-179,088,935	3.1
3 (4 regions)	135,468,146-190,948,780	5.4
4 (8 regions)	48,342,373-104,808,307	14.8
5 (3 regions)	23,252,089-165,063491	5.5
6 (9 regions)	53,360,831-133,733,043	21.6
7 (3 regions)	102,341,967-112,380,665	6.5
8 (1 region)	47,875,557-49,214,560	1.3
11 (7 regions)	26,971,799-56,611,798	10.2
12 (1 region)	91,022,984-92,050,203	1.0
13 (3 regions)	88,961,043-98,675,641	4.6
14 (1 region)	35,911,618-36,966,702	1.0
18 (8 regions)	836,110-54,243,554	17.7
20 (1 region)	21,533,924-23,028,137	1.5
X (6 regions)	3,143,656-114,350,574	8.3

Table 2. LOH regions in the index patient. Location relate to DNA draft hg19.

Gene	Ref. Base	Alt. Base	Homo/ Het	SNP Quality	Total Depth	Alt. Depth	Region	Change	Annotation
Patient									
CLDN16	G	-	hom	214	232	232	exonic	frameshift deletion	CLDN16:NM_006580:exon1:c.166delG:p.A56fs,
GMNC	C	T	hom	136	41	41	exonic	nonsynonymous SNV	GMNC:NM_001146686:exon2:c.G142A:p.D48N,
COQ2	A	G	hom	145	82	82	exonic	nonsynonymous SNV	COQ2:NM_015697:exon7:c.T1178C:p.V393A,
TRAF6	C	A	hom	15.9	2	2	exonic	nonsynonymous SNV	TRAF6:NM_145803:exon3:c.G269T:p.C90F,TRAF6:NM_004620:exon2:c.G269T:p.C90F,
Mother									
CLDN16	G	-	het	217	169	104	exonic	frameshift deletion	CLDN16:NM_006580:exon1:c.166delG:p.A56fs,
GMNC	C	T	het	66	45	20	exonic	nonsynonymous SNV	GMNC:NM_001146686:exon2:c.G142A:p.D48N,
COQ2	A	G	het	73	87	42	exonic	nonsynonymous SNV	COQ2:NM_015697:exon7:c.T1178C:p.V393A,
Father									
CLDN16	G	-	het	217	195	101	exonic	frameshift deletion	CLDN16:NM_006580:exon1:c.166delG:p.A56fs,
GMNC	C	T	het	44	35	17	exonic	nonsynonymous SNV	GMNC:NM_001146686:exon2:c.G142A:p.D48N,
COQ2	A	G	het	76	101	46	exonic	nonsynonymous SNV	COQ2:NM_015697:exon7:c.T1178C:p.V393A,

Table 3. CLDN16, GMNC, COQ2, and TRAF6 are identified as candidate genes. 3 variants (CLDN16, GMNC, COQ2) were homozygous in the patient and heterozygous in the parents, and 1 low-quality variant of interest (TRAF6) was identified in the patient but was not present in the parents' data set. Ref. Base is the wild-type base in the reference sequence, Alt. Base is the base identified in the patient's exome. Total depth indicates the number of reads mapped to that locus, and Alt. Depth is the number of reads with the alternate allele.

Alamut Algorithms	TRAF6	GMNC
Align GVGD	Deleterious; Class C65 (GV: 0.00, GD: 204.39)	Benign; Class 0 (GV: 44.60, GD: 11.33)
SIFT	Deleterious (Score: 0)	Deleterious (Score: 0.02)
Mutation Taster	Disease Causing (p-value:1)	Disease Causing (p-value: 1)
Polyphen-2	Probably Damaging (Score:1.00)	Probably Damaging (Score: 0.998)

Table 4. GMNC and TRAF6 are predicted to be pathogenic by in silico modelling. Align GDGV scores are classed on a spectrum from C0, C15, C25, C35, C45, C55, and C65; where C0 changes are the least likely to affect protein function, and C65 are the most likely. SIFT scores range from 0-1; scores less than 0.05 are predicted to be damaging and scores above 0.05 are predicted to be tolerated. Scores approaching the boundaries are predicted with greater confidence. Mutation Taster indicates if the change is a polymorphism or predicted to cause disease by integrating information from various databases. PolyPhen-2 classifies variants qualitatively as benign, possibly damaging, or probably damaging and gives a score of 0-1 where scores closer to 1 are predicted to be more damaging.

the variant, and one sibling does not carry the variant (Figure 5). The identified mutation is a missense mutation in exon 3 (c.G269T) and results in a cysteine to phenylalanine amino acid change at position 90 (C90F) in the N-terminal region of the TRAF6 protein.

2.4 Discussion

We have studied a consanguineous Cree family with a complex congenital immunodeficiency that could not be molecularly diagnosed with conventional methods. A bioinformatics approach including HZM, WES and *in silico* modelling was used to identify novel causes of the phenotype (Figure 5). The candidate gene *TRAF6* (Tumour Necrosis Factor Receptor Associated Factor 6) is a crucial adaptor molecule of the NF-κB pathway, and is involved in innate and adaptive immunity, ectodermal development, and osteoclast function.[78] This protein has broad tissue expression and is highly conserved among species;[78] it was first identified based on its interaction with the CD40 receptor and based on its similarity to other TRAF family proteins, but was also similar to proteins that bind the interleukin-1 receptor.[79,80] TRAF6 is distinct in the TRAF family; it is the only member to integrate signals between the TNFR and the TLR and IL-1R superfamilies.[81] TRAF6 has since been found to mediate NF-κB signals from numerous other immune receptors including the T-cell Receptor (TCR)[82] and B-cell Receptor (BCR)[83] and is involved in regulating lymphocyte development. TRAF6 also transduces signals from the RANK receptor involved in osteoclastogenesis for bone development,[84,85] and the EDAR receptor involved in ectodermal development.[86,87] *Traf6* knock-out in mouse results in perinatal lethality, and homozygous knock-out pups are not born in a Mendelian ratio.[88,89] Animals die within 2-3 weeks of birth and bear a severe phenotype as they develop. Homozygous mutants are 50-70%

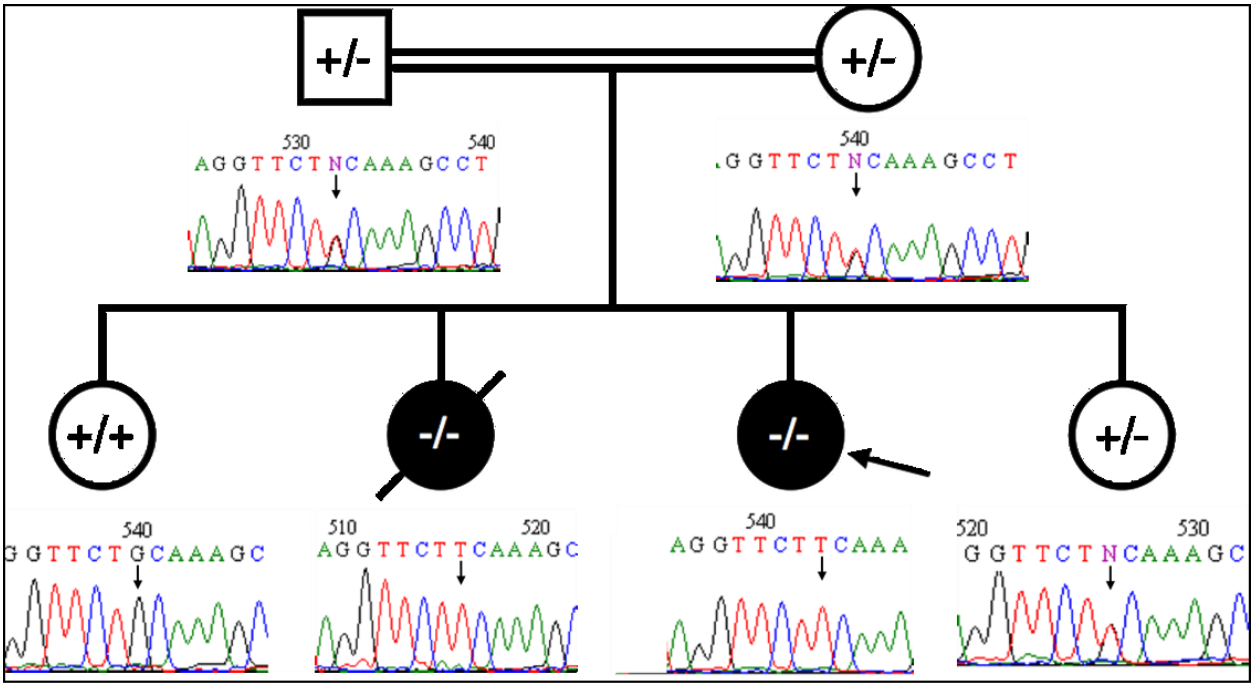

Figure 5. The TRAF6 mutation segregates with the phenotype. Both affected siblings were homozygous for the TRAF6 G>T missense mutation; consistent with the hypothesized autosomal recessive mode of inheritance. Both parents and one unaffected sibling were carriers of the mutation, and the other unaffected sibling was homozygous WT.

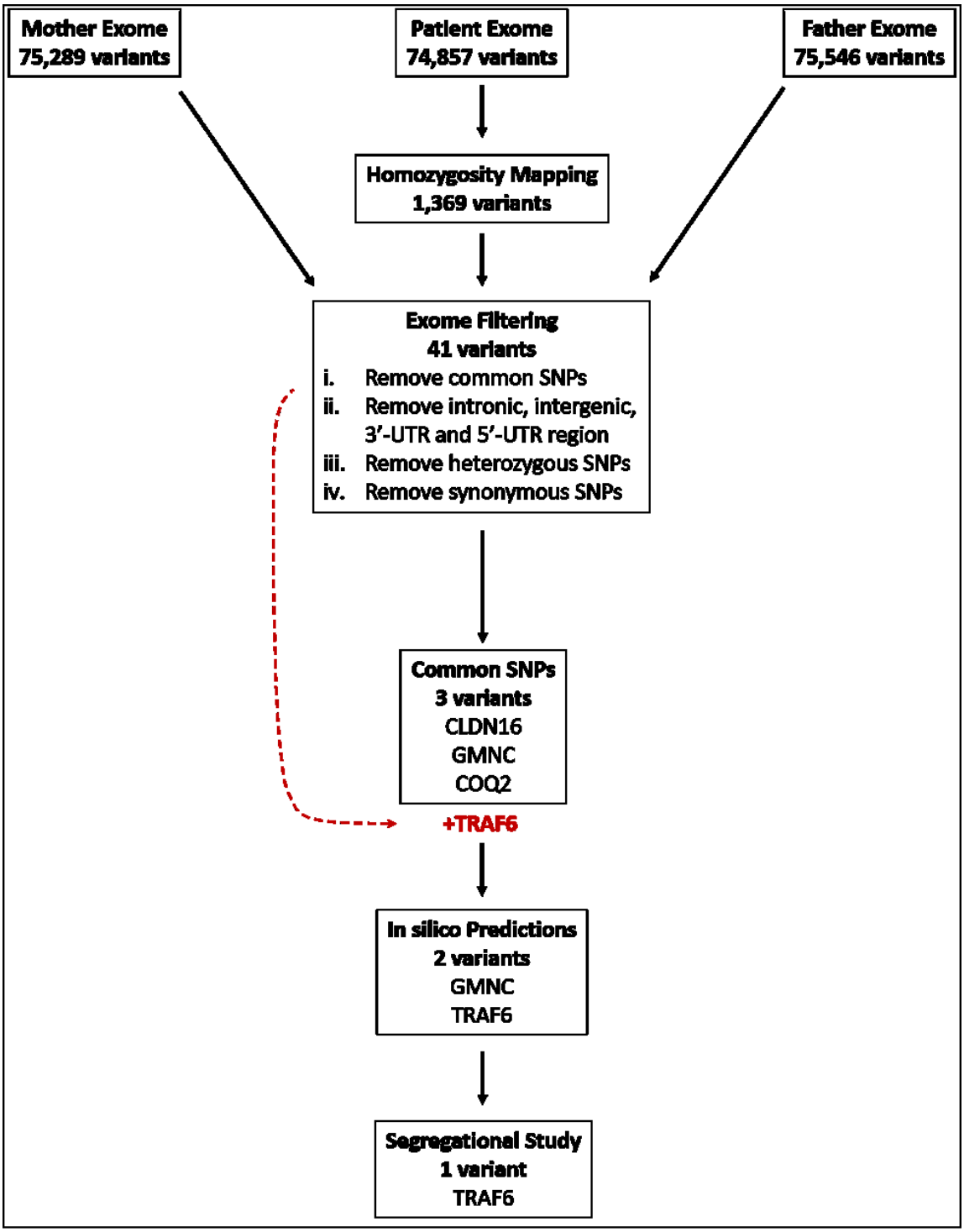

Figure 6. Gene discovery strategy identifies TRAF6 as a candidate gene. Homozygosity was performed for the patient, and an exome sequencing trio was performed for the patient and both parents. Homozygous variants in the patients were compared against heterozygous variants in the parents and identified 3 common variants. TRAF6 was identified in the HZM region of the patient's exome. Candidate genes were analyzed for predicted pathogenicity by in silico modelling. Variants predicted to be pathogenic were examined for segregation with the phenotype in the family.

smaller than control littermates at the time of death and exhibit splenomegaly and thymic atrophy; they have reduced numbers of immature B cells which fail to differentiate in response to CD40 ligand (CD40L) or LPS, and IL-1R dependent T-cell proliferation is impaired.[88,89] Homozygous *traf6* knock-out also results in osteopetrosis and causes a shortening of the long bones with metaphyseal splaying. Additionally, knock-out mice display features similar to hypohidrotic ectodermal dysplasia with abnormal hair follicles, an absence of sebaceous glands, and failed tooth eruption.[88–90] There have only been two associations of *TRAF6* mutations with human disease: a C-terminal frameshift mutation and a microdeletion of the *TRAF6* 5'non-coding region (Figure 7).[91,92] A heterozygous frameshift deletion of 8 nucleotides (c.1074-1081delCAATTTG; [p.Phe360fs]) in the 5'region in the last exon of *TRAF6* has been reported as a cause of Hypohidrotic Ectodermal Dysplasia in a single patient of Polish descent. This mutation was found to be *de novo* in this individual and was not found in 150 healthy controls or in the 1000 genomes database.[91] *In vitro* functional analysis showed that mutant TRAF6 was unable to bind to the EDARADD protein to activate NF-κB signaling, and that the mutant protein acts in a dominant negative manner to prevent WT TRAF6 interaction with EDARADD.[93] A homozygous 2064 Kb deletion on chromosome 11 (arr11p12; 36,530,297-38,595,131) including the *TRAF6* 5'non-coding region and the 2 upstream genes: Recombination Activating Gene 1 (*RAG1*) and *RAG2*, has been associated with SCID and osteopetrosis in a pair of fraternal twins from Israel.[92] *RAG1* and *RAG2* are known causes of SCID and are included on gene panels for the disorder but are not associated with osteopetrosis. The function of TRAF6 in osteoclastogenesis suggested that it may contribute to the phenotype observed in these patients.[92] I have identified a novel missense c.G269T variant in *TRAF6* as a candidate gene for an undiagnosed primary immunodeficiency with bone abnormalities and ectodermal dysplasia in an Alberta family of Cree descent. This was

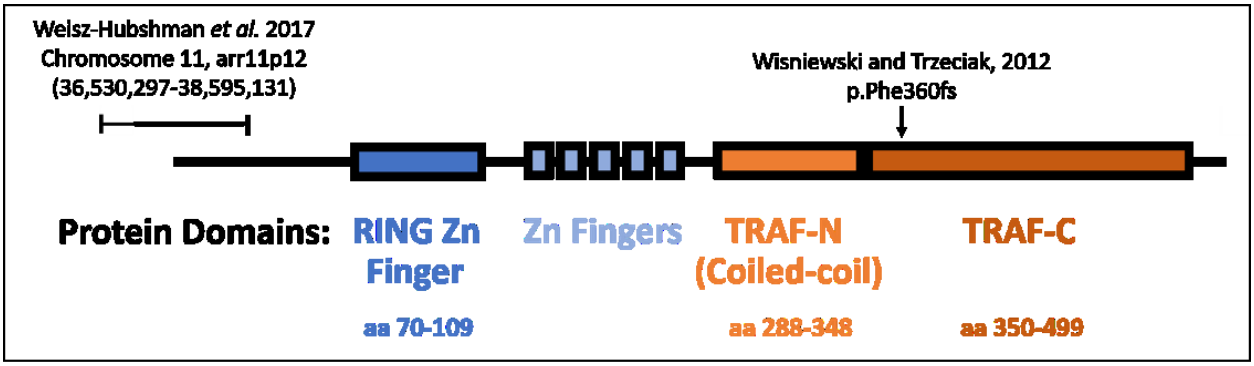

Figure 7. Two TRAF6 mutations have been associated with human phenotypes. The TRAF6 protein is composed of 4 major structural domains. Two mutations in TRAF6 have been associated with human disease; a deletion of the 5'non-coding region including the 2 upstream genes as a cause of immunodeficiency and osteopetrosis, and a frameshift deletion resulting in loss of most of the TRAF-C domain as a cause of Hypohidrotic Ectodermal Dysplasia.

the only candidate that was predicted to be pathogenic by *in silico* modelling and segregated with the phenotype in the family. The role of TRAF6 in the human immune system, bone and ectodermal development, together with the phenotype of the knock-out mouse and the preliminary association of TRAF6 with human phenotypes makes this gene a strong candidate for the disorder in this family.

Chapter Three:

Functional analysis of the C90F mutation in the context of the NF-κB signaling pathway

3.1 TRAF6 in the ubiquitin proteasome system and NF-κB Signaling

TRAF6 is a member of the TRAF family of proteins, which includes 7 proteins in mammals; TRAF1-7. These proteins were originally identified as intracellular signaling molecules for the TNFR family, but have since been shown to also function as signal transducers for the Toll and Interleukin 1 families of receptors.[79,94] TRAF proteins have no known enzymatic function, but contribute to cellular signaling by acting as adaptor molecules to bring other signaling proteins into proximity with each other. All TRAF proteins have a homologous TRAF domain in the C-terminal region of the protein (TRAF-C domain) which allows for receptor binding, as well as an upstream coiled-coil (TRAF-N) domain for homo- and hetero-oligomerization.[95] TRAF2-6 also share structural homology in the N-terminal region, which includes a Really Interesting New Gene (RING) finger domain followed by 5 or 7 zinc finger domains. This RING domain is highly conserved both within the TRAF protein family and among species (Figure 8). The association of these motifs with downstream kinase molecules makes them crucial for the signaling function of the TRAF protein.[96] The RING finger domain of TRAF6 allows it to function as a ubiquitin ligase to modulate protein function via post-translational modulation.[94] RING domain proteins make up the majority of E3 ubiquitin ligases,[97,98] which together with E1 ubiquitin activating enzymes and E2 ubiquitin conjugating enzymes, form the major proteins of the UPS.[99,100] The UPS is the primary system for the degradation and turnover of proteins in eukaryotic cells,[101] and plays a critical role in regulating many cellular processes, including: cell-cycle progression, DNA repair, membrane transport, and signal transduction.[102] Protein ubiquitination begins with the activation of ubiquitin protein by an E1 enzyme; this ATP-dependent reaction links the C-terminus of ubiquitin to the active cysteine of the E1 enzyme. The activated ubiquitin in then transferred to the

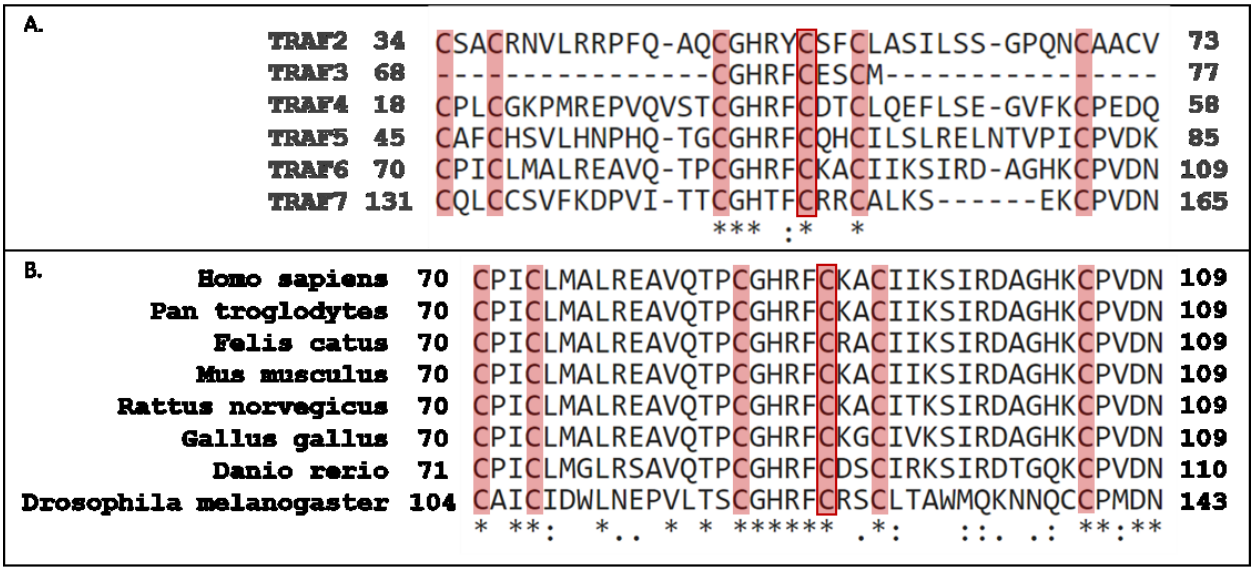

Figure 8. TRAF6 cysteine 90 is highly conserved. A. Amino acid conservation of the RING domain in the TRAF family. Cysteines are highlighted in red, and human TRAF6 cysteine 90 in highlighted and outlined in red. B. TRAF6 RING domain conservation among species. Sequences were aligned using Uniprot against the TRAF6 human RING domain (amino acids 70-109). Asterisks denote sites with a single, fully conserved residue, colons denote conservation between residues of strongly similar properties, and periods denote conservation between residues of weakly similar properties.

active cysteine of the E2 enzyme, and the E3 enzyme interacts with both the E2 and the protein to be targeted by ubiquitin.[100,103] The approximately 40 E2 and over 600 E3 enzymes in humans,[103–105] along with the nature of the ubiquitin linkages, allows for a high degree of target specificity of the UPS system.[103,106] The ubiquitin can be transferred either directly to the target substrate or another ubiquitin molecule, generally through a lysine residue and less often to the N-terminus.[99] The C-terminus of ubiquitin is able to link with any of the 7 lysine residues of another ubiquitin molecule to form poly-ubiquitin chains;[107,108] lysine 43 (K48) linked polyubiquitin chains are the best characterized and target proteins to be degraded by the 26S proteasome.[109] K63-linked polyubiquitin chains regulate proteins involved in DNA repair and cell signaling and are not involved in protein degradation.[102] Two mechanisms of E3 ubiquitin ligase function have been identified: they may act as catalytic intermediates to pass ubiquitin from the E2 to the target protein, or they mediate the transfer of ubiquitin from the E2 directly to the substrate by bringing the two proteins into proximity with one another.[106,110] The latter mechanism is used by the RING-type E3 ubiquitin ligases.[97,99,110] The RING domain of these proteins is characterized by 8 amino acids, generally cysteine and histidine, which coordinate with Zn+ ions in a cross-brace arrangement to serve as a binding platform for the E2 binding partner.[98,111] While the order of these residues varies between different RING proteins, the spacing between them is highly conserved.[99] TRAF6 activates the NF-κB pathway through the direct binding of NEMO to facilitate the K63-linked polyubiquitination of NEMO by the E2 complex Ubc13/UevA1.[112–115]

In the previous chapter, I described the identification of homozygous missense mutations in a candidate gene, *TRAF6*, c.G269T in individuals affected by a novel immunodeficiency which causes a radical amino acid change of the 4th cysteine in the RING domain of TRAF6 (Figure 9). The missense mutations alters the RNA codon to change the small, hydrophilic cysteine to a large,

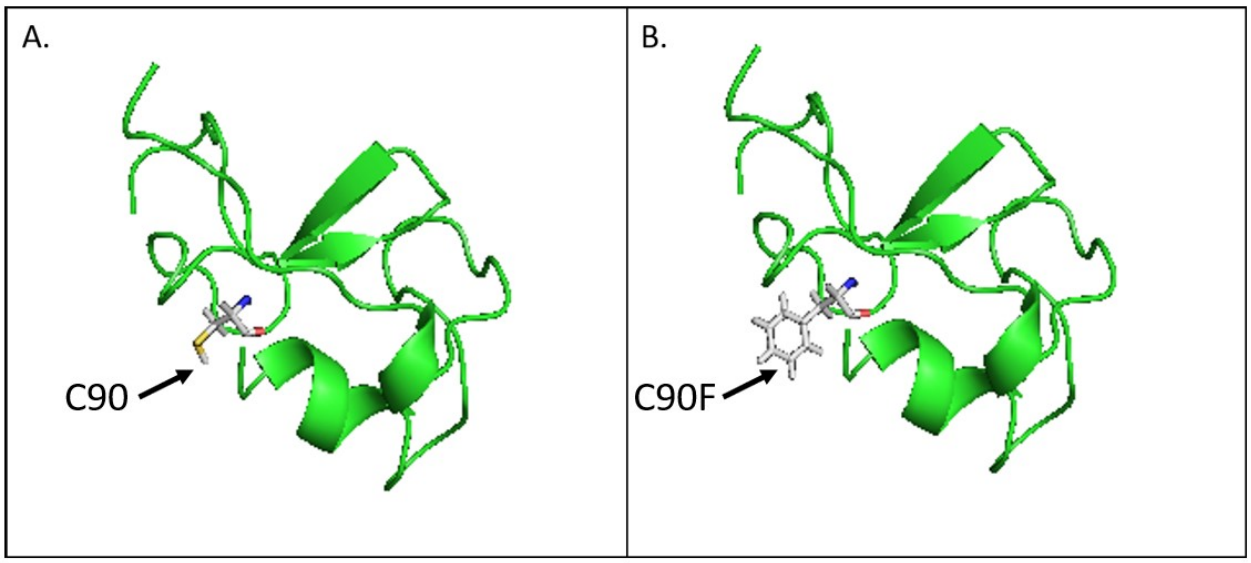

Figure 9. The TRAF6 mutation causes a cysteine to phenylalanine mutation in the protein. Structural representation of the TRAF6 RING domain produced in Pymol. A. The WT TRAF6 RING domain has a small, polar cysteine at position 90 (C90). B. The c.269G>T mutations replaces the cysteine with a large, hydrophobic phenylalanine at position 90 (C90F).

hydrophobic phenylalanine in the protein. This chapter presents experiments performed to functionally characterize the homozygous c.G269T mutation in *TRAF6*, which is hypothesized to impair the NF-κB pathway and cause a novel human disease. We believe that the loss of a cysteine in the RING domain will disrupt coordination with the Zn+ ion and impair proper folding of this structural domain. This impairment is hypothesized to abolish binding of the upstream E2, such that it cannot tag NEMO with ubiquitin to activate the IKK complex. We expect that the IKK complex will be unable to phosphorylate the IκB complex to mark it for degradation and release the NF-κB transcriptional subunits. We hypothesize that this will reduce or abolish NF-κB nuclear translocation and the transcription of NF-κB target genes.

3.2 Materials & Methods

3.2.1 Cell Culture

Human Fibroblasts

A primary fibroblast cell line harboring the homozygous *TRAF6* mutation was established from a skin biopsy collected from the patient (TRAF6 C90F/C90F). This was performed by the Department of Pathology at the University of Alberta Hospital. Control primary fibroblasts were established using skin samples from the patient's 2 surviving sisters, where one sister was a carrier for the TRAF6 mutation (TRAF6 +/C90F), and one sister was WT at both alleles (TRAF6 +/+). Control cell lines were established at The Centre for Applied Genomics (TCAG) in Toronto, Canada. Fibroblast cells were maintained in Dulbecco's Modified Eagle Medium (DMEM) (Gibco Cat. No. 11995-065) supplemented with 10% fetal bovine serum (FBS) (Gibco Cat. No. 12483-020) and 0.5% Penicillin-Streptomycine (Gibco Cat. No. 15140-122) and grown at 37°C with 5% humidified CO_2. Cell cultures were passaged when they reached >80% confluence. Cells were

utilized for only 12 passages after thawing. Frozen cell stocks were prepared when cells were >90% confluent; 1 T75 flask was used to prepare two 1 mL cell stocks. Spent media was aspirated and cells were washed with 10 mL 37°C Dulbecco's Phosphate Buffered Saline (DPBS) (Gibco Cat. No. 14190-144); DPBS was aspirated and cells were detached by incubation with 0.25% trypsin-EDTA (Gibco Cat. No. 25200-065) for <5 minutes at room temperature. 5 mL fresh 37°C media was added to detached cells, and cells were collected and centrifuged at 1000 RPM in the Sorvall ST8 (ThermoFisher Rotor 77-005-701) for 5 minutes. Media was aspirated from the cell pellet and cells were resuspended in 2 mL of *Recovery Cell Freezing Media* (Gibco Cat. No. 12648-010). Resuspended cells were aliquoted into 2 cryovials and slowly frozen at -80°C in isopropanol before transfer for long-term storage in liquid nitrogen. Cells were thawed by heating 1 vial (1 mL) of cells for <2 mins in a 37°C water bath before transfer to a T75 flask containing 13 mL of media; the vial was rinsed with 1 mL media which was then added to the T75 flask. Cells were grown at 37°C with 5% humidified CO_2.

Human Lymphoblastoid Cells

A lymphoblastoid cell line (LCL) harboring the homozygous *TRAF6* mutation was established by the Epstein-Barr virus (EBV) transformation of a blood sample collected from the patient (TRAF6 C90F/C90F). This was performed by the Department of Pathology and Laboratory Medicine at the University of California at Los Angeles (UCLA). Control LCLs were established using blood samples from the patient's 2 surviving sisters, where one sister was a carrier for the TRAF6 mutation (TRAF6 +/C90F), and one sister was WT at both alleles (TRAF6 +/+). Control cell lines were transformed by EBV at TCAG in Toronto, Canada. LCLs were maintained in Roswell Park Memorial Institute (RPMI) 1640 medium (Gibco Cat. No. 11875-093) supplemented

with 10-15% FBS and 1x Penicillin-Streptomycin-Glutamine (Gibco Cat. No. 10378-016) and grown with the flask in an upright position at 37°C with 5% humidified CO_2. Cell cultures were transferred to a fresh flask once a week. Frozen cell stocks were prepared according the protocol received from TCAG; 30-35 mL of cell culture was collected when media has just turned pale yellow. Cells were centrifuged at 1200 RPM in Sorvall ST8 (ThermoFisher Rotor 77-005-701) for 10 minutes and resuspended in 5 mL or *Recovery Cell Freezing Media*. Resuspended cells were aliquoted into 5 cryovials and slowly frozen at -80°C in isopropanol before transfer for long-term storage in liquid nitrogen. Cells were thawed according the protocol received from UCLA; 1 vial of cells was rapidly thawed for <2 mins in a 37°C water bath before transfer to a 15 mL falcon tube containing 10 mL of RPMI 1640 supplemented with 15% FBS and 1x Penicillin-Streptomycin-Glutamine. Cells were centrifuged at 1000 RPM for 5 minutes, media was aspirated and cells were resuspended in 3 mL of RPMI 1640 supplemented with 15% FBS and 1x Penicillin-Streptomycin-Glutamine. Cells were transferred to a T25 flask and grown with the flask in an upright position at 37°C with 5% humidified CO_2; 1-2 mL fresh growth media was added when cell culture media turned peach/yellow in color. Cells were transferred to a T75 flask when cell culture volume reached 10 mL.

Viability Resazurin Assay

LCLs were counted and established at a density of $1x10^6$ cells/mL in RPMI 1640; media was not supplemented with serum to promote LCL attachment to the plate. 100 µL was plated in a clear 96-well plate with 5-8 replicates were plated per cell line and grown overnight for 18 hours. 11 µL of resazurin (Sigma Cat. No. R7017) dye (440 µM in 1x phosphate buffered saline (PBS)) was added to each well and swirled to mix. Cell were incubated with resazurin dye at 37°C for 1.5-2

hours until the resazurin dye began changing color from dark blue to pink. Fluorescence was measured within 15 minutes of dye color change using excitation and emission settings of 544nm and 590 nm, respectively. A one-way analysis of variance (ANOVA) was used to determine any significant difference in viability between the 3 cell lines.

3.2.2 TRAF6 C90F Analysis

TRAF6 C90F mRNA abundance: RT-qPCR

Primary fibroblasts were plated for RNA extraction when cells were >80% confluent. Fibroblasts from 4x T75 flasks containing 15 mL cell culture were collected by trypsinization after washing with DPBS and centrifuged at 1000 rotations per minute (RPM) for 5 minutes. The media was aspirated and the pellet resuspended in 5 mL of 37°C DMEM supplemented with 10% FBS. Cells were counted and established at a density of $0.5x10^6$ cells/mL; 2 mL per well of resuspended culture was plated in a 6-well plate and cells were incubated for 20 hours at 37°C with 5% humidified CO_2. Media was aspirated and cells were washed with 2 mls of warm DPBS before RNA extraction with 400 µL Trizol (Invitrogen Cat. No. 15596026) following the TRIzol Reagent User Guide (Invitrogen Doc. Part. No. 15596026.PPS; Pub. No. MAN0001271; Rev. A.0). 20 µg of RNase-free glycogen (ThermoScientific Cat. No. R0551) was added to the isolated aqueous phase before RNA precipitation by isopropanol, and pelleted RNA was resuspended in RNase/DNase-free distilled water (Invitrogen Cat. No. 10977-015). RNA concentration was determined by nanodrop (GE NanoVue 4282 V1.7.3) and samples were stored at -80°C until cDNA synthesis. 500 ng of RNA was used as a template for cDNA synthesis by SuperScript III Reverse Transcriptase (Invitrogen Cat. No. 18080-093) and oligoDT primer (Life Technologies Cat. No. 58862) according to the Invitrogen First-Strand cDNA Synthesis protocol (Part. No.

18080.pps). cDNA was diluted 1/10 before performing qPCR using FastStart Essential DNA Green Master (Roche Cat. No. 06402712001) mix with TRAF6 qPCR primers binding in exon 5 5'- CCTTTGGCAAATGTCATCTGT-3' and the exon 6/7 junction 5'- CTCTGCATCTTTTCATGGCAAC-3', which yields a 2487 base-pair product before splicing and a 140 base-pair product post-splicing. Glucuronidase beta (*GUSB*) was served as a house keeping gene to determine expression levels using primers that bind in exon 2 5'- AGAGTGGTGCTGAGGATTGG-3' and exon 3 5'- CCCTCATGCTCTAGCGTGTC-3' to give a 392 base-pair unspliced fragment and 80 base-pair spliced fragment. Primer efficiencies were determined by standard curve; *TRAF6* efficiency=1.93 and *GUSB*=1.96. 2 µL diluted cDNA was mixed with 10 µL FastStart Essential DNA Green Master, 6 µL MQ H_2O, and 2 µL 2 µM TRAF6 primer mix or 4 µM *GUSB* primer mix. Template was preincubated at 95°C for 600 seconds and amplified over 45 cycles at 95°C for 10 seconds (ramp rate 4.4°C/s; no signal acquisition) and 58°C for 45 seconds (ramp rate 2.2°C/s; single signal acquisition). Sample was melted at 95°C for 10 seconds, 65°C for 60 seconds, and 97°C for 1s with a continuous signal acquisition, followed by cooling at 37°C for 30 seconds. qPCR data was analyzed using the $\Delta\Delta C_t$ comparative quantification algorithm described by Applied Biosystems to determine the range fold-change in gene expression. Briefly, after the ΔC_t was calculated the standard deviation of the ΔC_t of the technical replicates was determined using the formula $(s_1^2 + s_2^2)^{1/2}$, where s_1 is the standard deviation of the house keeping gene for a given condition and s_2 is the standard deviation of the target gene for a given condition. The $\Delta\Delta C_t$ was calculated using WT TRAF6 gene expression as a calibrator. Fold-change was expressed as a range by incorporating the standard deviation of the ΔC_t by calculating $2^{-\Delta\Delta Ct}$ to give the fold-change and the $2^{(-\Delta\Delta Ct \pm \text{st. dev } \Delta Ct)}$ was calculated to determine the range of fold-change, which is represented graphically by the error bars. A one-way

ANOVA was used to determine any significant difference in TRAF6 gene expression between the 3 cell lines. Statistical analysis was performed using the data from 3 biological replicates.

TRAF6 C90F protein abundance and stability: western blotting

Primary fibroblasts were plated for protein extraction when cells were >80% confluent. Fibroblasts from 4x T75 flasks containing 15 mL cell culture were collected by trypsinization after washing with DPBS and centrifuged in a Sorvall ST8 (ThermoFisher Rotor 77-005-701) at 1000 RPM for 5 minutes. The media was aspirated and the pellet resuspended in 5 mL of DMEM warmed to 37°C supplemented with 10% FBS. Cells were counted and established at a density of $1x10^6$ cells/mL; 1 mL per well of resuspended culture was plated in a 12-well plate and cells were incubated for 20 hours at 37°C with 5% humidified CO_2. Cells were either treated with 100 µM cycloheximide (CHX) (Sigma Cat. No. C7698) for 8-48 hours to examine protein stability, or media was aspirated from wells and fibroblasts were lysed in 50 µL of cold lysis buffer (20mM Tris pH 7.5, 25mM glycerol-2-phosphate, 150mM NaCl, 1% Triton X-100; supplemented with fresh phosphatase and protease inhibitors: 2mM Na_3VO_4 (100 mM in water pH 10), 1:100 PMSF (100 mM in isopropanol), respectively); the plate was incubated on ice for 10 minutes following cell lysis. Cells were collected by scraping and lysates were transferred to microcentrifuge tubes. Lysates were centrifuged in a Sorvall Legend Micro21R (ThermoScientific rotor 75-003-424)k at 14,200 RPM for 5 minutes at 4°C, and 40 µL supernatant was collected. Lysates were mixed with 20 µL 4x SDS Sample Buffer (240 mM Tris-HCl pH 6.8, 40% glycerol, 8% SDS, 5% β-mercaptoethanol, 0.1% bromophenol blue) and boiled at 98°C for 8 minutes. After boiling lysates were rapidly cooled on ice before being transferred to 4°C for short term storage (1 month), or -80°C for long term storage. Protein quantification was performed immediately after extraction

using the Micro BCA Protein Assay Kit (ThermoScientific Cat. No. 23235). Protein standards were prepared by serially diluting a 1.0 mL solution of 20 µg/µL bovine serum albumin (BSA) in PBS 1:1 with 500 µL PBS down to 2.5 µg/µL BSA in PBS. Unknown protein samples were prepared by adding 2 µL of protein lysate to 498 µL of PBS. BCA working reagent was prepared according to instructions contained in the kit, and 500 µL working reagent was added to 500 µL BSA standards and 500 µL unknown protein samples. Solutions were mixed by inverting and incubated for 30 minutes at 60°C. Solutions were cooled to room temperature for 15-30 minutes before measuring in the spectrophotometer. Protein concentration was determined using the Protein 595 Assay on the GeneQuant pro spectrophotometer. Fibroblast cell lines were examined for the abundance of TRAF6 protein by western blotting; 3 wells of technical replicates were loaded per cell line. 40 µg of protein was resolved on a 12% SDS-PAGE gel at 180 V for 1 hour and 25 minutes. Protein was transferred to 0.45 µm nitrocellulose membrane (BioRad Cat. No. 162-0115) by wet transfer at 80 V for 1 hour. After transfer the membrane was blocked for 60 minutes in Odyssey Blocking Buffer (Licor Cat. No. 927-40000). Membrane was incubated overnight at 4°C in a 1:1000 dilution rabbit-α-TRAF6 (Sigma Cat. No. HPA019805) and a 1:5000 dilution of mouse-α-tubulin E7 supernatant (Developmental Studies Hybridoma Bank AB_2315513).[116] Primary antibodies were diluted in a solution of 1:1 Licor Blocking Buffer and PBS+0.1% Tween-20 (PBS-T). After primary antibody incubation the membrane was washed 4x in PBS-T. The membrane was then incubated for 30 minutes at room temperature in a 1:20,000 dilution of dk-α-ms790 (Abcam Cat. No. ab186699) and 1:10,000 dilution of dk-α-rb680 (Abcam Cat. No. ab186692) fluorescently conjugated secondary antibodies in a 1:1 solution of Licor Blocking Buffer and PBS-T. After secondary antibody incubation the membrane was washed 4x in PBS-T. The membrane was then imaged with proteins facing down using the Licor Odyssey

Infrared Imaging System (Version 3.0.2.1). Protein samples from each cell line were run in triplicate and band intensity was quantified using Licor Application Software (Version 3.0). A one-way ANOVA was used to determine any significant difference in TRAF6 protein abundance (without CHX treatment) between the 3 cell lines. 5 biological replicates were performed for statistical analysis.

TRAF6 C90F RING domain structure: Nuclear Magnetic Resonance

Custom vectors for recombinant protein expression were ordered from Genscript. The sequences for the WT and C90F TRAF6 RING domain (Figure 10) were synthesized and cloned into the pGEX-6P-1 vector by Genscript using BamHI and NotI enzymes and received as sequence validated lyophilized pellet. Lyophilized plasmids were resuspended at 200ng/µL in RNase/DNase-free distilled water, and 100 ng of WT and mutant DNA was transformed into 50µL of competent BL21 RIPL *E. coli* (Agilent Cat. No. NC9122855) using electroporation. 20 µL transformed cells were plated onto LB-agar (Miller LB, Fisher Cat. No. L-13946) plates containing 100 µg/mL carbenicillin and 34 µg/mL chloramphenicol antibiotics and grown overnight at 37°C; a single colony was used to inoculate 50 mL of LB broth (Miller, Fisher Cat. No. L-13946) containing 100 µg/mL carbenicillin and 34 µg/mL and chloramphenicol and grown 37°C for 16 hours with 225 RPM shaking. Culture volumes were scaled up by inoculating 4x 500 mL LB broth + carbenicillin and chloramphenicol with 5 mL of liquid overnight culture and grown at 37°C in 2 L Erlenmeyer flasks for 2-3 hours until the OD^{600} reached ~0.6. Starter cultures were collected and centrifuged in an Avanti J-25 (rotor JLA 10.5)) at 4000 RPM for 10 mins at 40°C; the supernatant was decanted and cells were washed in 300-500 mL 37°C filter sterilized 1x MOPS wash buffer pH 7.4 (40 mM MOPS, 4 mM tricine, 50 mM NaCl) by breaking up the cell pellet and stirring cell

A.	B.
5'-AAGTATGAATGCCCCATCTGCTTGATGG CATTACGAGAAGCAGTGCAAACGCCATGC GGCCATAGGTTCT**G**CAAAGCCTGCATCATA AAATCAATAAGGGATGCAGGTCACAAATG TCCAGTTGACAATGAAATACTGCTGGAAA ATCAACTATTTCCAGACAAT**TTTGCAAAA-3'**	**5'-**AAGTATGAATGCCCCATCTGCTTGATGG CATTACGAGAAGCAGTGCAAACGCCATGC GGCCATAGGTTCT**T**CAAAGCCTGCATCATA AAATCAATAAGGGATGCAGGTCACAAATG TCCAGTTGACAATGAAATACTGCTGGAAA ATCAACTATTTCCAGACAAT**TTTGCAAAA-3'**

Figure 10. Custom vectors for expression of the TRAF6 RING domain for NMR. A. WT and B. mutant DNA sequence used to produce TRAF6 RING domain NMR vectors. Sequence corresponds to amino acids 67-112, where the RING domain appears in yellow and the mutant base-pair is bolded. Sequences were synthesized and cloned into the pGEX-6P-1 vector by Genscript.

mixture with a sterile spatula. Washed cells were centrifuged as above and cell pellet was resuspended in 500 mL 37°C filter sterilized 1x MOPS minimal media[117] (10 μM $FeSO_4 \cdot 7H_2O$ (fresh), 5 mM $(^{15}NH_4)_2SO_4$, 500 nM $CaCl_2 \cdot 2H_2O$, 523 μM $MgCl_2 \cdot 6H_2O$, 50 mM NaCl, 3 nM $(NH_4)Mo_7O_{24}$, 400 nM H_3BO_3, 30 nM $CoCl_2$, 10 nM $CuSO_4$, 80 nM $MnCl_2$, 10 nM $ZnSO_4$, 100 μM $ZnCl_2$, 1.32 mM K_2HPO_4, 20 mM glucose) containing ^{15}Nitrogen (Cambridge Isotope Laboratories Inc. Cat. No. NLM-713-PK) to label proteins[118] and 100 μg/mL carbenicillin and 34 μg/mL chloramphenicol and grown at 37°C for 1 hour in a 2 L baffled Erlenmeyer flask before inducing protein expression with 0.4 mM IPTG (Fisher Cat. No. BP1755-10). Induced cells were grown at 16°C for 20 hours before cell collection by centrifugation as above at 4°C; cell pellet was stored at -20°C until cell lysis. Cells were lysed on ice for protein extraction by scraping the pellet in 50-75 mL high salt 1x Tris Buffered Saline (TBS) (50mM Tris-HCl; 500 mM NaCl) pH 7.4 with 1 EDTA-free Protease Inhibitor tablet (Roche Cat. No. 16829900), 0.2 mg/mL lysozyme (Sigma L-6876), and 1:1000 β-mercaptoethanol (Sigma Cat. No. M6250). Lysed cells were sonicated for 2 minutes using 8 cycles of 15 seconds sonication at 50% amplitude followed by 45 seconds of rest for a total time of 8 minutes. 2-5 μL of crude lysate was collect for analysis by Coomassie gel before the sample was centrifuged in Avanti J-25 at 24000 rpm with JA25.5 rotor at 4°C for 20 minutes to clarify insoluble cellular components from the protein lysate. Protein supernatant was filtered with a 0.45 μm filter (Millipore Cat. No. HAWP04700) before Fast Protein Liquid Chromatography (FPLC) to isolate the GST-tagged TRAF6 RING domain. The GST FPLC column (Pharmacia Biotech GSTPrep FF 16/10 Code No. 17-5234-01) was equilibrated with high salt 1x TBS (+1:1000 β-mercaptoethanol) pH 7.4 before loading total protein sample volume onto the column. 2 μL of column flow through was collected for analysis by Coomassie gel with the remainder to be discarded. Tagged protein was eluted with the above

equilibration buffer including 10 mM glutathione (pH 7.4) (Fisher Cat. No. BP2521100), and eluted fractions containing WT or C90F GST-tagged RING domain were combined and 2-10 µL of sample was collected for analysis by Coomassie gel. The GST-tag was removed from the RING domain by incubation with 6.5 µL of 3C protease (expressed and purified in house) per mL of sample overnight at 4°C. 2-10 µL of cleaved protein was collected to monitor protein cleavage by Coomassie gel, if cleavage was complete then dialysis was used to remove glutathione from RING domain protein. Protein sample was transferred into 10x4.6 cm regenerated cellulose tubing (Fisher Cat. No. 21-152-9) with a molecular weight cut off (MWCO) of 3500 Da, and the dialysis tubing containing protein was incubated in 2L high salt 1x TBS with 1:1000 β-mercaptoethanol at 4°C with gentle stirring. After 2 hours the TBS solution was replaced and the dialysis was left to proceed overnight. TBS solution was changed an additional 2x with a 2 hour incubation between each buffer change. 2-10 µL protein sample was collected from the dialysis tubing for analysis by Coomassie gel and the remainder of the sample was loaded onto the GST FPLC column as described above to isolate the RING domain fragment from the GST-tag. Flow through containing the RING domain protein was collected and 2-10 µL of both flow through and eluted GST-tag were used for Coomassie gel staining. Size-exclusion FPLC was used to remove remaining traces of the GST-tag from the WT and mutant RING domain fragments. Before size-exclusion the protein sample was concentrated using Millipore Centrifugal filter units (Cat. No. UFC900324) and centrifuging at 5000 rpm for 15 minutes at 4°C until the sample volume was <1 mL. The Superdex 30 column (Pharmacia Biotech HiLoad26/60 Code No. 17-1140-01 Id No. 0644014) was equilibrated with 1x TBS (50 mM Tris-HCl; 150 mM NaCl) with 1:1000 β-mercaptoethanol and 10 nM $ZnCl_2$, and the total volume of protein sample was loaded onto the column. Protein fractions containing the GST-tag and the TRAF6 mutant or WT RING domain were collected and

analyzed by Coomassie staining, followed by concentration by centrifugation to <500 µL as described above, and Bradford assay. 300 µL of protein sample was supplemented with 5% deuterium oxide (D_2O) (Cambridge Isotope Laboratories Inc. Cat. No. DLM-6-PK) and fresh β-mercaptoethanol and was loaded onto a 5 mm Shigemi NMR tube. A plunger was inserted into the tube leaving 18mm of sample space between the base of the NMR tube and the plunger, and the sample was read by 2D ^{1}H-^{15}N heteronuclear single quantum correlation (HSQC) NMR spectroscopy.

3.2.3 NF-κB Signaling Analysis

Phosphorylation and degradation of IκB-α: western blotting (as above with changes noted)

Primary fibroblasts were plated and incubated for 20 hours before cytokine stimulation and protein extraction. Media was gently aspirated from the cells, and 1 mL fresh DMEM+10% FBS containing 10 ng/mL human IL-1β (Cell Signaling Cat. No. 8900) reconstituted at 50 µg/mL in DPBS, or 10 ng/mL human TNF-α (Sigma-Aldrich Cat. No. T0157) was added to each well. Wells were either untreated or treated for 2, 5, 10, 30, or 60 minutes. After cytokine treatment the media was removed from wells, and cells were lysed and protein concentration was determined by BCA assay as previously described. Fibroblast cell lines were examined for NF-κB activity by western blotting for phosphorylation and degradation of IκB-α after cytokine treatment. 60 µg of protein was resolved by SDS-PAGE as described above with the following changes. Membrane was incubated overnight at 4°C in a 1:5000 dilution of mouse-α-phospho-IκB-α (S32/36) (Cell Signaling Cat. No. 9246S) and 1:5000 dilution rabbit-α-IκB-alpha (Cell Signaling Cat. No. 4812S) primary antibodies. The membrane was incubated for 30 minutes at room temperature in a 1:20,000 dilution of dk-α-ms790 (Abcam Cat. No. ab186699) and 1:10,000 dilution of dk-α-rb680

(Abcam Cat. No. ab186692) fluorescently conjugated secondary antibodies. The membrane was sequentially probed with a 1:5000 dilution of primary mouse-α-tubulin E7 supernatant, and a 1:20,000 dilution of secondary dk-α-ms680 (Abcam Cat. No. 715-625-151).

Nuclear translocation of NF-κB: high-content assay for nuclear translocation

Primary fibroblasts were plated for NF-κB nuclear translocation assay when cells were >80% confluent. Cells were collected and established at a density of $1.25x10^5$ cells/mL; 100 µL per well of resuspended culture was plated in a black-bottomed 96-well plate (Greiner Cat. No. 655090); 5 replicates were plated per treatment condition. Cells were incubated for 20 hours at 37°C with 5% humidified CO_2. Media was gently aspirated from the cells by a multichannel pipette, and 50 µL fresh DMEM+10%FBS containing 10 ng/mL IL-1β was added to each well. Each set of replicates were either untreated or treated with 10 ng/mL IL-1β for 2, 5, 10, 15, 20, 30, or 60 minutes. After IL-1β treatment the media was gently aspirated from the cells by a multichannel pipette, and cells were quickly washed with 100 µL PBS. PBS was aspirated off the cells, and cells were fixed in 150 µL of 4% paraformaldehyde (PFA) (Sigma Cat. No. P6148) in PBS for 20 minutes at room temperature. PFA was removed and cells were permeabilized by washing 3x for 5 minutes with PBS+ 0.1% TritonX-100 at room temperature. Cells were blocked for >1 hour in 50 µL of 5% normal goat serum (Invitrogen Cat. No. 31872) in PBS-T (blocking buffer) at room temperature on a shaker. Cells were incubated overnight at 4°C on a shaker in 50 µL primary antibody solution containing rb-α-NF-κB (1:1000) (Santa Cruz Biotechnologies Cat. No. sc-372) in blocking buffer. Primary antibody was removed and cells were washed 4x for 5 mins with 100 µL PBS-T on a shaker. Cells were incubated for >1 hour at room temperature in the dark on a shaker in 50 µL secondary antibody/nuclear staining solution containing dk-α-rb488 (1:1000) (Life Technologies

Cat. No. A21206) fluorescently conjugated secondary antibody (Invitrogen) plus 1:1000 Hoechst Stain (Life Technologies Cat. No. H3569) in blocking buffer. Secondary antibody/nuclear staining solution was removed and cells were washed 4x for 2 mins with 100 µL PBS-T on a shaker in the dark. After the final wash with PBS-T cells were left in 100 µL PBS for imaging with the ImageXpress High Content System (Molecular Devices). Cells were imaged at 20X magnification and 9 regions were imaged per well; regions were non-overlapping to avoid photobleaching. Images were analyzed using the Perkin-Elmer Columbus Server to examine cells in a single visual plane; the total number of cells were defined by locating the nuclei according to Hoescht staining and the cytoplasm was located according to NF-κB staining in unstimulated cells. Partially visualized cells on the border of an imaged region were removed from analysis. Intensity of the nuclear region was calculated based on fluorescent levels of the NF-κB stain that colocalized with the Hoescht stain. A threshold to define nuclear translocation was set by comparing the nuclear intensity of unstimulated and stimulated WT cells. Any cell with fluorescent intensity above the specified threshold was interpreted to have undergone nuclear translocation.[119] A one-way ANOVA was used to determine any significant difference in NF-κB nuclear translocation between the 3 cell lines. 3 biological replicates were performed.

LCLs were plated for NF-κB nuclear translocation assay when cells were in log phase of growth (cell density= $0.5x10^6$-$1x10^6$ cells/mL) and the culture volume of the flasks was 20-25 mL. 15-20 mL cell culture was collected (5 mL remained for continued culture) and centrifuged in a Sorvall ST8 (ThermoFisher Rotor 77-005-701) at 1200 RPM for 1 minute. The media was aspirated and the pellet resuspended in 20 mL of warmed RPMI 1640 (+ L-glutamine); media was not supplemented with serum to attach lymphoblastoid cells to the plate. The HCS is only able to quantify fluorescent intensity of cells in a single visual plane. Cells were counted and established

at a density of $0.18x10^6$ cells/mL, and 100 µL was plated in a black bottomed 96-well plate; 3-5 replicates were plated per TNF-α treatment condition. Plated culture was grown at 37°C with 5% humidified CO_2 for 18 hours. Media was aspirated from adherent cells, and 50 µL fresh RPMI 1640 containing 10 ng/mL TNF-α was added to each well. Each set of replicates were either untreated or treated with 10 ng/mL TNF-α for 30, 60, 90 or 120 minutes. After TNF-α treatment the media was aspirated from the cells, and cells were quickly washed with 100 µL PBS. PBS was aspirated from the cells, and cells were fixed in 150 µL of 4% PFA in PBS for at least 20 minutes at room temperature. PFA was removed and cells were permeabilized by washing 3x for 5 minutes with PBS+ 0.1% TritonX-100. Cells were blocked for >1 hour in 50 µL of 5% normal goat serum in PBS-T (blocking buffer) at room temperature on a shaker. Cells were incubated overnight at 4°C on a shaker in 50 µL primary antibody solution containing rabbit-α-NF-κB (1:1000) in blocking buffer. Primary antibody was removed, and cells were washed 4x for 2 mins with 100 µL PBS-T on a shaker. Cells were incubated for >1 hour at room temperature in the dark on a shaker in 50 µL secondary antibody/nuclear staining solution containing dk-α-rb488 (1:1000) fluorescently conjugated secondary antibody (Invitrogen) plus 1:1000 Hoechst Stain (Invitrogen) in blocking buffer. Secondary antibody/nuclear staining solution was removed, and cells were washed 4x for 2 mins with 100 µL PBS-T on a shaker in the dark. After the final wash with PBS-T cells were left in 100 µL PBS for imaging with the Operetta High Content System (Perkin-Elmer Part No. HH12000000). Nuclear translocation was quantified with Harmony Software (Perkin-Elmer) according to the method described above.[119] Cells were stored in PBS in the dark at 4°C until imaging with imaging. A one-way ANOVA was used to determine if a potential significant difference in NF-κB nuclear translocation could exist between the 3 cell lines. Statistical analysis was performed by comparing technical replicates of a single biological replicate and should be

interpreted with caution.

Transcription of NF-κB target genes: qPCR (as above with changes noted)

Fibroblasts were plated and incubated as above, and either untreated or incubated with 10 ng/mL IL-1β for 1 hour before RNA extraction with Trizol. LCLs were unstimulated and $2x10^6$ cells were lysed with Trizol and RNA extraction was performed as previously. qPCR for *IκB-α*, *A20*, and *IL-8* was performed as above. Primer sequences are as follows: *IκB-α* forward 5'-GCAAAATCCTGACCTGGTGT-3' and reverse 5'- GCTCGTCCTCTGTGAACTCC-3'; *A20* forward 5'- AGGACTGCTTCATCGTCTTG-3' and reverse 5'-CTTCCTTGAGCTTCTTGCAG-3'; and *IL-8* forward 5'- TAGCAAAATTGAGGCCAAGG-3' and reverse 5'- AGCAGACTAGGGTTGCCAGA-3'. Primer efficiencies were determined by standard curve: *IκB-α*=1.94, *A20*=1.98, and *IL-8*=1.97. qPCR reactions were carried out using the reaction and cycling conditions above, and final primer concentrations of 0.1 μM for *IκB-α* and *A20*, and 0.2 μM for *IL-8*. Data was analyzed using the $\Delta\Delta C_t$ comparative quantification algorithm described by Applied Biosystems to determine the range fold-change in gene expression as described above; *GUSB* was used as a house keeping gene to normalize gene expression, and WT untreated was used as a calibrator for the target gene of interest. A one-way ANOVA was used to determine any significant difference in target gene induction between the 3 fibroblast cell lines, and statistical analysis was performed on 3 biological replicates. A one-tailed t-test for unequal variance for each gene was used to determine if any potential difference could exist between target gene expression between WT and patient LCLs; statistical analysis was performed by comparing technical replicates of a single biological replicate and should be interpreted with caution.

3.2.4 Rescue of NF-κB Signaling Defects in Patient Fibroblasts

Nucleofection with Amaxa Human Dermal Fibroblast Nucleofector Kit

A plasmid containing WT TRAF6 in the vector pCMV6-XL4 was purchased from Origene (Cat. No. SC109845), and the empty vector was generated by NotI digestion (ThermoScientific Cat. No. FD0594) to remove the TRAF6 insert. Patient fibroblasts were collected at >80% confluence, established at a density of $0.5x10^6$ cells/mL per nucleofection condition in Falcon tubes (1 mL/tube), and centrifuged to remove media. Cell were nucleofected using the *Amaxa Human Dermal Fibroblast Nucleofector kit* (Lonza Cat. No. VPD-1001) according to the kit protocol. Cell pellets were resuspended in 100 µL complete nucleofection solution (Human dermal fibroblast nucleofector solution + supplement) and 300 µg of plasmid DNA was added and the mixture was transferred to the cuvette. Cells were transfected using the *U-023 high transfection efficiency for normal human dermal fibroblasts (NHDF) adult* program preset in the Amaxa Nucleofector. Immediately after transfection 500 µL of warm DMEM+10% FBS was added to the cuvette and the transfected cells were gently mixed by pipetting and transferred to a new falcon tube containing 1.5 mL warm DMEM+10% FBS. The total 2 mL cell solution was plated in a 6 well plate and incubated for 20 hours at 37°C with 5% humidified CO_2.

RNA extraction and qPCR

IL-1β stimulation of fibroblast cells, and RNA extraction and RT-qPCR for *IκB-α*, *A20*, and *IL-8* was performed as above. Data was analyzed as described above; *GUSB* was used as a house keeping gene to normalize gene expression, and patient untreated and transfected with empty vector was used as a calibrator for the target gene of interest. A one-tailed t-test for unequal variance was performed to determine any significant difference in target gene induction in patient

cells transfected with empty vector or WT *TRAF6* after IL-1β stimulation. Statistical analysis was performed on 3 biological replicates.

3.3 Results

3.3.1 Lymphoblastoid Cell Viability

Patient and carrier LCLs presented a challenge to grow; patient cells were consistently difficult to grow, and carrier cells were variable in their growth from frozen stocks received after transformation. To determine if there was a difference in cell viability compared to WT a resazurin assay was used; reduction of resazurin to resorufin due to cell metabolism of NADH to NAD^+ results in the release of a florescent signal proportional to cell viability.[120] Incubation of patient and carrier cells with resazurin dye resulted in much lower fluorescent intensity than that observed in WT LCLs, suggesting that patient and carrier LCLs exhibit lower cellular viability. One-way ANOVA revealed a statistically significant difference in cell viability between all cell lines, p-value=<0.0001. Paired t-tests revealed statistically significant differences in cell viability between the patient and WT sibling (***, p value=0.0009), and the carrier sibling and WT sibling (**, p-value=0.0043). (Figure 11). Statistical analysis was performed using technical replicates of a single biological replicate; due to challenges maintaining mutant LCLs it was difficult to reproduce experiments with lymphoblastoid cells.

3.3.2 TRAF6 C90F Analysis

Nonsense mutations and missense mutations that alter pre-mRNA splicing can cause changes in mRNA length and abundance, particularly if the mutation results in nonsense mediated decay.[121,122] RT-qPCR was used to investigate if the c.296G>T mutation has any effect on mRNA

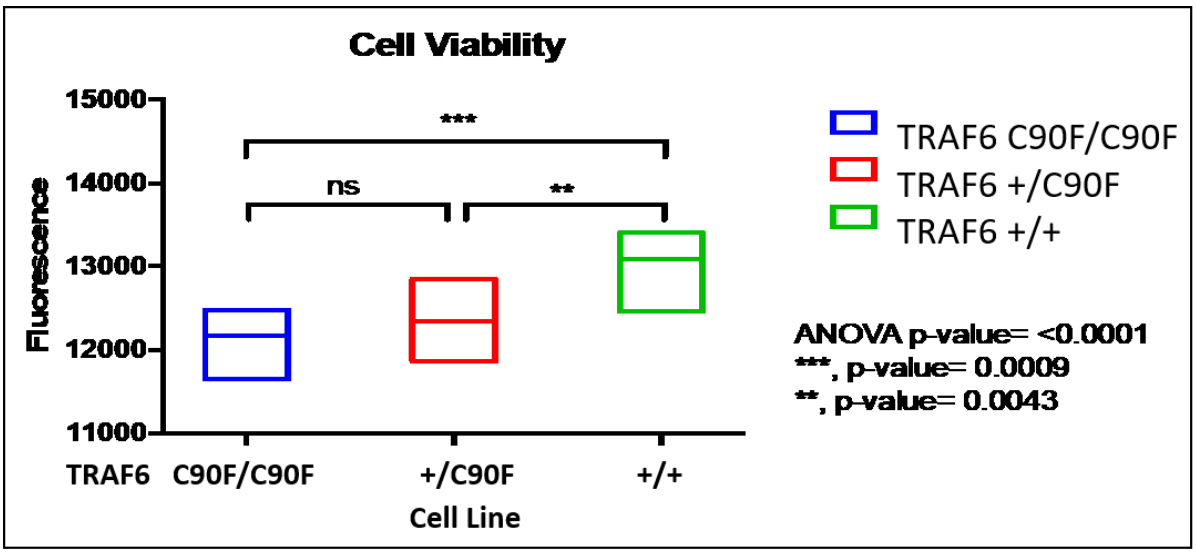

Figure 11. Cell viability is decreased in patient and carrier lymphoblastoid cells. Patient (TRAF6 C90F/C90F), carrier (TRAF6 +/C90F), and WT (TRAF6 +/+) LCLs were incubated with resazurin dye and fluorescence was determined as a measure of viability. One-way ANOVA revealed a significant difference in cell viability between the cell lines, with a p-value of <0.0001. Paired t-tests revealed statistically significant differences in cell viability between the patient and wild-type (WT) sibling (***, p value=0.0009), and the carrier sibling and WT sibling (**, p- value=0.0043). Based on 5 technical replicates of a single biological replicate.

abundance compared to WT levels. Patient TRAF6 gene expression compared to WT and carrier levels was analyzed by RT-qPCR and showed that there is no difference in the amount mRNA present in patient compared to control fibroblast cells (Figure 12). This prompted the investigation of the effect of the mutation at the protein level. The C90F mutation to the RING domain of TRAF6 is hypothesized to impair folding of this domain, and western blotting for TRAF6 protein was performed to determine if this mutation affects the abundance of TRAF6 protein. Analysis of TRAF6 protein abundance by western blotting suggests that the missense mutation is sufficient to cause a dramatic reduction in protein levels in both patient and carrier cells compared to WT cells, as TRAF6 protein from patient and carrier fibroblasts results in much lower band intensity (Figure 13a). Visualization of TRAF6 C90F/C90F protein from patient cells is only possible by loading at least 40 μg of protein extract; whereas, 20 μg of protein from WT extracts is sufficient to observe TRAF6 bands. Therefore, 40 μg of protein was loaded from all cell lines to visual protein from WT, carrier, and patient cells on the same gel (Figure13). Band quantification indicates that the patient and carrier fibroblast cells express significantly less TRAF6 protein than WT cells (One-way ANOVA p-value=7.64×10^{-6}), with carrier and patient cells expressing approximately 45% and 71% less TRAF6 protein than wild-type fibroblast cells. Translational repression using cycloheximide treatment was carried out to examine the half-life of the mutant TRAF6 protein. Western blotting showed that TRAF6 protein extracted from carrier and WT fibroblast cells is remarkably stable and does not begin to degrade until after 48 hours of treatment with 100 μM cycloheximide. However, TRAF6 C90F from the patient cells begins to decrease after just 8 hours of cycloheximide treatment, suggesting that the mutation reduces the stability of the protein (Figure 13b). The C90F mutation is in the RING domain of the TRAF6 protein, which is essential

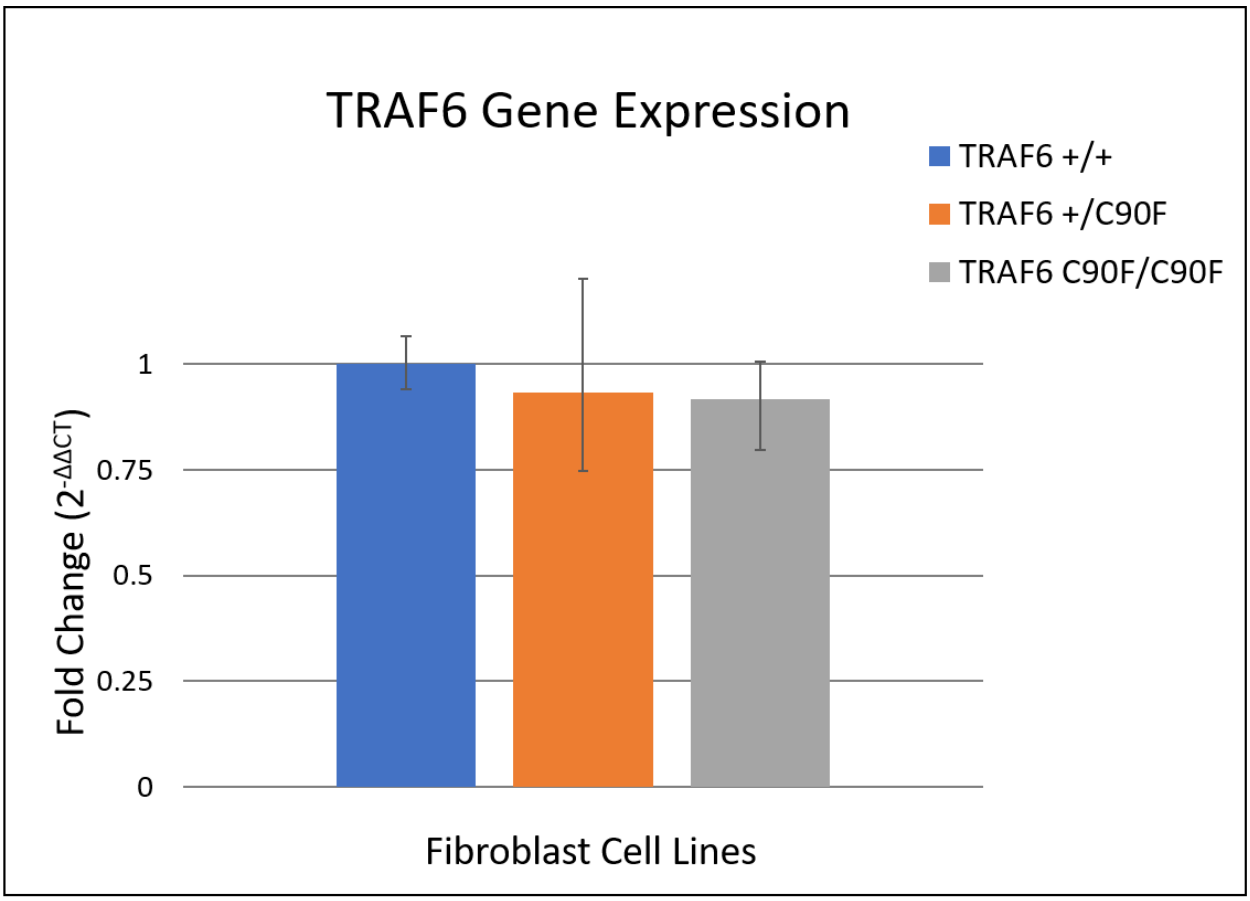

B.

Cell Line	TRAF6
TRAF6 +/+	1.00 (0.94-1.07)
TRAF6 +/C90F	0.93 (0.75-1.20)
TRAF6 C90F/C90F	0.92 (0.80-1.01)

Figure 12. TRAF6 gene expression is the same in patient and control cell lines. TRAF6 gene expression in WT (TRAF6 +/+), carrier (+/C90F), and patient (TRAF6 C90F/C90F) fibroblasts by RT-qPCR. Fold-change in gene expression was determined by normalizing TRAF6 values against an internal control (GUSB) and WT expression. A. Error bars represent the standard deviation between the 3 technical replicates per biological replicate. B. The range in fold-change of gene expression based on the standard deviation among technical replicates is shown in brackets. Data shown represent the average of 3 biological replicates

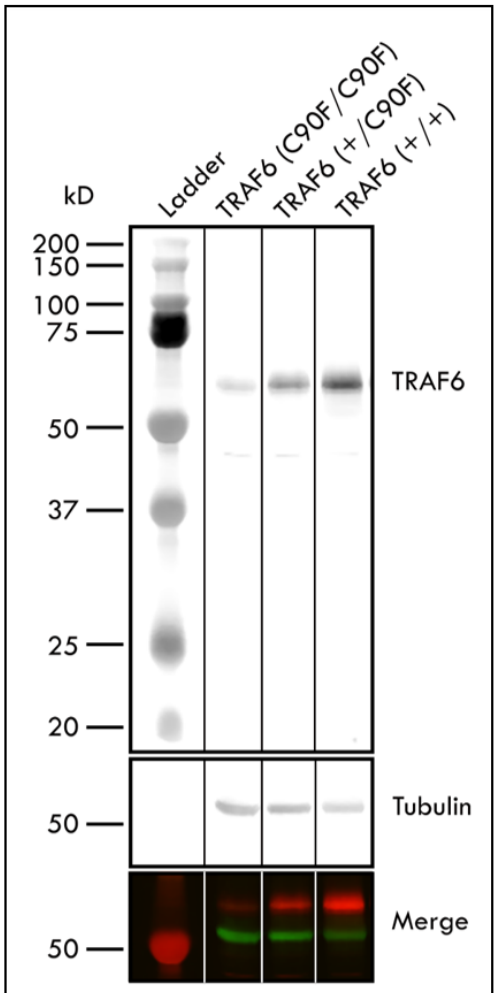

Figure 13. TRAF6 protein abundance and stability is decreased in patient cells. TRAF6 protein in patient (TRAF6 C90F/C90F), carrier (TRAF6 +/C90F), and WT (TRAF6 +/+) fibroblasts by western blot. Membrane was probed with rbαTRAF6 (60 kD) and msαTubulin (50 kD) primary antibodies, and protein was visualized by Licor imaging. A. Endogenous protein from fibroblasts. One-way Anova revealed a significant difference in TRAF6 band intensity between the 3 cell lines (p-value=$3.1x10^{-5}$) based on 5 biological replicates. Each protein sample was run in triplicate on the same blot for quantification. Duplicates of each sample were removed; lines represent where the blot was cropped and reassembled. B. Cells were treated with 10 uM CHX before lysis. WT and carrier untreated/DMSO/8 hr CHX were run on 1 blot, and carrier 24/36/48 hr CHX and patient samples were run on a 2nd blot. Lines represent where the blot was cropped and reassembled for continuity.

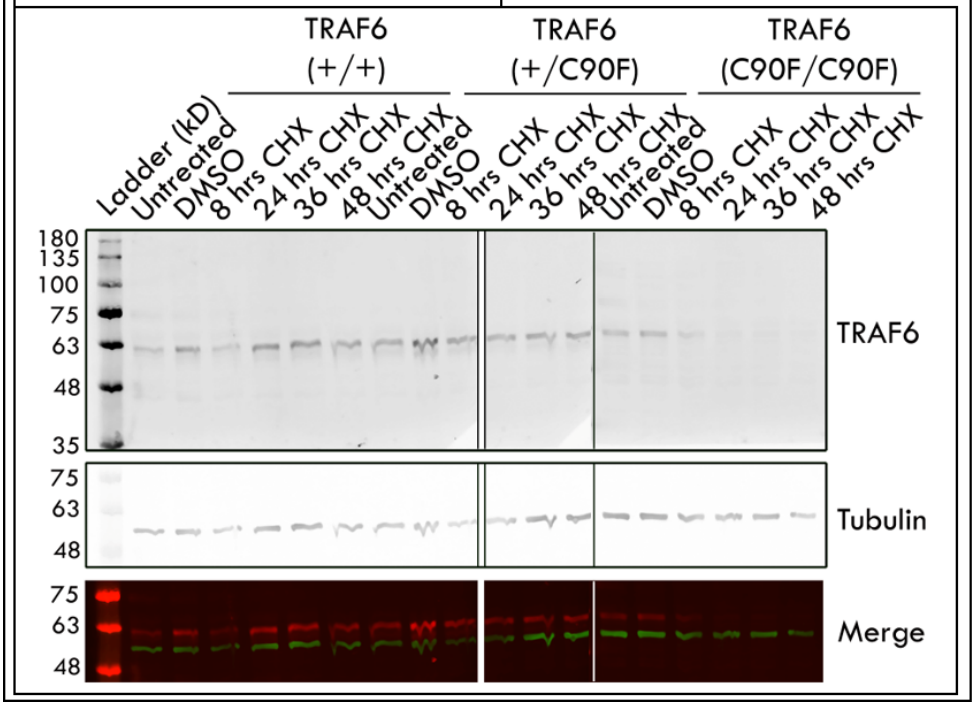

for mediating NEMO ubiquitination and NF-κB pathway activation in response to numerous cytokines.[112] NMR spectroscopy was used to examine the effect of the mutation on the RING domain structure by expressing the recombinant protein in *E. coli*. NMR spectroscopy was used to examine the structural effect of the C90F mutation on the TRAF6 RING domain. The WT TRAF6 RING domain was successfully expressed in *E.coli* and purified by FPLC (Figure 14), and produced a spectrum (Figure 15) that is consistent with a folded protein and previously documented TRAF6 RING domain structure.[123] However, it was not possible to purify a sufficient amount of the mutant RING domain to obtain a spectrum. The C90F TRAF6 RING domain was expressed at very low levels in *E. coli* (Figure 16a) and the small amount that was isolated was lost during the purification process (Figure 16b). It is possible that the mutant RING domain is insoluble, so proteins obtained from the lysate supernatant and pellet of *E. coli* expressing the WT and mutant TRAF6 RING domains were compared by Coomassie staining. When protein was extracted a second time the mutant RING domain was still expressed at a much lower level than WT; however, there is a large amount of insoluble TRAF6 protein in the pellets of both the WT and mutant RING domain (Figure 16c).

3.3.3 NF-κB Signaling Analysis

Mutation to the TRAF6 RING domain is hypothesized to impair activation of the IKK complex via loss of ubiquitination of NEMO and subsequently results in impaired activation of NF-κB signaling. The NF-κB pathway can be activated through multiple membrane receptors and by numerous cytokines, including IL-1β and TNF-α.[24–26,28,32] TRAF6 is unique in the TRAF family as it is the only member to mediate signals from the IL-1/TLR families; TRAF2 and 5 are the main adaptors in response to TNF-α stimulation.[32,79,96] NF-κB signaling was investigated at multiple

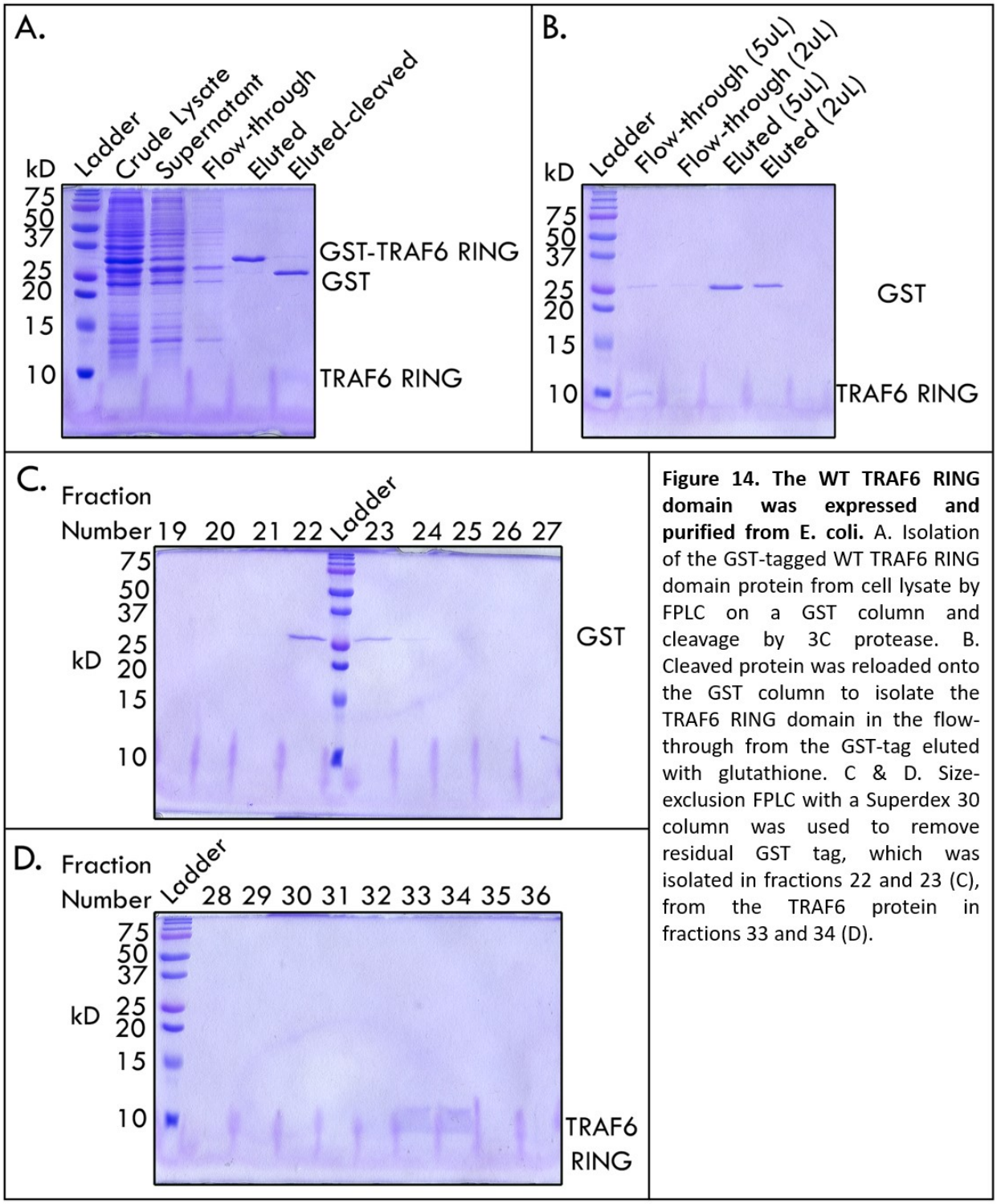

Figure 14. The WT TRAF6 RING domain was expressed and purified from E. coli. A. Isolation of the GST-tagged WT TRAF6 RING domain protein from cell lysate by FPLC on a GST column and cleavage by 3C protease. B. Cleaved protein was reloaded onto the GST column to isolate the TRAF6 RING domain in the flow-through from the GST-tag eluted with glutathione. C & D. Size-exclusion FPLC with a Superdex 30 column was used to remove residual GST tag, which was isolated in fractions 22 and 23 (C), from the TRAF6 protein in fractions 33 and 34 (D).

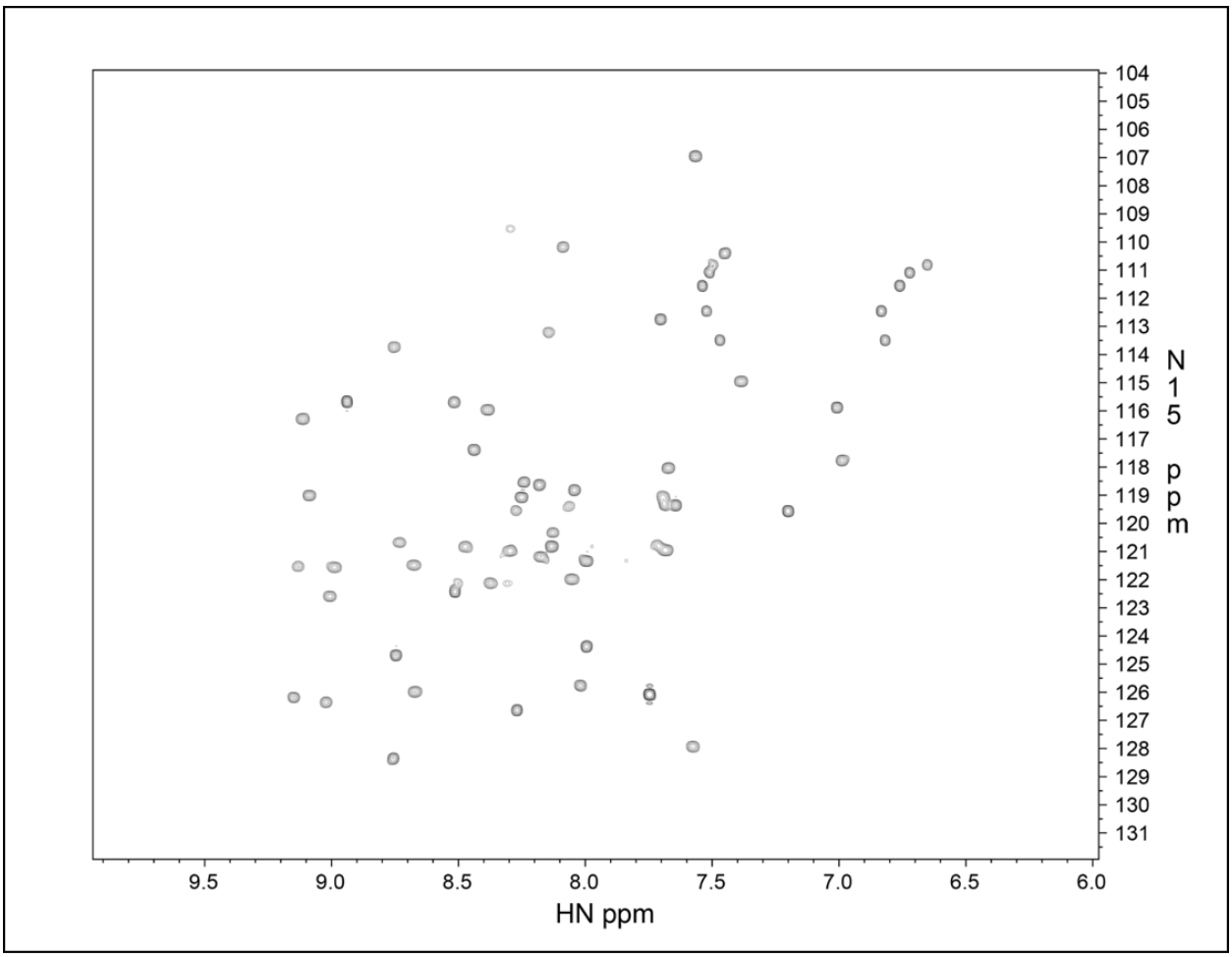

Figure 15. The WT TRAF6 RING domain produces a spectrum consistent with a folded protein. Protein was expressed and purified from E. coli and a 2D 1H-15N-HSQC spectrum was obtained on a 600 MHz NMR spectrophotometer. The X-axis represents signals from protons and the Y-axis shows signals from 15 nitrogen. Interactions between protons and ^{15}N are plotted.

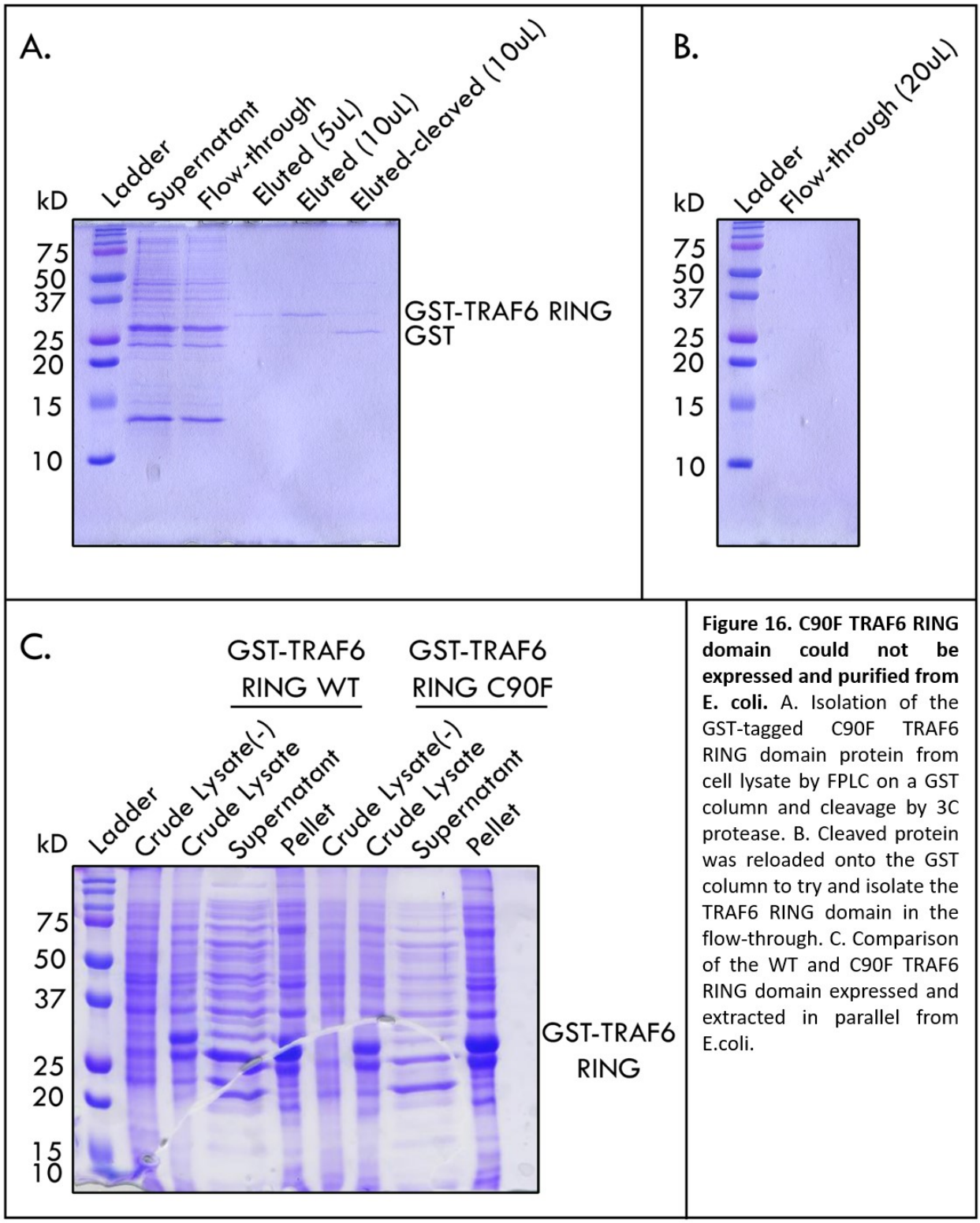

Figure 16. C90F TRAF6 RING domain could not be expressed and purified from E. coli. A. Isolation of the GST-tagged C90F TRAF6 RING domain protein from cell lysate by FPLC on a GST column and cleavage by 3C protease. B. Cleaved protein was reloaded onto the GST column to try and isolate the TRAF6 RING domain in the flow-through. C. Comparison of the WT and C90F TRAF6 RING domain expressed and extracted in parallel from E.coli.

points of the signaling cascade to identify if there was complete failure of activation, or if compensatory mechanisms could exist at certain levels in the pathway. IKK complex activation allows for phosphorylation and degradation of the IκB-α protein and subsequent release of the NF-κB transcription factor. Western blotting showed that patient fibroblast cells were unable to phosphorylate and degrade the IκB-α protein, a requirement for NF-κB translocation to the nucleus, in response to IL-1β stimulation at all treatment times tested. Expression of phospho-IκB-α is never observed, and total IκB-α remains abundant. Whereas, carrier and homozygous WT cells were both competent to execute this signaling process rapidly within minutes of cytokine stimulation (Figure 17); after just 2 minutes of IL-1β stimulation IκB-α becomes phosphorylated and by 10 minutes of treatment it is beginning to degrade. Interestingly, patient fibroblasts were competent to execute this process in response to TNF-α; within 5 minutes of cytokine stimulation IκB-α was phosphorylated and by 30 minutes the protein was degraded, similar to WT and carrier fibroblasts (Figure 18).

IκB-α sequesters NF-κB in the nucleus; therefore, the subsequent signaling step of NF-κB nuclear translocation was evaluated using IL-1β as a stimulus. Consistent with the loss of IκB-α phosphorylation and degradation patient cells were unable to translocate the NF-κB transcriptional subunits to the nucleus following up to 60 minutes of IL-1β stimulation. The fluorescent signal for NF-κB protein never colocalizes with the nuclear stain above untreated levels in patient fibroblasts. Carrier and homozygous WT cells responded quickly to cytokine treatment and translocated NF-κB to the nucleus within 10 minutes of IL-1β stimulation, with NF-κB protein accumulating maximally in the nucleus by 30 minutes of treatment (Figure 19a). Quantification of nuclear translocation for an average of 5000 cells per cell line per condition showed that at 30 minutes of stimulation 95% of WT and 93% of carrier cells had a nuclear NF-κB fluorescent intensity above

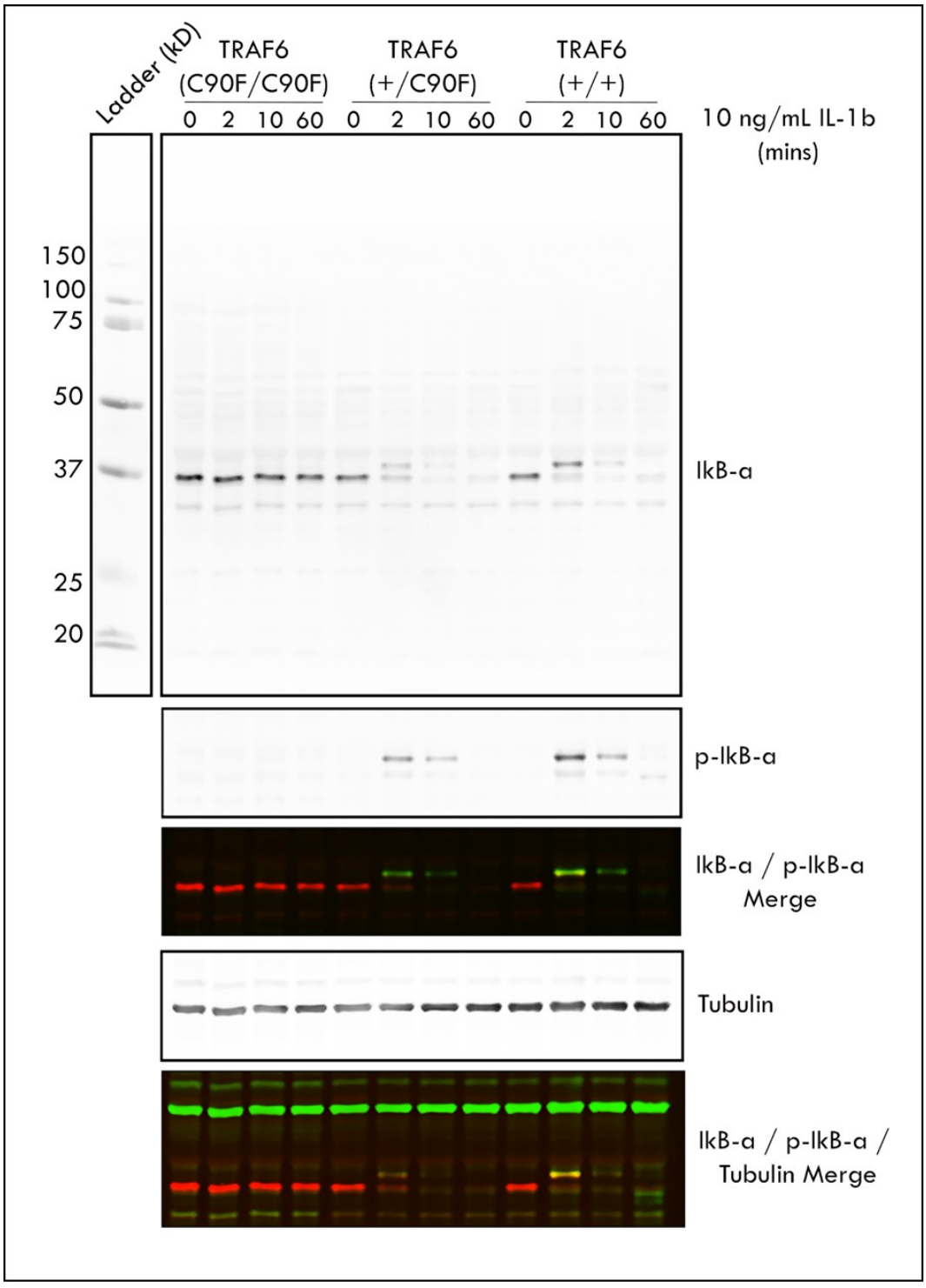

Figure 17. IkB-a phosphorylation and degradation does not occur after IL-1b stimulation of patient cells. Total and phospho-IkB-α protein in patient (TRAF6 C90F/C90F), carrier (TRAF6 +/C90F), and wild-type (TRAF6 +/+) fibroblasts. Cells were stimulated with IL-1β before cell lysis. The membrane was probed first with msαphospho-IkB-α (39 kD) and rbαIkB-α (37 kD) primary antibodies and visualized by Licor imaging, followed by probing with msαTubulin (50 kD) primary antibody and visualization.

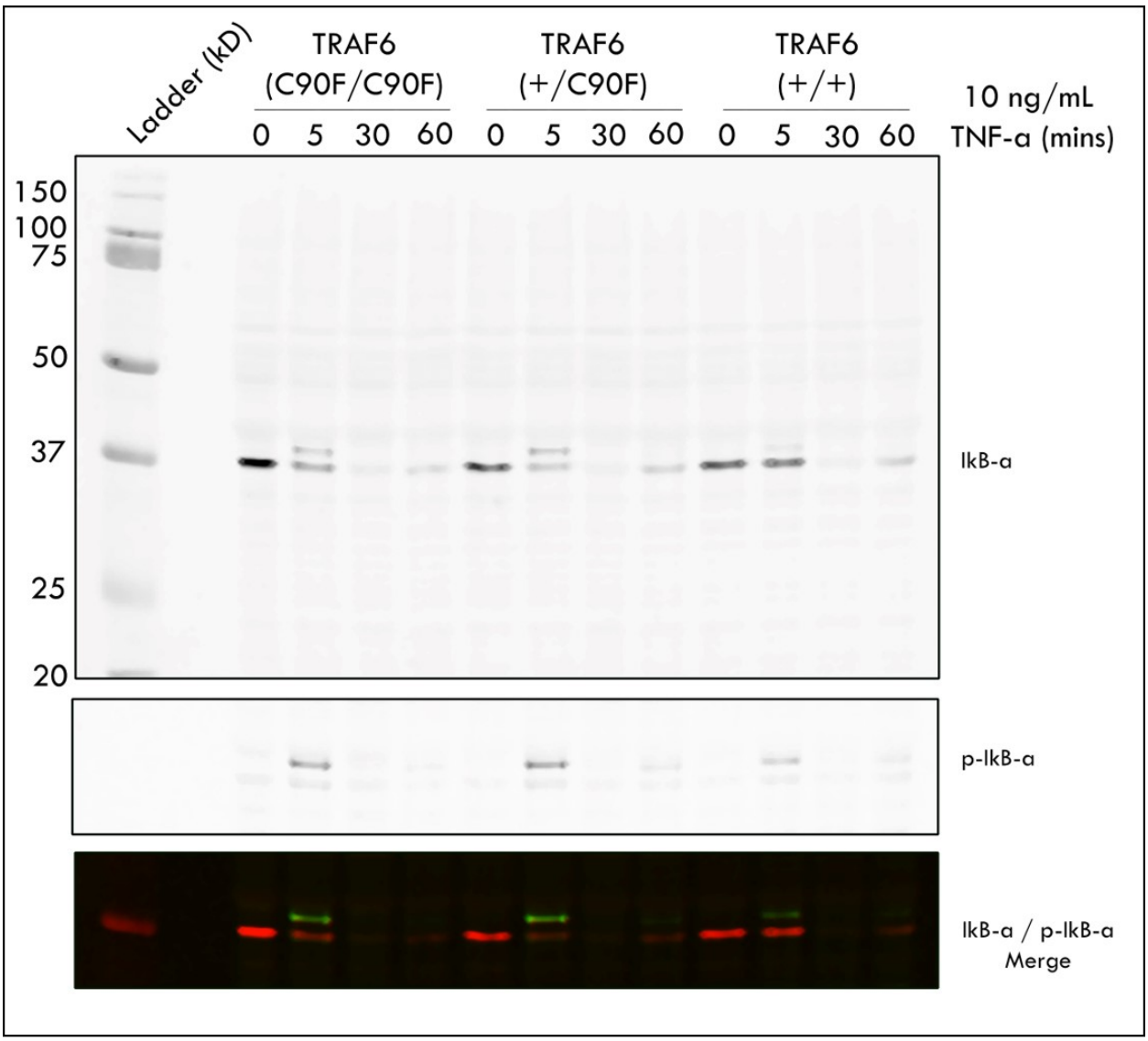

Figure 18. IkB-α phosphorylation and degradation after TNF-α stimulation is normal in patient cells. Total and phospho-IkB-α protein in patient (TRAF6 C90F/C90F), carrier (TRAF6 +/C90F), and wild-type (TRAF6 +/+) fibroblasts. Cells were stimulated with TNF-a before cell lysis. The membrane was probed with msαphospho-IkB-α (39 kD) and rbαIkB-α (37 kD) primary antibodies and visualized by Licor imaging.

untreated levels; indicating that the transcription factor had moved to the nucleus. However, throughout cytokine stimulation to 60 minutes only 6.5% of patient cells had nuclear NF-κB intensity above basal levels (Figure 19b). One-way ANOVA showed a statistically significant difference in nuclear translocation between cell lines (p-value=$3.99x10^{-7}$). Consistent with the results for IκB-α phosphorylation and degradation, nuclear translocation of NF-κB was completely abolished in patient fibroblasts following IL-1β stimulation.

Preliminary examination of NF-κB nuclear translocation in LCLs after stimulation with TNF-α suggests that patient (TRAF6 C90F/C90F) LCLs have reduced NF-κB nuclear translocation compared to carrier (TRAF6 +/C90F) and WT (TRAF6 +/+) derived LCLs regardless of TNF-α stimulation. Furthermore, LCLs heterozygous for the *TRAF6* mutation have lower NF-κB nuclear translocation than WT LCLs at all TNF-α treatment times tested. Similar to the responses observed in patient fibroblast cells (Figure 19), the data shows that patient LCLs respond to TNF-α treatment by transporting NF-κB to the nucleus; however, accumulation in the nucleus is lower than control cell lines at all TNF-α treatment lengths (Figure 20a). Analysis of the 5 technical replicates of a single experiment by one-way ANOVA indicates a statistically significant difference in NF-κB nuclear translocation between the three cell lines (p=0.006) (Figure 20b). However, this data has been challenging to reproduce in independent experiments, as patient and carrier LCLs are difficult to maintain.

Translocation of the NF-κB transcription factor to the nucleus allows for subsequent transcription of the NF-κB target genes *IκB-α*, *A20* and *IL-8* among many. *IκB-α* and *A20* are both negative regulators of NF-κB signaling and are induced upon pathway stimulation.[24,25] A20 is a multifunctional ubiquitin editing enzyme; it has N-terminal deubiquinating activity and a C-terminal E3 ligase activity to mediate NF-κB activity by deubiquitinating the K63 linked chains

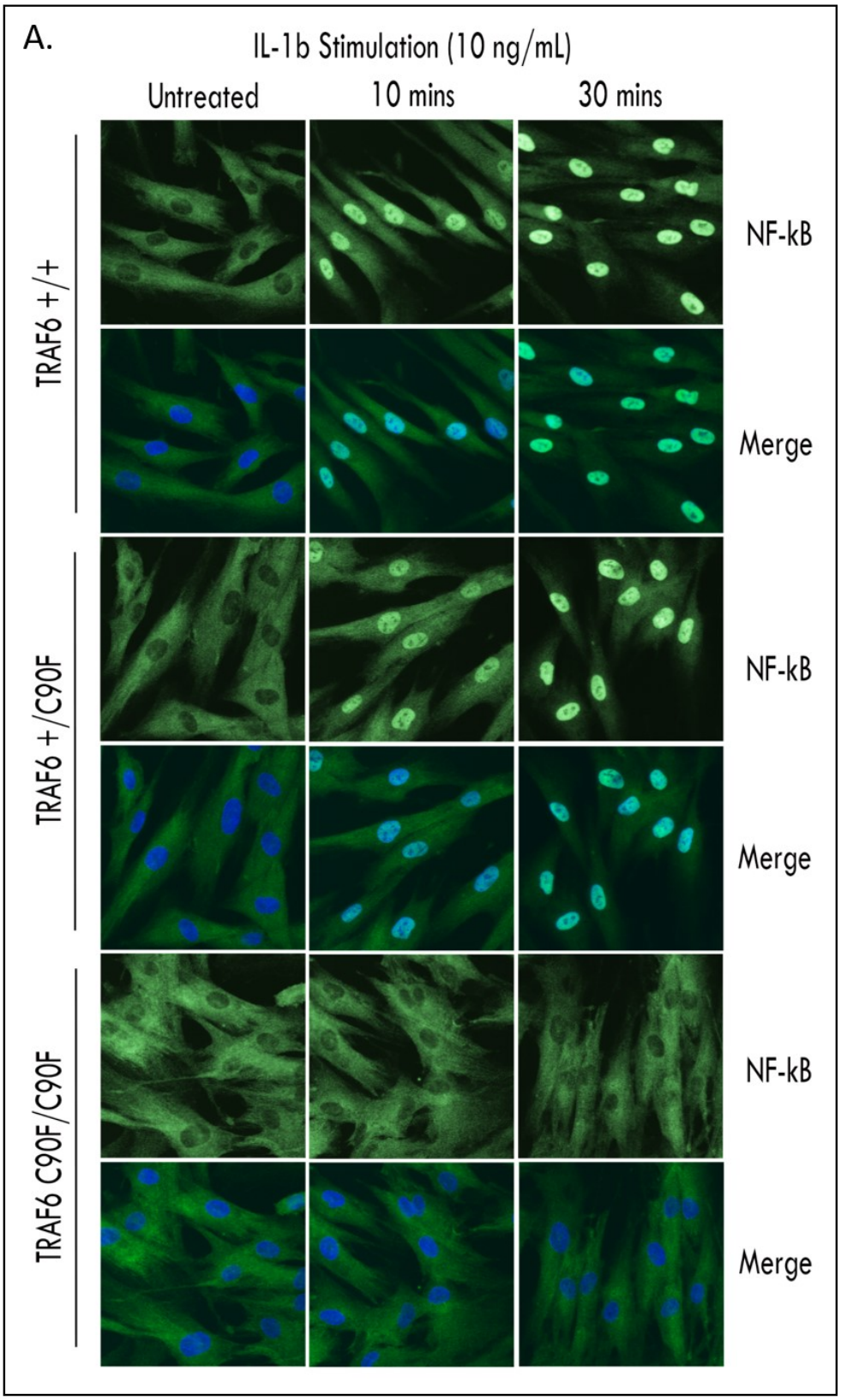

Figure 19. IL-1β dependent NF-κB nuclear translocation is abolished in patient fibroblasts.

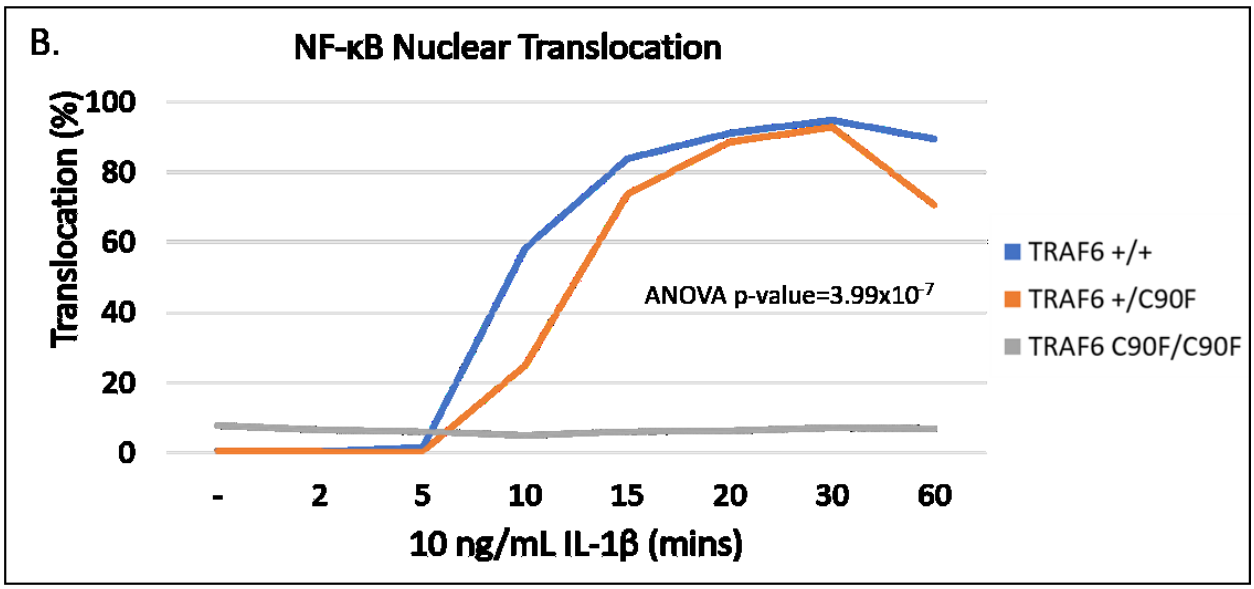

Figure 19. IL-1β dependent NF-κB nuclear translocation is abolished in patient fibroblasts. NF-kB protein in patient (TRAF6 C90F/C90F), carrier (TRAF6 +/C90F), and wild-type (TRAF6 +/+) fibroblasts imaged by HCS. Cells were stimulated with IL-1β before treatment with para-formaldehyde. A. Cells were probed with rbαNF-kB (p65) primary antibody and Hoecsht stain. B. Nuclear translocation was quantified with the Columbus Server (Perkin-Elmer). One-way ANOVA p-value=3.99×10^{-7}.

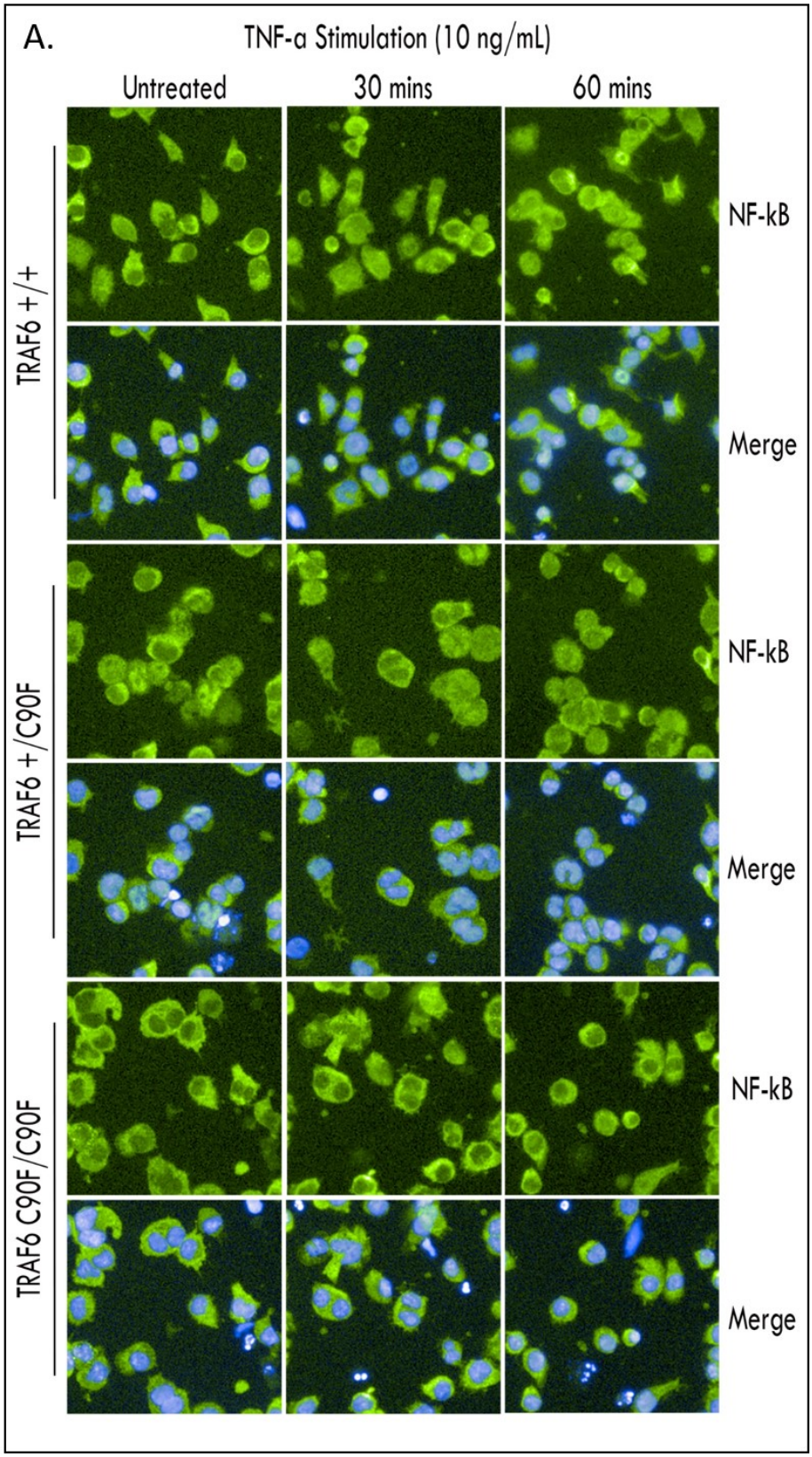

Figure 20. NF-κB nuclear translocation is impaired in patient lymphoblastoid cells.

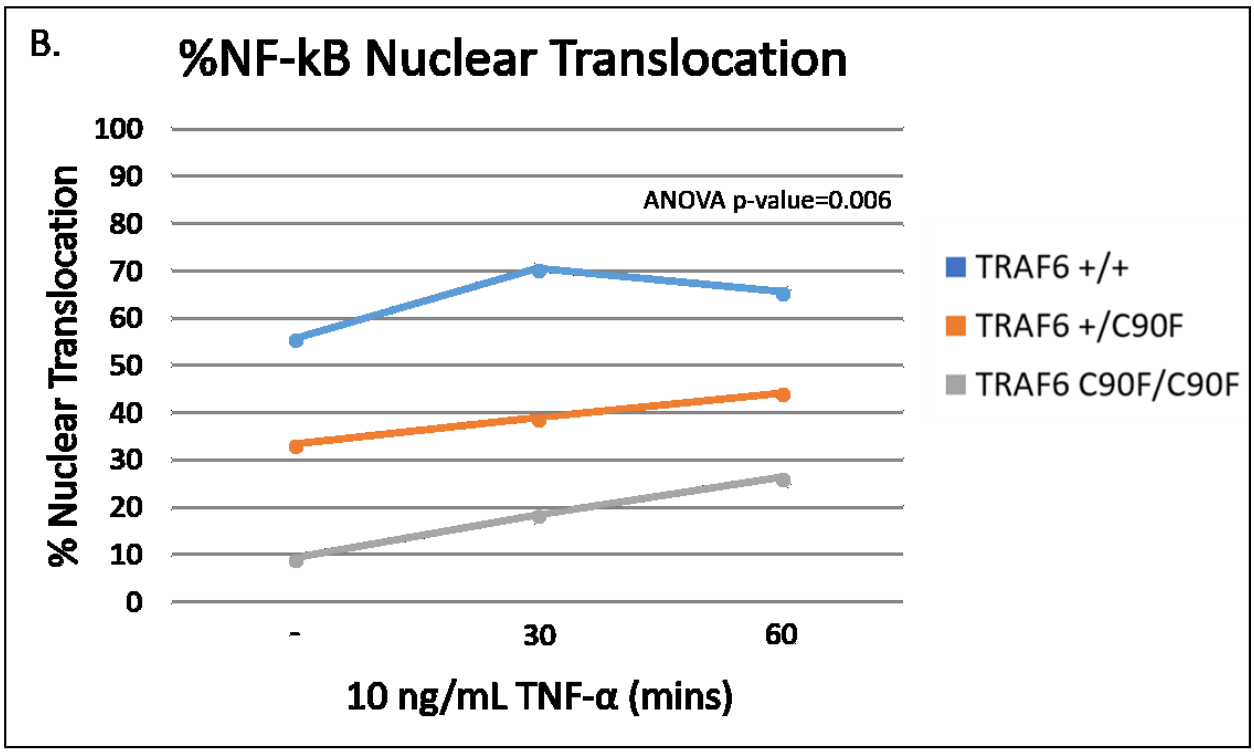

Figure 20. NF-κB nuclear translocation is impaired in patient lymphoblastoid cells. NF-κB protein in patient (TRAF6 C90F/C90F), carrier (TRAF6 +/C90F), and wild-type (TRAF6 +/+) LCLs imaged by Operetta. Cells were stimulated with TNF-α before treatment with para-formaldehyde. A. Cells were probed with rbαNF-kB (p65) primary antibody and Hoecsht stain. B. Nuclear translocation was quantified with Harmony software (Perkin-Elmer). One-way ANOVA p-value=0.006 (based on technical replicates of 1 biological replicate).

on NEMO, or by conjugating other regulatory proteins with K48 linked ubiquitin for proteasomal degradation.[124] IL-8 is secreted by fibroblasts as a part of the inflammatory response to IL-1β stimulation.[125] Fibroblasts were stimulated with IL-1β and RT-qPCR was used to examine the expression of *IκB-α*, *A20*, and *IL-8*. Upon 1 hour stimulation with IL-1β WT and carrier fibroblast cells exhibited strong induction of all three NF-κB target genes, whereas patient fibroblasts showed a small change in gene induction in response to IL-1β (Figure 21). One-way ANOVA indicated a significant difference in target gene expression induction between cell lines, with carrier and WT cells inducing a fold-change of 17-25x for *IκB-α* (p-value=4.03×10^{-8}), 87-147x for *A20* (p-value=5.44×10^{-9}), and 118-153x for *IL-8* (p-value=1.2×10^{-7}) over unstimulated gene expression levels.

Immortalization of human B-cells by transformation with Epstein-Barr virus results in constitutive NF-κB signaling through the CD40 receptor.[126] This constitutive signaling was used as a proxy for NF-κB activity in the absence of cytokine activation. Preliminary results suggest patient lymphoblastoid cells have decreased expression of NF-κB target genes compared to wildtype LCLs (Figure 22). One-tailed t-test for unequal variance showed a significant difference in fold-change in patient gene expression for *IκB-α* (p-value=0.003), *A20* (p-value=2.39×10^{-6}), and *IL-8* (p-value=0.004) compared to WT gene expression. However, due to challenges propagating the patient LCLs only one biological replicate was performed, and statistical analysis was performed using technical replicates.

3.3.4 TRAF6 Rescue of NF-κB Target Gene Expression

The NF-κB pathway encompasses numerous constituents, many of which are known to cause human disease (Table 1). The patient could harbor a mutation in another component of the pathway

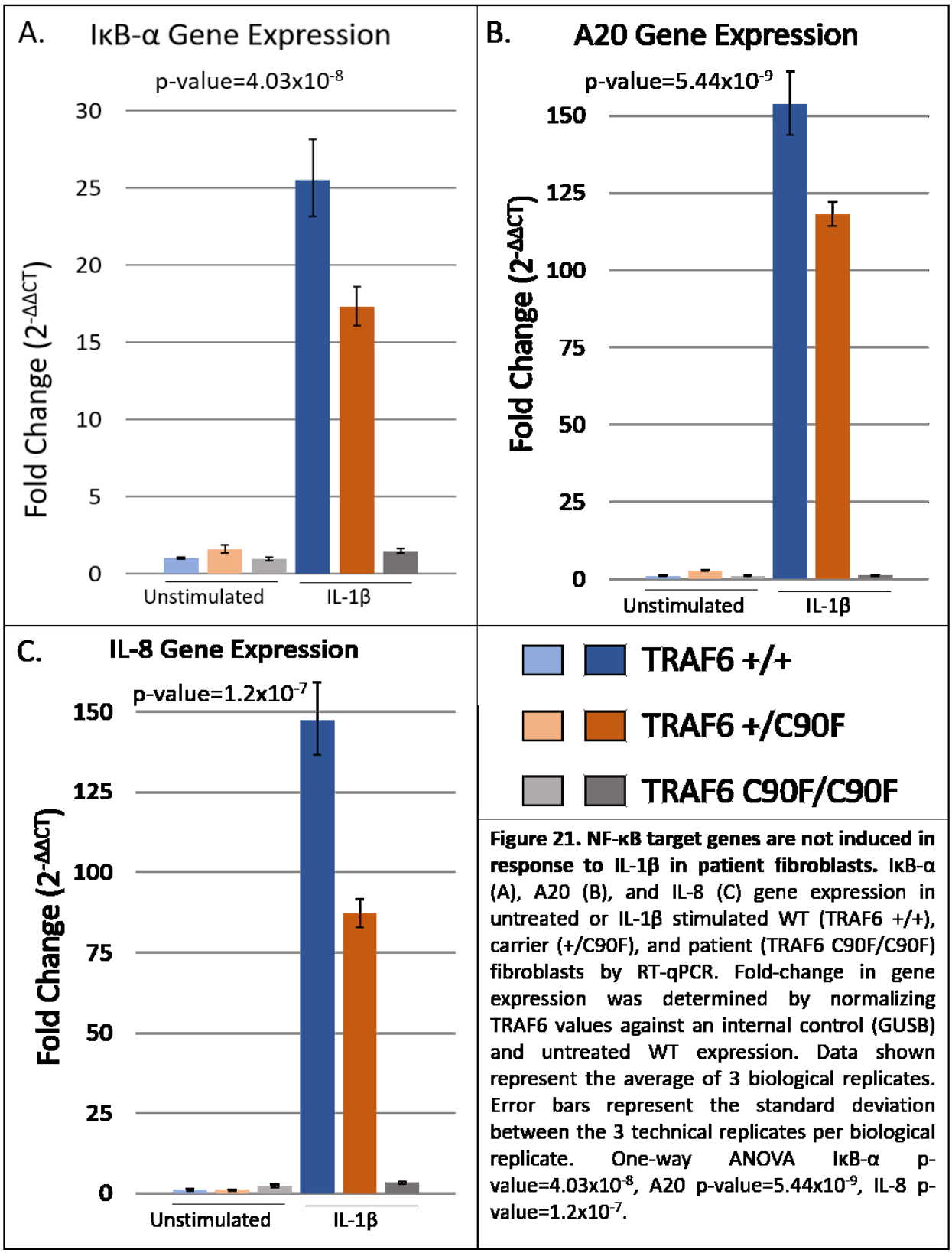

Figure 21. NF-κB target genes are not induced in response to IL-1β in patient fibroblasts. IκB-α (A), A20 (B), and IL-8 (C) gene expression in untreated or IL-1β stimulated WT (TRAF6 +/+), carrier (+/C90F), and patient (TRAF6 C90F/C90F) fibroblasts by RT-qPCR. Fold-change in gene expression was determined by normalizing TRAF6 values against an internal control (GUSB) and untreated WT expression. Data shown represent the average of 3 biological replicates. Error bars represent the standard deviation between the 3 technical replicates per biological replicate. One-way ANOVA IκB-α p-value=4.03×10^{-8}, A20 p-value=5.44×10^{-9}, IL-8 p-value=1.2×10^{-7}.

Cell Line	Stimulation	IkB-α	A20	IL-8
TRAF6 +/+	Untreated	1.00 (0.93-1.08)	1.00 (0.87-1.18)	1.00 (0.93-1.07)
	IL-1β	25.55 (23.16-28.18)	147.30 (136.38-159.22)	153.74 (143.80-164.40)
TRAF6 +/C90F	Untreated	1.60 (1.38-1.86)	0.96 (0.83-1.12)	2.64 (2.50-2.78)
	IL-1β	17.31 (16.10-18.62)	87.01 (82.71-91.60)	118.07 (114.43-121.87)
TRAF6 C90F/C90F	Untreated	0.96 (0.87-1.06)	2.14 (1.75-2.63)	0.99 (0.93-1.06)
	IL-1β	1.49 (1.35-1.64)	3.19 (2.82-3.62)	1.19 (1.11-1.28)

Figure 21d. NF-κB target genes are not induced in response to IL-1β in patient fibroblasts. IκB-α, A20, and IL-8 gene expression in untreated or IL-1 β stimulated WT (TRAF6 +/+), carrier (+/C90F), and patient (TRAF6 C90F/C90F) fibroblasts by RT-qPCR. Fold-change in gene expression was determined by normalizing TRAF6 values against an internal control (GUSB) and untreated WT expression. The range in fold-change of gene expression based on the standard deviation among technical replicates is shown in brackets. Data shown represent the average of 3 biological replicates. One-way ANOVA IκB-α p-value=4.03×10^{-8}, A20 p-value=5.44×10^{-9}, IL-8 p-value=1.2×10^{-7}.

A.

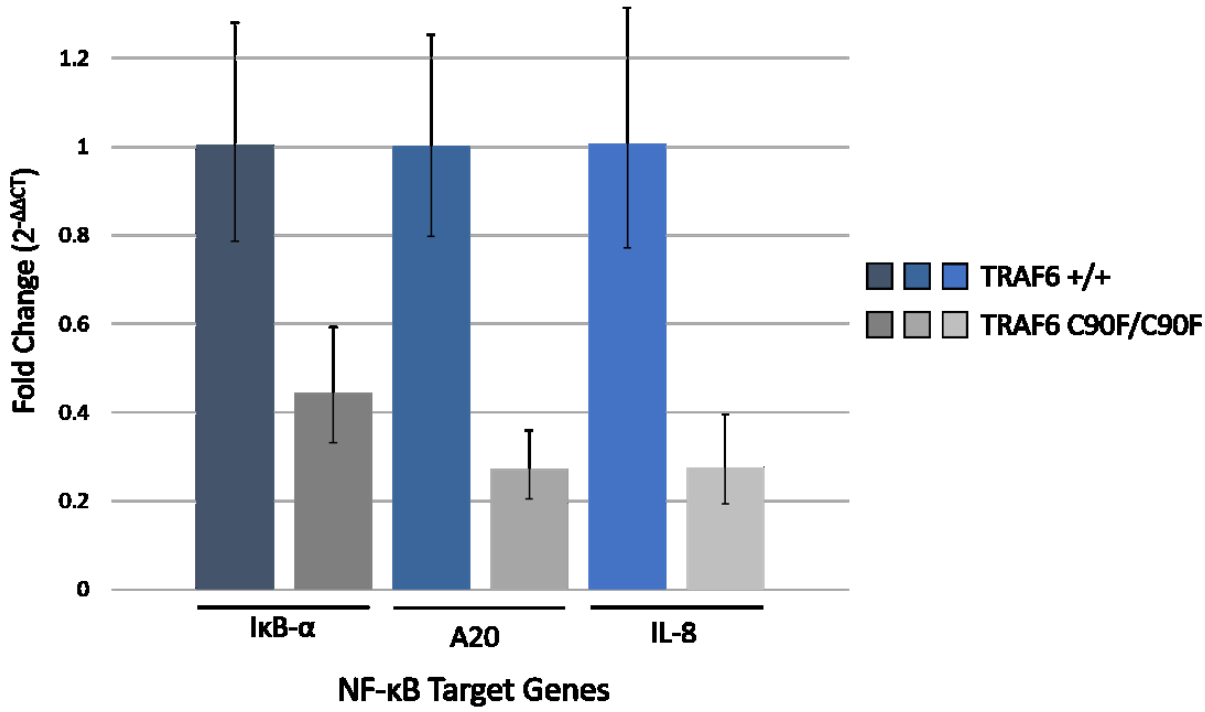

B.

Cell Line	IkB-α	A20	IL-8
TRAF6 +/+	1.00 (079-1.28)	1.00 (0.80-1.25)	1.00 (0.77-1.31)
TRAF6 C90F/C90F	0.44 (0.33-0.59)	0.27 (0.21-0.36)	0.28 (0.19-0.39)

Figure 22. NF-κB target gene expression is reduced in patient lymphoblastoid cells. IκB-α, A20, and IL-8 gene expression in WT (TRAF6 +/+) and patient (TRAF6 C90F/C90F) LCLs by RT-qPCR. Fold-change in gene expression was determined by normalizing TRAF6 values against an internal control (GUSB) and WT expression. A. Error bars represent the standard deviation between the 3 technical replicates. One-tailed t-test for unequal variance IκB-α p-value=0.003, A20 p-value=2.39×10^{-6}, IL-8 p-value=0.004 based on technical replicates from 1 biological replicate. B. The range in fold-change of gene expression based on the standard deviation among technical replicates is shown in brackets.

that was undetected by our filtering strategy. To provide support that the TRAF6 C90F mutation is the cause of the defective NF-κB pathway activation in our patient's cells a wild-type copy of the *TRAF6* gene was introduced and expressed in patient fibroblast cells to rescue the IL-1β mediated signaling impairment. Transfection of WT *TRAF6* but not empty vector allowed patient fibroblasts to induce the NF-κB target genes *IκB-α*, *A20*, and *IL-8* following IL-1β stimulation (Figure 23). Gene expression was not induced to the level observed in WT or carrier fibroblast cells, but patient cells were now competent to induce gene expression above baseline levels in the presence of the cytokine, which was not possible in untransfected cells (Figure 20) or in cells transfected with the empty vector. One-tailed t-test for unequal variances showed a significant difference in the fold-change of NF-κB target gene expression in response to IL-1β in fibroblasts transfected with WT *TRAF6* or empty vector, where an average fold-change increase of 21.5 for *IκB-α* (p-value=0.02), 13.2 for *A20* (p-value=0.01), and 16.3 for *IL-8* (p-value=0.02) was observed for stimulated cells expressing WT *TRAF6*. Analysis is based on 3 biological replicates.

3.4 Discussion

Functional analysis of the homozygous *TRAF6* C90F mutation showed defects at the protein level and on NF-κB pathway activation. Overall, the data indicate that the C90F mutation reduces the stability of TRAF6 protein and results in a significant decrease in cellular protein abundance. Both carrier and patient protein levels were decreased compared to WT; carrier levels were roughly 45% lower than WT which is expected with heterozygosity of a loss of function allele. TRAF6 protein stability was unaffected in carrier cells, likely because the bulk of the protein in the cell is from the WT *TRAF6* allele. Expressing the recombinant RING domain independently suggests that the mutation is interferes with protein expression levels, as sufficient mutant protein could not

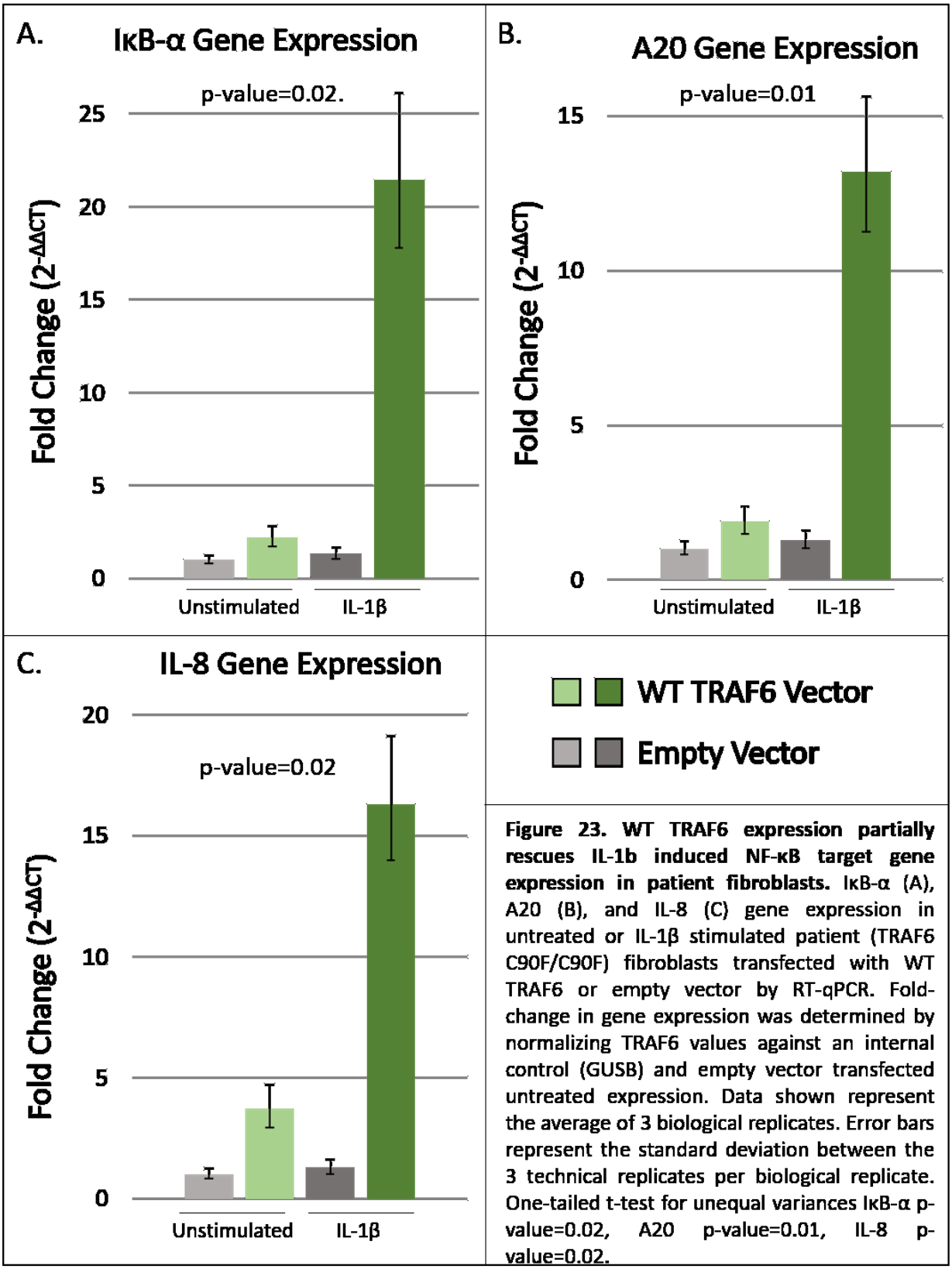

Figure 23. WT TRAF6 expression partially rescues IL-1b induced NF-κB target gene expression in patient fibroblasts. IκB-α (A), A20 (B), and IL-8 (C) gene expression in untreated or IL-1β stimulated patient (TRAF6 C90F/C90F) fibroblasts transfected with WT TRAF6 or empty vector by RT-qPCR. Fold-change in gene expression was determined by normalizing TRAF6 values against an internal control (GUSB) and empty vector transfected untreated expression. Data shown represent the average of 3 biological replicates. Error bars represent the standard deviation between the 3 technical replicates per biological replicate. One-tailed t-test for unequal variances IκB-α p-value=0.02, A20 p-value=0.01, IL-8 p-value=0.02.

Vector	Stimulation	IkB-α	A20	IL-8
Empty Vector	Untreated	1.00 (0.81-1.25)	1.00 (0.81-1.26)	1.00 (0.83-1.23)
	IL-1β	1.32 (1.04-1.69)	1.29 (1.04-1.61)	1.29 (1.04-1.61)
WT TRAF6	Untreated	2.21 (1.73-2.83)	1.89 (1.50-2.38)	3.73 (2.95-4.72)
	IL-1β	21.45 (17.79-26.12)	13.21 (11.27-15.63)	16.28 (13.99-19.13)

Figure 23d. WT TRAF6 expression partially rescues IL-1b induced NF-κB target gene expression in patient fibroblasts. IκB-α, A20, and IL-8 gene expression in untreated or IL-1β stimulated patient (TRAF6 C90F/C90F) fibroblasts transfected with WT TRAF6 or empty vector by RT-qPCR. Fold-change in gene expression was determined by normalizing TRAF6 values against an internal control (GUSB) and empty vector transfected untreated expression. The range in fold-change of gene expression based on the standard deviation among technical replicates is shown in brackets. One-tailed t-test for unequal variances IκB-α p-value=0.02, A20 p-value=0.01, IL-8 p-value=0.02 based on 3 biological replicates.

be obtained for structural analysis. To try and overcome this issue *E. coli* cultures could be further scaled up to try and isolate more protein for purification. Additionally, if the mutant protein can be successfully expressed but is degraded over the course of purification because it is unstable, then protocols for refolding zinc binding proteins could be used to try and obtain and NMR spectrum from the mutant protein. It is possible that the protein is so unfolded that it is sequestered in inclusion bodies in the cell to be processed for degradation. Analysis of the insoluble protein fraction could not conclusively support this hypothesis as large amounts of WT and C90F TRAF6 was observed in the lysate pellet. Furthermore, introduction of WT TRAF6 into patient cells rescued signaling defects suggesting that the specific defect in TRAF6 is underlying the impaired signaling. These data support pathogenicity of the TRAF6 C90F variant, as faulty NF-κB signaling is known to cause immunodeficiency.[127]

Impaired NF-κB signaling is a known cause of human immunodeficiency[127] and IL-1β mediated NF-κB pathway activation is completely abolished in patient cells. Western blotting, nuclear translocation, and RT-qPCR data indicate that the TRAF6 C90F mutation causes a loss of IL-1β dependent NF-κB signaling in patient fibroblast cells. The impaired NF-κB signaling in patient cells represents an IL-1β specific deficiency, rather than a global loss of pathway activation, as TNF-α responses are intact in both fibroblasts and lymphoblastoid cells (Figure 15 & 16). This is consistent with previous literature which has shown that TRAF6 is unique in the TRAF family, as it is the only member which has been shown to transduce signals through the IL-R family; whereas, TRAFs 2 and 5 are primarily responsible from mediating inputs from the TNF receptor.[79] The distinct role of TRAF6 in the protein family and the NF-κB pathway[81] could be underlying the patient's distinct inflammatory response. NEMO, IKK-β and IκB-α are core proteins in the canonical NF-κB pathway and central mediators of signaling.[25] TRAF6 bridges interactions

between these major proteins and specific receptors and would be expected to result in a discrete response.[78] Immunodeficiency due to mutations in *IKBKG*, *IKBKB*, or *NFKBIA* would be expected to result in a different phenotype than that caused by a TRAF6 mutation. Further investigations using additional methods of NF-κB activation, including stimulation with LPS and CD40-ligand, could help to more fully characterize the specific signaling defect underlying the patient's immunodeficiency. Future investigations should examine NF-κB signaling in an immune cell type.

Preliminary data using NF-κB nuclear translocation assay and RT-qPCR suggest that NF-κB activity is also impaired in patient LCLs, but additional experiments are required to verify this finding. A potential issue with use of LCLs for the NF-κB nuclear translocation assay could be the serum starvation required to adhere the cells to the plate. NF-κB is activated in response to many cellular stresses[128] so serum starvation may have contributed to the high variability of NF-κB activation observed among technical replicates, especially since serum starvation has been shown to activate the pathway in some cell types.[129] Experiments in lymphoblastoid cells have presented a challenge as patient LCLs are difficult to maintain. LCL transformation and immortalization requires constitutive activation of the NF-κB pathway through the CD40 receptor by latent membrane protein-1 (LMP-1).[126,130] TRAF6 is responsible for mediating the signals via LMP-1 to activate NF-κB signaling,[131] so the patient's mutation may have interfered with the immortalization process and impair the NF-κB signals required for LCL cell growth. Alternative immune cells for future investigations could be macrophages, but the mutant cell line would have to be engineered as it is not possible to obtain patient samples. A cell line with the C90F mutation could be created many ways; CRISPR-cas9 using the homology directed repair mechanism could be used to introduce the missense mutation into WT macrophages, or existing patient fibroblasts could be reprogrammed into induced pluripotent stem cells by expression of the Yamanaka factors

and then differentiated into macrophages. Transient expression of the WT gene by transfection into macrophage cells is not ideal as NF-κB signaling mediated by endogenous TRAF6 protein would make results interpretation challenging.

It is unclear if the observed signaling defects are due to an insufficient amount of TRAF6 protein to mediate signaling, or a structural defect resulting in an inability of the mutant to interact with binding partners. This could be tested by overexpressing the mutant protein in patient cells and determining whether TRAF6 protein levels increase, and if any increase is capable of rescuing NF-κB signaling. Investigating the ability of the mutant TRAF6 to interact with binding partners could be examined by using co-immunoprecipitation for known interactors of TRAF6. NEMO, Ubc13, Tab2, and IRAK-1 interact with TRAF6 via the RING domain;[30,112,132,133] whereas, EDAR and other members of the TRAF family dimerize with TRAF6 via the TRAF domain.[84,85,87] Determination of which, if any, interactions are impaired could hint at the mechanism underlying the patient's signaling defect. Furthermore, TRAF6 interactions are dependent on the receptor which the pathway is activated through; understanding the specific cytokine limitations of the mutation could help toward characterizing the patient's distinct immune response. Data so far have shown a significant decrease in TRAF6 C90F protein in mutant cells, and a complete abolition of IL-1β mediated NF-κB signaling in patient fibroblasts. The ability of WT TRAF6 expression to rescue these defects suggests that the TRAF6 C90F mutation is underlying the impaired NF-κB response to IL-1β observed in patient cells.

Chapter Four:

General Discussion and Conclusions

4.1 Results Summary

We have studied a consanguineous family of Cree ancestry who have had 2 children born with a severe congenital immunodeficiency. The first child died at 40 days of life due to infection, and the second child began experiencing infections at 2 weeks of age resulting in her permanent hospitalization at 2 months. While in hospital the patient developed features of ectodermal dysplasia and skeletal scans revealed abnormal bone development. A diagnosis could not be provided by conventional medical and genetic testing, prompting the search of novel causes of immunodeficiency. The patient's phenotype bore striking similarities to males who have hypomorphic mutations in *IKBKG* gene encoding the protein NEMO,[134,135] which is a central component of the NF-κB pathway coordinating signals through major immune receptors.[25] These individuals also experience immunodeficiency with ectodermal dysplasia and metaphyseal splaying similar to our patient. However, NEMO is encoded on the X-chromosome and females with *IKBKG* mutations experience a milder phenotype.[136] The severity of our patient's disorder and the improbability of an X-inactivation skew to occur in both patients II-2 and II-3 did not support *IKBKG* as the cause in this family. However, similarities to patients with mutations in NEMO suggested that the causative gene might be in the NF-κB pathway. The fact that the parents are related by blood and belong to a consanguineous population from Northern Alberta suggested potentially an autosomal recessive mode of inheritance in this family.

A bioinformatics approach using HZM, WES and *in silico* modelling was used to search for candidate genes. HZM was used due to consanguinity in the family and a WES trio of the patient and parents was performed and analyzed under an autosomal recessive mode. This strategy yielded 3 candidate genes: *CLDN16*, *GMNC* and *COQ2*. TRAF6 was identified as a low-quality variant in the patient's exome data set after HZM but failed to amplify in the parents and was therefore

eliminated by the initial filtering strategy. *TRAF6* was included as a candidate gene due to the protein's function in the NF-κB pathway. The *TRAF6* and *GMNC* variants were predicted to be pathogenic by *in silico* modelling, but only the *TRAF6* variant segregated with the phenotype in the family. Sanger sequencing confirmed homozygosity of the *TRAF6* variant in the patient and revealed that each parent was heterozygous for the variant. The identified variant is a homozygous missense mutation (c.G269T) in *TRAF6* (NM_145803) causing a non-synonymous amino acid substitution of a cysteine to a phenylalanine in the RING domain, which is critical for the protein's function in NF-κB signaling.

TRAF6 activates the NF-κB pathway by ubiquitination of NEMO and activation of the IKK complex in response to IL-1β stimulation and is involved in transducing signals through numerous other immune receptors.[78] TRAF6 also contributes to bone and ectodermal development by coordinating signals through the RANK and EDAR receptors, respectively.[90,137] The function of TRAF6 in these processes based on existing literature provided a potential explanation of the patient's complex immune, skeletal, and ectodermal phenotype.[30,47,112,138,57,78,83,85,86,88–90] Therefore, *TRAF6* was considered a very strong candidate gene for functional analysis. Identification of *TRAF6* as a candidate gene was only possible using HZM, as conventional exome filtering strategies would have missed the variant. Indeed, initial exome filtering before the availability of HZM data failed to identify *TRAF6* as a candidate gene. A limitation of WES is poor or no coverage of some parts of the exome, which can lead to inaccuracies in variant calling and inclusion.[63] Initial use of homozygosity mapping reduced the analysis to less than 2% of the ~75,000 variants identified in the patient's exome and made it possible to examine individual low-quality SNPs for potential inclusion, as was the case with *TRAF6*. Importantly, TRAF6 was only covered by two reads in the patient's exome and not at all in the parents; if TRAF6 had also failed

to amplify in the patient it would have been impossible to identify with this strategy. This underscores a limitation of WES as a tool for gene discovery, but also highlights the importance of understanding technological barriers to overcome them. It underlines the fundamental need for correct and detailed clinical phenotyping of patients, as in this case we started the project with the suggestion that our gene of interest would likely be part of the NF-κB pathway. HZM and filtering for low quality variants were then instrumental to the success of the gene discovery strategy. The identification of *TRAF6* as a candidate gene for our project indicates that even in the era of next generation sequencing detailed observation of patient's clinical features, and family history remain an essential point of departure for a successful project as technological advancements, while powerful, are not perfect.

TRAF6 is a RING-type E3 ubiquitin ligase involved in the conjugation of K63-inked ubiquitin onto the protein NEMO to activate NF-κB signaling.[78,82,138] RING domain proteins are characterized by zinc coordination through their cysteine residues to facilitate interaction with the E2 ubiquitin conjugating enzyme and the target substrate.[99] Functional analysis of the patient's cysteine to phenylalanine missense mutation focused on examining the effect of the mutation on the TRAF6 protein and on NF-κB signaling. The mutation was found to decrease TRAF6 abundance and stability in patient fibroblast cells, but it is unclear what was the effect of the mutation on TRAF6 RING domain structure as it was not possible to express the mutant domain in *E. coli* for analysis by NMR. NF-κB signaling was impaired in patient lymphoblastoid cells, and pathway activation was completely abolished in patient fibroblast cells in response to IL-1β but TNF-α signaling remained intact, as expected.

Early clinical investigation revealed that the patient did not have an inflammatory response typical of any specific SCID subtype; complicating the diagnosis. The role of TRAF6 in mediating

inflammatory signals from some immune receptors but not others could be underlying her unique immune profile. Further analysis of NF-κB and other immune signaling pathways with additional cytokines and on a different cell type (macrophages) could allow for a more complete understanding of the patient's phenotype. The observed decrease in TRAF6 protein was not sufficient to suggest that the missense mutation was the cause of the defective NF-κB signaling in patient fibroblast and lymphoblastoid cells. A WT copy of the *TRAF6* gene was introduced into patient fibroblasts to provide evidence that the C90F mutation is responsible for the impaired pathway activation, and this was found to rescue activation of NF-κB target genes in response to IL-1β. Taken together these data provide evidence that the homozygous *TRAF6* c.G269T [p.C90F] missense mutation impairs NF-κB signaling, a known cause of immunodeficiency, and this mutation could be underlying the complex phenotype observed in our patient. Our study shows that functional studies of biological processes remain fundamental for understanding the intricacies of human disorders, and a *sine qua non* condition for the development of personalized treatment of genetic disorders in the future.

4.2 Significance for family

Identification of a candidate gene had a profound impact on patient management and family care. Early experiments provided functional support for the pathogenicity of the identified variant and allowed the patient to receive a bone-marrow transplant (BMT) to potentially cure her immunodeficiency. BMT is the typical treatment for most types of SCID; other modalities are used for some forms of SCID such as Omenn Syndrome and ADA deficiency. However, BMT is the treatment of choice for individuals with NEMO mutations and was considered the most appropriate option for our patient. BMT represents a highly effective treatment when administered in the first

3 months of life and with the appropriate donor. The ideal donor is an HLA-matched sibling or parent in consanguineous families; other donors can be successful but the risk for graft-versus-host disease or graft failure is higher.[139,140] The patient's siblings and parents were not matches to provide a bone marrow transplant, and the patient received a transplant from an unrelated donor at 24 months. The BMT was completed and the patient discharged from the hospital after recovery. After discharge the patient died due to infection. BMT reconstituted the immune system and had an effect on the skin and adnexa, including correction of the rash, and the patient was able to grow hair while the two teeth seen at the last medical appointment were peg-shaped as seen in ED cases (Figure 3f). Although, the patient showed marrow engraftment, she appears to have died from an infection at home a year later. An autopsy was performed but unfortunately we are not in possession of the report from the medical examiner. It is possible that elements of the ectodermal dysplasia may have contributed to her demise. A skeletal survey was suggested post-mortem but again we have not had access to her X-rays to date. While we cannot comment if earlier intervention would have increased her chances of survival, the results of our study will allow timely intervention in future detected cases. New births in the family have been promptly tested to prevent dangerous delays in treatment.

In addition to impacting patient treatment, identification of a candidate gene has allowed for personalized genetic counselling for the patient's family. *TRAF6* has not previously been shown to cause immunodeficiency and is not tested for commercially or through provincial screening program. Identifying the cause of the disorder in this family could allow the addition of *TRAF6* to the list of genes to be clinically tested in patients with SCID increasing the chances of finding other affected individuals who may have negative results at this time. This will require confirmation of *TRAF6* as a cause of immunodeficiency. Furthermore, the patient's parents belong to large sib-

ships; the extended family's pedigree shows multiple loops of consanguinity (Figure 24) and this mutation could represent a risk for other individuals in this family, and the larger consanguineous Cree community. Partnerships with the community could help to identify additional carriers and determine if a founder effect exists, which could allow for carrier screening and improved health outcomes for this underserved community.

4.3 **Significance for the field**

The functional work presented here represents evidence TRAF6 as a genetic cause of immunodeficiency. This finding contributes to the current body of work expanding the role of *TRAF6* as a cause of human disease. There have been two other clinical cases of mutations in *TRAF6*. A heterozygous frameshift mutation resulting in a truncated TRAF6 protein has been associated with ectodermal dysplasia in a single Polish case, and a pair of Israeli twins with immunodeficiency and bone defects were found to have a homozygous deletion encompassing the 5' non-coding region of *TRAF6*.[91,92] Significantly, the Israeli deletion also included the 2 upstream genes *RAG1* and *RAG2*, which are known causes of immunodeficiency but have not been associated with bone defects. The authors hypothesized that the deletion in TRAF6 may be underlying the skeletal abnormalities observed in these patients.[92] We have also been in collaboration with researchers at the University of Missouri at Kansas City (UMKC) who have identified a homozygous nonsense mutation in *TRAF6* as a cause of immunodeficiency and osteopetrosis in a Turkish family. This mutation results in loss of approximately half of the C-TRAF domain in the C-terminal region of the protein; this is downstream of the heterozygous mutation identified in the Polish individual. Preliminary work by our group and the researchers at UMKC suggests that the mutation identified in the Turkish family also abolishes IL-1β dependent

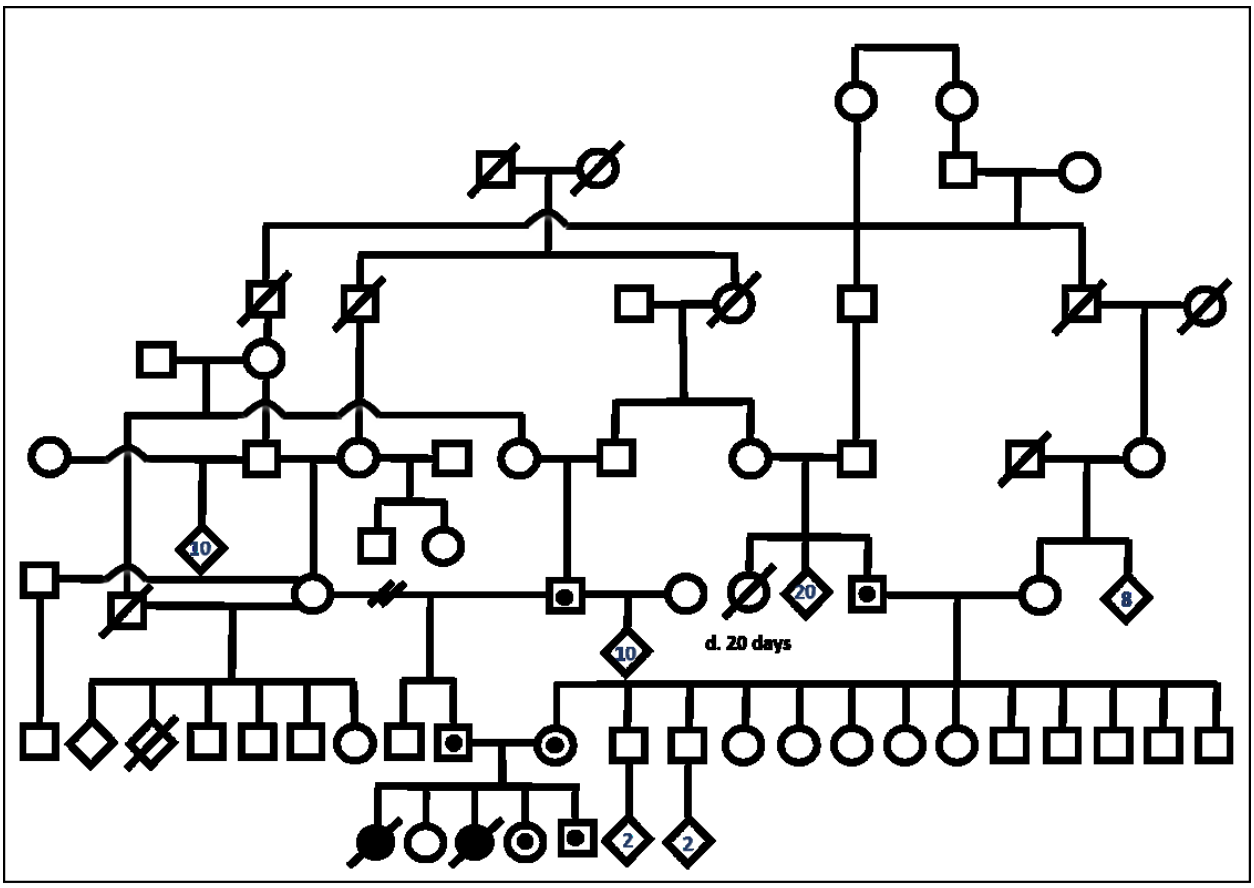

Figure 24. The patient's large consanguineous family. Pedigree of the extended family from a consanguineous Cree community. Denoted carriers (indicated by a black dot in the circle/square) have undergone genetic testing for the TRAF6 c.G269T variant. Only grandparents have been tested to date, beyond the nuclear family. Diamond symbols with numbers (X) indicate X number of male and female children.

NF-κB signaling (personal correspondence). Much work remains to be done to understand how the spectrum of *TRAF6* mutations causes human disease; the specific phenotype seems to be dependent on mode of inheritance and the domain harboring the mutation. TRAF6 has several functional domains and the specific phenotype is likely dependent on which domain is impaired by a given mutation (Figure 25). The TRAF domain is involved in binding the cytoplasmic region of cell surface receptors such as CD40, RANK, and EDAR[87,131] and for homo- or heterodimerization with other TRAF family proteins.[94] Specifically, the TRAF-C domain is responsible for receptor interactions and the TRAF-N domain dimerization, whereas, the RING domain is more important for cytoplasmic signaling downstream of the IL-1/TLR and TCR/BCR receptor families.[94,141] A major focus of future functional analysis could compare the effect of the 4 identified TRAF6 mutations (Figure 25) on cell signaling through the different RING or TRAF domain dependent receptors.

It is currently unclear how the different *TRAF6* mutations cause osteopetrosis in the knock-out mouse and Israeli and Turkish families, given that osteoporosis was observed in our patient.[88,89,92] Bone development and maintenance is a dynamic process involving the breakdown and rebuilding of bone tissue by osteoclasts and osteoblasts, respectively. When calcium is required by the body osteoclasts breakdown bone, and when calcium in plentiful osteoblasts build the bone back up. This remodeling process also helps to maintain bone integrity by eliminating old bone tissue and replacing it with new.[137] TRAF6 is the only known TRAF family member to cause skeletal abnormalities when absent, and is required for osteoclast differentiation in response to RANK receptor stimulation by RANKL.[137] Osteoclastogenesis by RANK signaling is positively regulated by TGF-β and TNF-α, and negatively regulated by INF-γ and IFN-β signals.[142] IFN-γ is secreted by T-cells to counter the action of RANKL stimulation and inhibits osteoclastogenesis

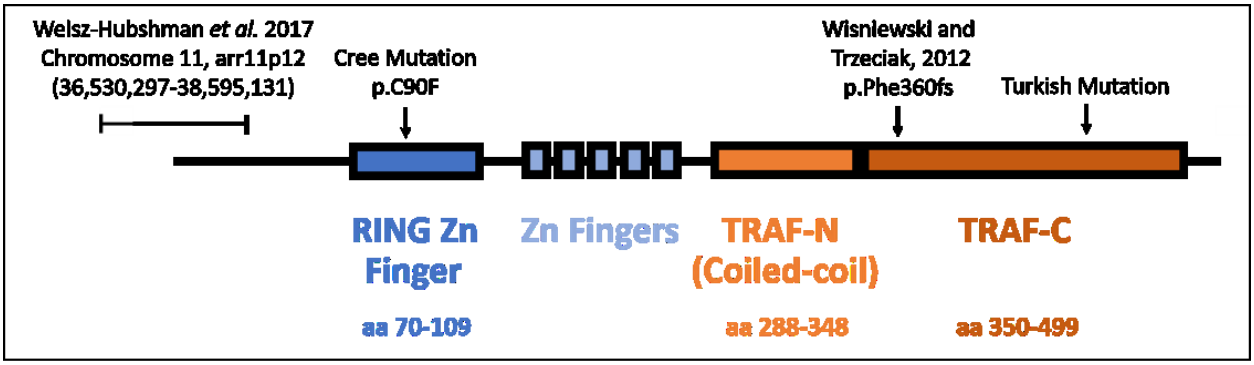

Figure 25. Four TRAF6 mutations are associated with human phenotypes. The TRAF6 protein is composed of 4 major structural domains. Homozygous mutations throughout the TRAF6 protein in Israeli, Cree, and Turkish individuals have been associated with immunodeficiency and bone abnormalities. A homozygous missense mutation in the RING domain and a heterozygous frameshift mutation in the TRAF-C domain have been associated with ectodermal dysplasia.

through the degradation of TRAF6. In contrast RANKL stimulation upregulates TRAF6 protein expression to drive osteoclastogenesis.[51] TRAF6 is degraded through the action of the ubiquitin proteasome system. However, the exact mechanism is currently unclear.[52] We have shown that the C90F mutant protein is detectable in patient cells. It is possible that this low level of protein is sufficient to mediate RANK signaling through the intact TRAF domain and drive osteoclastogenesis. If INF-γ mediated TRAF6 ubiquitination and degradation is RING dependent, then negative regulation of osteoclastogenesis may be impaired by the C90F mutation. This could result in an excess of osteoclasts leading to osteoporosis, in contrast to the osteopetrosis experienced by patients with TRAF domain mutations. This hypothesis is complicated by research suggesting that RANK signaling is not entirely RING-independent. While the TRAF domain of TRAF6 is responsible for RANK receptor binding it has been shown that a ligase defective mutant of TRAF6, caused by mutation of cysteine 70 to an alanine, is incapable of rescuing defective RANK signaling in TRAF6-deficient monocytes.[137] These data suggest that RANK signaling relies on a functional RING domain. Future work with both the RING and TRAF domain mutants of TRAF6 could be used to develop a more complete understanding of RANK signaling regulation and bone homeostasis.

An additional complication is the observation that a heterozygous [p.F360fs] TRAF6 mutation has been associated with ectodermal dysplasia, yet carriers of the C90F mutation and the Turkish mutation seem to be unaffected.[91] Functional analysis of the F360fs mutation revealed that the heterozygous *TRAF6* mutation acts as a dominant negative to inhibit WT TRAF6 protein interaction with EDARRAD.[93] EDARADD serves as an adaptor for the ectodysplasia receptor EDAR and mutations to these genes are known to cause ectodermal dysplasia.[22,143] There are multiple hypotheses as to why the heterozygous C90F mutation does not cause ectodermal

dysplasia. The C90F mutation is unstable and may not be present at sufficient levels to effectively titrate out the WT TRAF6 copy and is therefore incapable of fully acting as a dominant negative. Furthermore, the RING domain is not considered to be involved in homodimerization and would not be expected to cause ectodermal dysplasia by the same mechanism as a TRAF domain mutation. The more interesting cases to consider are the Polish patient and the parents of the Turkish patients, all these individuals have heterozygous truncating mutations resulting in loss of part of the TRAF domain but only one has been diagnosed with ED. One possibility is that the Turkish heterozygotes do have mild ED that has gone undiagnosed. Preliminary data show that the Turkish mutation behaves as a null, more like the mutation studied in our patients, and the disorder in our patients and the Turkish patients are due to abrogation of the downstream NF-κB effects supported by results of the lack on nuclear translocation (personal correspondence). Due to the severity of the mutation in our patients and Turkish patients it is plausible that the carriers do have sufficient amount of TRAF6 protein to support normal signaling while the amount of protein is reduced as seen in carriers of autosomal recessive disorders, who usually are not affected. The nonsense Turkish *TRAF6* mutation could prompt nonsense mediated decay (NMD) of the mutant allele, and no protein would be produced to act as a dominant negative. NMD was originally identified as a quality control mechanism to prevent the expression of aberrant proteins in the cell, where the presence of a premature termination codon (PTC) was sufficient to prompt degradation. However, that view has changed and NMD is now considered a highly regulated process requiring numerous factors that can impact expression of WT and mutant mRNAs.[144] Splicing plays a role in the execution of NMD, for an mRNA to be efficiently degraded by NMD the PTC generally needs to be at least 50 nucleotides upstream of an exon-exon junction; therefore, PTCs in the final exon often do not prompt this quality control mechanism.[145] Control of NMD by multiple factors

rather than a PTC alone means it is possible that, despite the similarities, the Turkish mutation may cause NMD while the Polish mutation does not. Additionally, the F360fs mutation occurs upstream of the Turkish mutation resulting in loss of most of the TRAF-C domain; whereas, the Turkish mutation does not truncate the protein until midway through the domain. The TRAF-N region of the TRAF domain is known to be more important for homo- and heterodimerization, and the TRAF-C domain more involved in receptor interactions. The Polish mutation is considerably closer to the TRAF-N domain and may be more likely to impair the function of this domain than the Turkish mutations. Understanding the different phenotype-genotype correlations will improve our understanding of how *TRAF6* mutations cause human disease and enhance patient care and could provide new insight into the many molecular functions of TRAF6.

4.3 Future Directions

Examining the different mutations in a cellular context is challenging without access to patient derived cells, as the function of endogenous TRAF6 can make results challenging to interpret. Genome engineering techniques represent a useful strategy to address this issue when patient cells are not available. Introducing specific mutations through CRISPR-cas9 using the homology directed repair (HDR) pathway would be ideal, but labor intensive than the non-homologous end joining (NHEJ) repair pathway, as the guide RNA and donor template would have to be optimized for each mutation. A potential alternative would be to knock out endogenous *TRAF6* using CRISPR-cas9 and NHEJ, and if cells are viable to express each mutation stably or transiently in cells. Stable gene expression is generally preferred as it avoids variations in transfection efficiencies between conditions and biological replicates, thereby improving data interpretation and reproducibility. However, methods of stable gene expression are not without

issue; differing locations of exogenous gene integration in the genome can have unexpected consequences and make data interpretation challenging.

Access to patient derived cell lines has been a major strength of this project as it has allowed for the analysis of the mutation in the absence of unrelated, external factors. Before this work there had been associations of *TRAF6* mutations with human disease, but none were strong enough to implicate *TRAF6* as a notable cause of any disorder. The extensive functional analysis achieved in this work, and our collaboration with other scientists studying *TRAF6* as a cause of immunodeficiency, makes a substantial contribution to the implication of *TRAF6* as a new cause of a novel type of immunodeficiency.

A limitation of this study is that it only addresses the effect of the mutation in the context of cellular NF-κB signaling, and a defect observed at the cellular level may not translate to a phenotype *in vivo*. Furthermore, we have only shown a loss of pathway activation in response to IL-1β stimulation, yet many cytokines are responsible for mediating an immune and inflammatory response. As mentioned before, TRAF6 is unique in the TRAF protein family as it is the only member to transduce signals from the IL-1 receptor; the other TRAF proteins serve as adaptors for the TNF receptor superfamily. However, TRAF6 is still involved in signaling from many other receptors and its distinct role could contribute to the patient's unique inflammatory response. Examination of the TRAF6 C90F mutation as a cause of disease beyond a cellular level could be accomplished by creating an animal model of the mutation. If immunodeficiency is observed in a model organism this would be strong evidence that the C90F mutation, and other *TRAF6* mutations in general, cause human disease. A mouse model is an obvious choice, as a *Traf6* knock out mouse already exists and would provide a useful comparison for other *TRAF6* variants.[88–90] However, zebrafish represent a vertebrate model that would be more efficient and economical to produce

than a mouse model. Indeed, *traf6* is already being examined in terms of conservation and tissue expression,[146] and in the context of an infectious disease model in zebrafish.[147] We have obtained funding for such studies and a zebrafish model is being currently developed by Dr. Jason Berman from Dalhousie University. Further functional analysis in cells and a model organism, in addition to identification of more individuals with mutations in *TRAF6*, will strengthen the evidence that *TRAF6* mutations are an important cause of human disease and help to provide more patients and families with diagnoses and treatment.

References

1. Delves, P.J., Martin, S.J., Burton, D.R., and Roitt, I.M. (2011). Roitt's essential immunology.

2. Janeway, C. (2001). Immunobiology 5 : the immune system in health and disease (Garland Pub).

3. Yang, S.-H., Gao, C.-Y., Li, L., Chang, C., Leung, P.S.C., Gershwin, M.E., and Lian, Z.-X. (2018). The molecular basis of immune regulation in autoimmunity. Clin. Sci. (Lond). *132*, 43–67.

4. Tang, D., Kang, R., Coyne, C.B., Zeh, H.J., and Lotze, M.T. (2012). PAMPs and DAMPs: signal 0s that spur autophagy and immunity. Immunol. Rev. *249*, 158–175.

5. Di Gioia, M., and Zanoni, I. (2015). Toll-like receptor co-receptors as master regulators of the immune response. Mol. Immunol. *63*, 143–152.

6. Callewaert, L., Van Herreweghe, J.M., Vanderkelen, L., Leysen, S., Voet, A., and Michiels, C.W. (2012). Guards of the great wall: bacterial lysozyme inhibitors. Trends Microbiol. *20*, 501–510.

7. Paul, W.E. (2013). Fundamental immunology (Wolters Kluwer Health/Lippincott Williams & Wilkins).

8. Speck, N.A., and Gilliland, D.G. (2002). Core-binding factors in haematopoiesis and leukaemia. Nat. Rev. Cancer *2*, 502–513.

9. Kobayashi, S.D., and DeLeo, F.R. (2009). Role of neutrophils in innate immunity: a systems biology-level approach. Wiley Interdiscip. Rev. Syst. Biol. Med. *1*, 309–333.

10. Davies, L.C., Jenkins, S.J., Allen, J.E., and Taylor, P.R. (2013). Tissue-resident macrophages. Nat. Immunol. *14*, 986–995.

11. Reagan, M.R., and Rosen, C.J. (2016). Navigating the bone marrow niche: translational

insights and cancer-driven dysfunction. Nat. Rev. Rheumatol. *12*, 154–168.

12. Hewitt, E.W. (2003). The MHC class I antigen presentation pathway: strategies for viral immune evasion. Immunology *110*, 163–169.

13. Sawicki, M.W., Dimasi, N., Natarajan, K., Wang, J., Margulies, D.H., and Mariuzza, R.A. Structural basis of MHC class I recognition by natural killer cell.

14. Klein, L., Kyewski, B., Allen, P.M., and Hogquist, K.A. (2014). Positive and negative selection of the T cell repertoire: what thymocytes see (and don't see). Nat. Rev. Immunol. *14*, 377–391.

15. Cirillo, E., Giardino, G., Gallo, V., D'Assante, R., Grasso, F., Romano, R., Lillo, C. Di, Galasso, G., and Pignata, C. (2015). Severe combined immunodeficiency-an update. Ann. N. Y. Acad. Sci. *1356*, 90–106.

16. Kwan, A., Abraham, R.S., Currier, R., Brower, A., Andruszewski, K., Abbott, J.K., Baker, M., Ballow, M., Bartoshesky, L.E., Bonilla, F.A., et al. (2014). Newborn Screening for Severe Combined Immunodeficiency in 11 Screening Programs in the United States. JAMA *312*, 729.

17. van der Burg, M., and Gennery, A.R. (2011). The expanding clinical and immunological spectrum of severe combinded immunodeficiency. Eur. J. Pediatr. *170*, 561–571.

18. Van Der Burg, M., Van Zelm, M.C., and Notarangelo, L.D. (2014). Clinical spectrum of SCID: the key is in the thymus?

19. Boisson-Dupuis, S., Bustamante, J., El-Baghdadi, J., Camcioglu, Y., Parvaneh, N., El Azbaoui, S., Agader, A., Hassani, A., El Hafidi, N., Mrani, N.A., et al. (2015). Inherited and acquired immunodeficiencies underlying tuberculosis in childhood. Immunol. Rev. *264*, 103–120.

20. Döffinger, R., Smahi, A., Bessia, C., Geissmann, F., Feinberg, J., Durandy, A., Bodemer, C.,

Kenwrick, S., Dupuis-Girod, S., Blanche, S., et al. (2001). X-linked anhidrotic ectodermal dysplasia with immunodeficiency is caused by impaired NF-κB signaling. Nat. Genet. *27*, 277–285.

21. D'Assante, R., Fusco, A., Palamaro, L., Giardino, G., Gallo, V., Cirillo, E., and Pignata, C. (2015). Unraveling the Link Between Ectodermal Disorders and Primary Immunodeficiencies. Int. Rev. Immunol. 1–14.

22. Smahi, A., Courtois, G., Rabia, S.H., Döffinger, R., Bodemer, C., Munnich, A., Casanova, J.-L., and Israël, A. (2002). The NF-kappaB signalling pathway in human diseases: from incontinentia pigmenti to ectodermal dysplasias and immune-deficiency syndromes. Hum. Mol. Genet. *11*, 2371–2375.

23. Kawai, T., Nishikomori, R., and Heike, T. (2012). Diagnosis and Treatment in Anhidrotic Ectodermal Dysplasia with Immunodeficiency. Allergol. Int. *61*, 207–217.

24. Oeckinghaus, A., Hayden, M.S., and Ghosh, S. (2011). Crosstalk in NF-κB signaling pathways. Nat. Immunol. *12*, 695–708.

25. Gilmore, T.D. (2006). Introduction to NF-κB: players, pathways, perspectives. Oncogene *25*, 6680–6684.

26. Scheidereit, C. (2006). IκB kinase complexes: gateways to NF-κB activation and transcription. Oncogene *25*, 6685–6705.

27. Perkins, N.D. (2006). Post-translational modifications regulating the activity and function of the nuclear factor kappa B pathway. Oncogene *25*, 6717–6730.

28. Hayden, M.S., West, A.P., and Ghosh, S. (2006). NF-κB and the immune response. Oncogene *25*, 6758–6780.

29. Liu, T., Zhang, L., Joo, D., and Sun, S.-C. (2017). NF-κB signaling in inflammation. Signal

Transduct. Target. Ther. *2*, 17023.

30. Conze, D.B., Wu, C.-J., Thomas, J.A., Landstrom, A., and Ashwell, J.D. (2008). Lys63-linked polyubiquitination of IRAK-1 is required for interleukin-1 receptor- and toll-like receptor-mediated NF-kappaB activation. Mol. Cell. Biol. *28*, 3538–3547.

31. Loiarro, M., Gallo, G., Fantò, N., De Santis, R., Carminati, P., Ruggiero, V., and Sette, C. (2009). Identification of critical residues of the MyD88 death domain involved in the recruitment of downstream kinases. J. Biol. Chem. *284*, 28093–28103.

32. Hayden, M.S., and Ghosh, S. (2014). Regulation of NF-κB by TNF family cytokines. Semin. Immunol. *26*, 253–266.

33. Orange, J.S., Levy, O., Brodeur, S.R., Krzewski, K., Roy, R.M., Niemela, J.E., Fleisher, T.A., Bonilla, F.A., and Geha, R.S. (2004). Human nuclear factor κB essential modulator mutation can result in immunodeficiency without ectodermal dysplasia. J. Allergy Clin. Immunol. *114*, 650–656.

34. Zonana, J., Elder, M.E., Schneider, L.C., Orlow, S.J., Moss, C., Golabi, M., Shapira, S.K., Farndon, P.A., Wara, D.W., Emmal, S.A., et al. (2000). A Novel X-Linked Disorder of Immune Deficiency and Hypohidrotic Ectodermal Dysplasia Is Allelic to Incontinentia Pigmenti and Due to Mutations in IKK-gamma (NEMO). Am. J. Hum. Genet. *67*, 1555–1562.

35. Filipe-Santos, O., Bustamante, J., Haverkamp, M.H., Vinolo, E., Ku, C.-L., Puel, A., Frucht, D.M., Christel, K., von Bernuth, H., Jouanguy, E., et al. (2006). X-linked susceptibility to mycobacteria is caused by mutations in NEMO impairing CD40-dependent IL-12 production. J. Exp. Med. *203*, 1745–1759.

36. Pannicke, U., Baumann, B., Fuchs, S., Henneke, P., Rensing-Ehl, A., Rizzi, M., Janda, A., Hese, K., Schlesier, M., Holzmann, K., et al. (2013). Deficiency of Innate and Acquired

Immunity Caused by an *IKBKB* Mutation. N. Engl. J. Med. *369*, 2504–2514.

37. Lahtela, J., Nousiainen, H.O., Stefanovic, V., Tallila, J., Viskari, H., Karikoski, R., Gentile, M., Saloranta, C., Varilo, T., Salonen, R., et al. (2010). Mutant *CHUK* and Severe Fetal Encasement Malformation. N. Engl. J. Med. *363*, 1631–1637.

38. Courtois, G., Smahi, A., Reichenbach, J., Döffinger, R., Cancrini, C., Bonnet, M., Puel, A., Chable-Bessia, C., Yamaoka, S., Feinberg, J., et al. (2003). A hypermorphic IκBα mutation is associated with autosomal dominant anhidrotic ectodermal dysplasia and T cell immunodeficiency. J. Clin. Invest. *112*, 1108–1115.

39. Wade, E.M., Daniel, P.B., Jenkins, Z.A., McInerney-Leo, A., Leo, P., Morgan, T., Addor, M.C., Adès, L.C., Bertola, D., Bohring, A., et al. (2016). Mutations in MAP3K7 that Alter the Activity of the TAK1 Signaling Complex Cause Frontometaphyseal Dysplasia. Am. J. Hum. Genet. *99*, 392–406.

40. Le Goff, C., Rogers, C., Goff, W. Le, Pinto, G., Bonnet, D., Chrabieh, M., Alibeu, O., Nistchke, P., Munnich, A., Picard, C., et al. (2016). Heterozygous Mutations in MAP3K7, Encoding TGF-β-Activated Kinase 1, Cause Cardiospondylocarpofacial Syndrome.

41. Thienpont, B., Zhang, L., Postma, A. V., Breckpot, J., Tranchevent, L.-C., Van Loo, P., Møllgård, K., Tommerup, N., Bache, I., Tümer, Z., et al. (2010). Haploinsufficiency of TAB2 Causes Congenital Heart Defects in Humans. Am. J. Hum. Genet. *86*, 839–849.

42. Picard, C., Puel, A., Bonnet, M., Ku, C.-L., Bustamante, J., Yang, K., Soudais, C., Dupuis, S., Feinberg, J., Fieschi, C., et al. (2003). Pyogenic Bacterial Infections in Humans with IRAK-4 Deficiency. Science (80-.). *299*, 2076–2079.

43. Medvedev, A.E., Lentschat, A., Kuhns, D.B., Blanco, J.C.G., Salkowski, C., Zhang, S., Arditi, M., Gallin, J.I., and Vogel, S.N. (2003). Distinct mutations in IRAK-4 confer

hyporesponsiveness to lipopolysaccharide and interleukin-1 in a patient with recurrent bacterial infections. J. Exp. Med. *198*, 521–531.

44. Ku, C.-L., Picard, C., Erdös, M., Jeurissen, A., Bustamante, J., Puel, A., von Bernuth, H., Filipe-Santos, O., Chang, H.-H., Lawrence, T., et al. (2007). IRAK4 and NEMO mutations in otherwise healthy children with recurrent invasive pneumococcal disease. J. Med. Genet. *44*, 16–23.

45. von Bernuth, H., Picard, C., Jin, Z., Pankla, R., Xiao, H., Ku, C.-L., Chrabieh, M., Mustapha, I.B., Ghandil, P., Camcioglu, Y., et al. (2008). Pyogenic Bacterial Infections in Humans with MyD88 Deficiency. Science (80-.). *321*, 691–696.

46. Treon, S.P., Xu, L., Yang, G., Zhou, Y., Liu, X., Cao, Y., Sheehy, P., Manning, R.J., Patterson, C.J., Tripsas, C., et al. (2012). MYD88 L265P Somatic Mutation in Waldenström's Macroglobulinemia. N. Engl. J. Med. *367*, 826–833.

47. Cui, C.-Y., and Schlessinger, D. (2006). EDA signaling and skin appendage development. Cell Cycle *5*, 2477–2483.

48. Tao, R., Jin, B., Guo, S.Z., Qing, W., Feng, G.Y., Brooks, D.G., Liu, L., Xu, J., Li, T., Yan, Y., et al. (2006). A novel missense mutation of the EDA gene in a Mongolian family with congenital hypodontia. J. Hum. Genet. *51*, 498–502.

49. Monreal, A.W., Ferguson, B.M., Headon, D.J., Street, S.L., Overbeek, P.A., and Zonana, J. (1999). Mutations in the human homologue of mouse dl cause autosomal recessive and dominant hypohidrotic ectodermal dysplasia. Nat. Genet. *22*, 366–369.

50. Bal, E., Baala, L., Cluzeau, C., El Kerch, F., Ouldim, K., Hadj-Rabia, S., Bodemer, C., Munnich, A., Courtois, G., Sefiani, A., et al. (2007). Autosomal dominant anhidrotic ectodermal dysplasias at the EDARADD locus. Hum. Mutat. *28*, 703–709.

51. Takayanagi, H., Kim, S., and Taniguchi, T. (2002). Signaling crosstalk between RANKL and interferons in osteoclast differentiation. Arthritis Res. *4*, S227.

52. Takayanagi, H., Kim, S., Matsuo, K., Suzuki, H., Suzuki, T., Sato, K., Yokochi, T., Oda, H., Nakamura, K., Ida, N., et al. (2002). RANKL maintains bone homeostasis through c-Fos-dependent induction of interferon-β. Nature *416*, 744–749.

53. Walsh, M.C., and Choi, Y. (2014). Biology of the RANKLâ€“RANKâ€“OPG System in Immunity, Bone, and Beyond. Front. Immunol. *5*, 511.

54. Otero, J.E., Dai, S., Alhawagri, M.A., Darwech, I., and Abu-Amer, Y. (2010). IKKβ activation is sufficient for RANK-independent osteoclast differentiation and osteolysis. J. Bone Miner. Res. *25*, 1282–1294.

55. Abu-Amer, Y. (2013). NF-κB signaling and bone resorption. Osteoporos. Int. *24*, 2377–2386.

56. Boyce, B.F., Xiu, Y., Li, J., Xing, L., and Yao, Z. (2015). NF-κB-Mediated Regulation of Osteoclastogenesis. Endocrinol. Metab. (Seoul, Korea) *30*, 35–44.

57. Darnay, B.G., Besse, A., Poblenz, A.T., Lamothe, B., and Jacoby, J.J. (2007). TRAFs in RANK Signaling. In TNF Receptor Associated Factors (TRAFs), (New York, NY: Springer New York), pp. 152–159.

58. Hughes, A.E., Ralston, S.H., Marken, J., Bell, C., MacPherson, H., Wallace, R.G.H., van Hul, W., Whyte, M.P., Nakatsuka, K., Hovy, L., et al. (2000). Mutations in TNFRSF11A, affecting the signal peptide of RANK, cause familial expansile osteolysis. Nat. Genet. *24*, 45–48.

59. Johnson-Pais, T.L., Singer, F.R., Bone, H.G., McMurray, C.T., Hansen, M.F., and Leach, R.J. (2003). Identification of a Novel Tandem Duplication in Exon 1 of the TNFRSF11A Gene in Two Unrelated Patients With Familial Expansile Osteolysis. J. Bone Miner. Res. *18*, 376–380.

60. Guerrini, M.M., Sobacchi, C., Cassani, B., Abinun, M., Kilic, S.S., Pangrazio, A., Moratto, D., Mazzolari, E., Clayton-Smith, J., Orchard, P., et al. (2008). Human osteoclast-poor osteopetrosis with hypogammaglobulinemia due to TNFRSF11A (RANK) mutations. Am. J. Hum. Genet. *83*, 64–76.

61. Sobacchi, C., Frattini, A., Guerrini, M.M., Abinun, M., Pangrazio, A., Susani, L., Bredius, R., Mancini, G., Cant, A., Bishop, N., et al. (2007). Osteoclast-poor human osteopetrosis due to mutations in the gene encoding RANKL. Nat. Genet. *39*, 960–962.

62. Whyte, M.P., Obrecht, S.E., Finnegan, P.M., Jones, J.L., Podgornik, M.N., McAlister, W.H., and Mumm, S. (2002). Osteoprotegerin Deficiency and Juvenile Paget's Disease. N. Engl. J. Med. *347*, 175–184.

63. O'Donnell-Luria, A.H., and Miller, D.T. (2016). A Clinician's perspective on clinical exome sequencing. Hum. Genet. *135*, 643–654.

64. Ng, S.B., Buckingham, K.J., Lee, C., Bigham, A.W., Tabor, H.K., Dent, K.M., Huff, C.D., Shannon, P.T., Jabs, E.W., Nickerson, D.A., et al. (2010). Exome sequencing identifies the cause of a mendelian disorder. Nat. Genet. *42*, 30–35.

65. Wang, Q., Shashikant, C.S., Jensen, M., Altman, N.S., and Girirajan, S. (2017). Novel metrics to measure coverage in whole exome sequencing datasets reveal local and global non-uniformity. Sci. Rep. *7*, 885.

66. Gilissen, C., Hoischen, A., Brunner, H.G., and Veltman, J.A. (2012). Disease gene identification strategies for exome sequencing. Eur. J. Hum. Genet. *20*, 490–497.

67. Boycott, K.M., and Ardigó, D. (2017). Addressing challenges in the diagnosis and treatment of rare genetic diseases. Nat. Rev. Drug Discov. *17*, 151–152.

68. Timmermans, S., Tietbohl, C., and Skaperdas, E. (2017). Narrating uncertainty: Variants of

uncertain significance (VUS) in clinical exome sequencing. Biosocieties *12*, 439–458.

69. Ku, C.-S., Cooper, D.N., and Patrinos, G.P. (2016). The Rise and Rise of Exome Sequencing. Public Health Genomics *19*, 315–324.

70. Ernani, F.P., and Leproust, E.M. Agilent's SureSelect Target Enrichment System.

71. Grantham, R. (1974). Amino acid difference formula to help explain protein evolution. Science *185*, 862–864.

72. Tavtigian, S. V, Deffenbaugh, A.M., Yin, L., Judkins, T., Scholl, T., Samollow, P.B., de Silva, D., Zharkikh, A., and Thomas, A. (2006). Comprehensive statistical study of 452 BRCA1 missense substitutions with classification of eight recurrent substitutions as neutral. J. Med. Genet. *43*, 295–305.

73. Vaser, R., Adusumalli, S., Ngak Leng, S., Sikic, M., and Ng, P.C. (2015). SIFT missense predictions for genomes. Nat. Protoc. *11*,.

74. Schwarz, J.M., Cooper, D.N., Schuelke, M., and Seelow, D. (2014). MutationTaster2: mutation prediction for the deep-sequencing age. Nat. Methods *11*, 361–362.

75. Adzhubei, I.A., Schmidt, S., Peshkin, L., Ramensky, V.E., Gerasimova, A., Bork, P., Kondrashov, A.S., and Sunyaev, S.R. (2010). A method and server for predicting damaging missense mutations. Nat. Methods *7*, 248–249.

76. Adzhubei, I., Jordan, D.M., and Sunyaev, S.R. (2013). Predicting functional effect of human missense mutations using PolyPhen-2. Curr. Protoc. Hum. Genet. *Chapter 7*, Unit7.20.

77. Shabayek, S., and Spellerberg, B. (2018). Group B Streptococcal Colonization, Molecular Characteristics, and Epidemiology. Front. Microbiol. *9*, 437.

78. Walsh, M.C., Lee, J., and Choi, Y. (2015). Tumor necrosis factor receptor- associated factor 6 (TRAF6) regulation of development, function, and homeostasis of the immune system.

Immunol. Rev. *266*, 72–92.

79. Cao, Z., Xiong, J., Takeuchi, M., Kurama, T., and Goeddel, D. V. (1996). TRAF6 is a signal transducer for interleukin-1. Nature *383*, 443–446.

80. Ishida, T., Mizushima, S. i, Azuma, S., Kobayashi, N., Tojo, T., Suzuki, K., Aizawa, S., Watanabe, T., Mosialos, G., Kieff, E., et al. (1996). Identification of TRAF6, a novel tumor necrosis factor receptor-associated factor protein that mediates signaling from an amino-terminal domain of the CD40 cytoplasmic region. J. Biol. Chem. *271*, 28745–28748.

81. Ye, H., Arron, J.R., Lamothe, B., Cirilli, M., Kobayashi, T., Shevde, N.K., Segal, D., Dzivenu, O.K., Vologodskaia, M., Yim, M., et al. (2002). Distinct molecular mechanism for initiating TRAF6 signalling. Nature *418*, 443–447.

82. Sun, L., Deng, L., Ea, C.-K., Xia, Z.-P., and Chen, Z.J. (2004). The TRAF6 ubiquitin ligase and TAK1 kinase mediate IKK activation by BCL10 and MALT1 in T lymphocytes. Mol. Cell *14*, 289–301.

83. Maruyama, K., Kawagoe, T., Kondo, T., Akira, S., and Takeuchi, O. (2012). TRAF family member-associated NF-κB activator (TANK) is a negative regulator of osteoclastogenesis and bone formation. J. Biol. Chem. *287*, 29114–29124.

84. Darnay, B.G., Haridas, V., Ni, J., Moore, P.A., and Aggarwal, B.B. (1998). Characterization of the intracellular domain of receptor activator of NF-kappaB (RANK). Interaction with tumor necrosis factor receptor-associated factors and activation of NF-kappab and c-Jun N-terminal kinase. J. Biol. Chem. *273*, 20551–20555.

85. Darnay, B.G., Ni, J., Moore, P.A., and Aggarwal, B.B. (1999). Activation of NF-kappaB by RANK requires tumor necrosis factor receptor-associated factor (TRAF) 6 and NF-kappaB-inducing kinase. Identification of a novel TRAF6 interaction motif. J. Biol. Chem. *274*, 7724–

7731.

86. Sinha, S.K., Zachariah, S., Quiñones, H.I., Shindo, M., and Chaudhary, P.M. (2002). Role of TRAF3 and -6 in the activation of the NF-kappa B and JNK pathways by X-linked ectodermal dysplasia receptor. J. Biol. Chem. *277*, 44953–44961.

87. Morlon, A., Munnich, A., and Smahi, A. (2005). TAB2, TRAF6 and TAK1 are involved in NF-κB activation induced by the TNF-receptor, Edar and its adaptator Edaradd. Hum. Mol. Genet. *14*, 3751–3757.

88. Lomaga, M.A., Yeh, W.C., Sarosi, I., Duncan, G.S., Furlonger, C., Ho, A., Morony, S., Capparelli, C., Van, G., Kaufman, S., et al. (1999). TRAF6 deficiency results in osteopetrosis and defective interleukin-1, CD40, and LPS signaling. Genes Dev. *13*, 1015–1024.

89. Naito, A., Azuma, S., Tanaka, S., Miyazaki, T., Takaki, S., Takatsu, K., Nakao, K., Nakamura, K., Katsuki, M., Yamamoto, T., et al. (1999). Severe osteopetrosis, defective interleukin-1 signalling and lymph node organogenesis in TRAF6-deficient mice. Genes Cells *4*, 353–362.

90. Naito, A., Yoshida, H., Nishioka, E., Satoh, M., Azuma, S., Yamamoto, T., Nishikawa, S., and Inoue, J. (2002). TRAF6-deficient mice display hypohidrotic ectodermal dysplasia. Proc. Natl. Acad. Sci. U. S. A. *99*, 8766–8771.

91. Wisniewski, S.A., and Trzeciak, W.H. (2012). A rare heterozygous TRAF6 variant is associated with hypohidrotic ectodermal dysplasia. Br. J. Dermatol. *166*, 1353–1356.

92. Weisz Hubshman, M., Basel-Vanagaite, L., Krauss, A., Konen, O., Levy, Y., Garty, B.Z., Smirin-Yosef, P., Maya, I., Lagovsky, I., Taub, E., et al. (2017). Homozygous deletion of RAG1, RAG2 and 5′ region TRAF6 causes severe immune suppression and atypical osteopetrosis. Clin. Genet. *91*, 902–907.

93. Fujikawa, H., Farooq, M., Fujimoto, A., Ito, M., and Shimomura, Y. (2013). Functional studies for the *TRAF6* mutation associated with hypohidrotic ectodermal dysplasia. Br. J. Dermatol. *168*, 629–633.

94. Bradley, J.R., and Pober, J.S. (2001). Tumor necrosis factor receptor-associated factors (TRAFs). Oncogene *20*, 6482–6491.

95. Xie, P. (2013). TRAF molecules in cell signaling and in human diseases. J. Mol. Signal. *8*, 7.

96. Grech, A., Quinn, R., Srinivasan, D., Badoux, X., and Brink, R. Complete structural characterisation of the mammalian and Drosophila TRAF genes: implications for TRAF evolution and the role of RING finger splice variants. Mol. Immunol. *37*, 721–734.

97. Metzger, M.B., Hristova, V.A., and Weissman, A.M. (2012). HECT and RING finger families of E3 ubiquitin ligases at a glance. J. Cell Sci. *125*, 531–537.

98. Chasapis, C.T., and Spyroulias, G.A. (2009). RING finger E(3) ubiquitin ligases: structure and drug discovery. Curr. Pharm. Des. *15*, 3716–3731.

99. Metzger, M.B., Pruneda, J.N., Klevit, R.E., and Weissman, A.M. (2014). RING-type E3 ligases: master manipulators of E2 ubiquitin-conjugating enzymes and ubiquitination. Biochim. Biophys. Acta *1843*, 47–60.

100. DIPANKAR NANDI, PANKAJ TAHILIANI, A.K. and D.C. (2006). The ubiquitin-proteasome system. J.Biosci. *31*, 137–155.

101. Schmidt, M., and Finley, D. (2014). Regulation of proteasome activity in health and disease. Biochim. Biophys. Acta - Mol. Cell Res. *1843*, 13–25.

102. Tokunaga, F., Sakata, S., Saeki, Y., Satomi, Y., Kirisako, T., Kamei, K., Nakagawa, T., Kato, M., Murata, S., Yamaoka, S., et al. (2009). Involvement of linear polyubiquitylation of NEMO in NF-κB activation. Nat. Cell Biol. *11*, 123–132.

103. Deshaies, R.J., and Joazeiro, C.A.P. (2009). RING Domain E3 Ubiquitin Ligases. Annu. Rev. Biochem. *78*, 399–434.

104. Schulman, B.A., and Wade Harper, J. (2009). Ubiquitin-like protein activation by E1 enzymes: the apex for downstream signalling pathways. Nat. Rev. Mol. Cell Biol. *10*, 319–331.

105. Ye, Y., and Rape, M. (2009). Building ubiquitin chains: E2 enzymes at work. Nat. Rev. Mol. Cell Biol. *10*, 755–764.

106. Ardley, H.C., and Robinson, P.A. (2005). E3 ubiquitin ligases. Essays Biochem. *41*, 15.

107. Grice, G.L., and Nathan, J.A. (2016). The recognition of ubiquitinated proteins by the proteasome. Cell. Mol. Life Sci. *73*, 3497–3506.

108. Saeki, Y. (2017). Ubiquitin recognition by the proteasome. J. Biochem. *161*, mvw091.

109. Pickart, C.M. (1997). Targeting of substrates to the 26S proteasome. FASEB J. *11*, 1055–1066.

110. Berndsen, C.E., and Wolberger, C. (2014). New insights into ubiquitin E3 ligase mechanism. Nat. Struct. Mol. Biol. *21*, 301–307.

111. Freemont, P.S. (2000). Ubiquitination: RING for destruction? Curr. Biol. *10*, R84–R87.

112. Lamothe, B., Besse, A., Campos, A.D., Webster, W.K., Wu, H., and Darnay, B.G. SITE-SPECIFIC K63-LINKED TRAF6 AUTO- UBIQUITINATION IS A CRITICAL DETERMINANT OF IKK ACTIVATION.

113. Gautheron, J., Pescatore, A., Fusco, F., Esposito, E., Yamaoka, S., Agou, F., Ursini, M. V., and Courtois, G. (2010). Identification of a new NEMO/TRAF6 interface affected in incontinentia pigmenti pathology. Hum. Mol. Genet. *19*, 3138–3149.

114. Yin, Q., Lin, S.-C., Lamothe, B., Lu, M., Lo, Y.-C., Hura, G., Zheng, L., Rich, R.L., Campos, A.D., Myszka, D.G., et al. (2009). E2 interaction and dimerization in the crystal

structure of TRAF6. Nat. Struct. Mol. Biol. *16*, 658–666.

115. Deng, L., Wang, C., Spencer, E., Yang, L., Braun, A., You, J., Slaughter, C., Pickart, C., and Chen, Z.J. (2000). Activation of the IκB Kinase Complex by TRAF6 Requires a Dimeric Ubiquitin-Conjugating Enzyme Complex and a Unique Polyubiquitin Chain. Cell *103*, 351–361.

116. Chu, D.T.W., and Klymkowsky, M.W. (1989). The appearance of acetylated α-tubulin during early development and cellular differentiation in Xenopus. Dev. Biol. *136*, 104–117.

117. Neidhardt, F.C., Bloch, P.L., and Smith, D.F. (1974). Culture medium for enterobacteria. J. Bacteriol. *119*, 736–747.

118. Marley, J., Lu, M., and Bracken, C. (2001). A method for efficient isotopic labeling of recombinant proteins. J. Biomol. NMR *20*, 71–75.

119. Fraser, B., Maranchuk, R.A., and Foley, E. (2014). A High-Content RNAi Screen Identifies Ubiquitin Modifiers That Regulate TNF-Dependent Nuclear Accumulation of NF-ÎºB. Front. Immunol. *5*, 322.

120. Riss, T.L., Moravec, R.A., Niles, A.L., Duellman, S., Benink, H.A., Worzella, T.J., and Minor, L. (2004). Cell Viability Assays (Eli Lilly & Company and the National Center for Advancing Translational Sciences).

121. Faustino, N.A., and Cooper, T.A. (2003). Pre-mRNA splicing and human disease. Genes Dev. *17*, 419–437.

122. Tazi, J., Bakkour, N., and Stamm, S. (2009). Alternative splicing and disease. Biochim. Biophys. Acta - Mol. Basis Dis. *1792*, 14–26.

123. Mercier, P., Lewis, M.J., Hau, D.D., Saltibus, L.F., Xiao, W., and Spyracopoulos, L. (2007). Structure, interactions, and dynamics of the RING domain from human TRAF6. Protein Sci. *16*, 602–614.

124. Vereecke, L., Beyaert, R., and van Loo, G. (2009). The ubiquitin-editing enzyme A20 (TNFAIP3) is a central regulator of immunopathology. Trends Immunol. *30*, 383–391.

125. Abruzzo, L. V, Thornton, A.J., Liebert, M., Grossman, H.B., Evanoff, H., Westwick, J., Strieter, R.M., and Kunkel, S.L. (1992). Cytokine-induced Gene Expression of Interleukin-8 in Human Transitional Cell Carcinomas and Renal Cell Carcinomas. Am. J. Pathol. *140*,.

126. Zhao, B., Barrera, L.A., Ersing, I., Willox, B., Schmidt, S.C.S., Greenfeld, H., Zhou, H., Mollo, S.B., Shi, T.T., Takasaki, K., et al. (2014). The NF-κB genomic landscape in lymphoblastoid B cells. Cell Rep. *8*, 1595–1606.

127. Paciolla, M., Pescatore, A., Conte, M.I., Esposito, E., Incoronato, M., Lioi, M.B., Fusco, F., and Ursini, M. V (2015). Rare mendelian primary immunodeficiency diseases associated with impaired NF-κB signaling. Genes Immun. *16*, 239–246.

128. Mercurio, F., and Manning, A.M. (1999). NF-κB as a primary regulator of the stress response. Oncogene *18*, 6163–6171.

129. Kohno, T., Kubo, Y., Yasui, K., Haraguchi, M., Shigematsu, S., Chua, K.J., Matsuyama, T., and Hayashi, H. (2012). Serum Starvation Activates NF-κB Through G Protein β2 Subunit-Mediated Signal. DNA Cell Biol. *31*, 1636–1644.

130. Hussain, T., and Mulherkar, R. (2012). Lymphoblastoid Cell lines: a Continuous in Vitro Source of Cells to Study Carcinogen Sensitivity and DNA Repair. Int. J. Mol. Cell. Med. *1*, 75–87.

131. (2007). TNF Receptor Associated Factors (TRAFs) (New York, NY: Springer New York).

132. Muroi, M., and Tanamoto, K. (2008). TRAF6 distinctively mediates MyD88- and IRAK-1-induced activation of NF-κB. J. Leukoc. Biol. *83*, 702–707.

133. Walsh, M.C., Kim, G.K., Maurizio, P.L., Molnar, E.E., and Choi, Y. (2008). TRAF6

autoubiquitination-independent activation of the NFkappaB and MAPK pathways in response to IL-1 and RANKL. PLoS One *3*, e4064.

134. Ricci, S., Romano, F., Nieddu, F., Picard, C., and Azzari, C. (2017). OL-EDA-ID Syndrome: a Novel Hypomorphic NEMO Mutation Associated with a Severe Clinical Presentation and Transient HLH. J. Clin. Immunol. *37*, 7–11.

135. Ramírez-Alejo, N., Alcántara-Montiel, J.C., Yamazaki-Nakashimada, M., Duran-McKinster, C., Valenzuela-León, P., Rivas-Larrauri, F., Cedillo-Barrón, L., Hernández-Rivas, R., and Santos-Argumedo, L. (2015). Novel hypomorphic mutation in IKBKG impairs NEMO-ubiquitylation causing ectodermal dysplasia, immunodeficiency, incontinentia pigmenti, and immune thrombocytopenic purpura. Clin. Immunol. *160*, 163–171.

136. Fusco, F., Pescatore, A., Conte, M.I., Mirabelli, P., Paciolla, M., Esposito, E., Lioi, M.B., and Ursini, M.V. (2015). EDA-ID and IP, Two Faces of the Same Coin: How the Same *IKBKG* / *NEMO* Mutation Affecting the NF-κB Pathway Can Cause Immunodeficiency and/or Inflammation. Int. Rev. Immunol. *34*, 445–459.

137. Lamothe, B., Webster, W.K., Gopinathan, A., Besse, A., Campos, A.D., and Darnay, B.G. (2007). TRAF6 ubiquitin ligase is essential for RANKL signaling and osteoclast differentiation. Biochem. Biophys. Res. Commun. *359*, 1044–1049.

138. Yin, Q., Lin, S.-C., Lamothe, B., Lu, M., Lo, Y.-C., Hura, G., Zheng, L., Rich, R.L., Campos, A.D., Myszka, D.G., et al. (2009). E2 interaction and dimerization in the crystal structure of TRAF6. Nat. Struct. Mol. Biol. *16*, 658–666.

139. Good, R.A. (1987). Bone Marrow Transplantation Symposium: Bone Marrow Transplantation for Immunodeficiency Diseases. Am. J. Med. Sci. *294*, 68–74.

140. Cowan, M.J. (1991). Bone marrow transplantation for the treatment of genetic diseases.

Clin. Biochem. *24*, 375–381.

141. Bradshaw, R.A., and Dennis, E.A. (2010). Handbook of cell signaling. Volume 1 (Elsevier/Academic Press).

142. Yasui, T., Hirose, J., Tsutsumi, S., Nakamura, K., Aburatani, H., and Tanaka, S. (2011). Epigenetic regulation of osteoclast differentiation: Possible involvement of Jmjd3 in the histone demethylation of Nfatc1. J. Bone Miner. Res. *26*, 2665–2671.

143. Bal, E., Baala, L., Cluzeau, C., El Kerch, F., Ouldim, K., Hadj-Rabia, S., Bodemer, C., Munnich, A., Courtois, G., Sefiani, A., et al. (2007). Autosomal dominant anhidrotic ectodermal dysplasias at the EDARADD locus. Hum. Mutat. *28*, 703–709.

144. Raimondeau, E., Bufton, J.C., and Schaffitzel, C. (2018). New insights into the interplay between the translation machinery and nonsense-mediated mRNA decay factors. Biochem. Soc. Trans.

145. Neu-Yilik, G., Amthor, B., Gehring, N.H., Bahri, S., Paidassi, H., Hentze, M.W., and Kulozik, A.E. (2011). Mechanism of escape from nonsense-mediated mRNA decay of human beta-globin transcripts with nonsense mutations in the first exon. RNA *17*, 843–854.

146. Phelan, P.E., Mellon, M.T., and Kim, C.H. (2005). Functional characterization of full-length TLR3, IRAK-4, and TRAF6 in zebrafish (Danio rerio). Mol. Immunol. *42*, 1057–1071.

147. Stockhammer, O.W., Rauwerda, H., Wittink, F.R., Breit, T.M., Meijer, A.H., and Spaink, H.P. (2010). Transcriptome analysis of Traf6 function in the innate immune response of zebrafish embryos. Mol. Immunol. *48*, 179–190.